Topologic and topographic controls on flow networks and transport

by

Scott Raulerson

(Under the Direction of C. Rhett Jackson)

Abstract

Hydrological connectivity describes how different portions of the landscape interact in some form of water-mediated transfer of matter or energy. Hydrological connectivity between portions of the landscape (hillslopes, wetlands, streams) has major implications on the environmental functioning of a watershed as a whole. Understanding what governs these interactions can provide insight into individual watershed processes and can be used for more robust watershed management. In this dissertation, there are three separate but related studies primarily looking at the influence of topography and watershed structure on the flow of water and solutes at three low-relief, permeable, and groundwater-driven headwater catchments of Upper Fourmile Creek, which drains the Savannah River Site in the Upper Atlantic Coastal Plain of South Carolina. The first study investigates the longitudinal depiction of watershed structure and characteristics like topography, stream networks, groundwater levels, and land use through three case studies. These case studies provide examples of applying longitudinal depictions to stream networks, watershed hydrologic behavior and land use distributions. This longitudinal depiction of flow networks revealed large variability in slope-area relationships for low-order streams, clearly shows the influence groundwater connections have on the permanence of surface water features and quantifies the effect of land use relative to topographic position. The second study introduces a topographically based, GIS-driven, two-dimensional groundwater model for predicting water table position and groundwater travel times. This model was introduced and then used in Upper Fourmile Creek to estimate water position and compared to groundwater records, and then used to calculate groundwater travel times to provide context for nitrate transport on site. The third study investigates the fate and transport of excess nitrogen in the form of nitrate from an intensively management short-rotation woody crop plantation through the riparian zone of an intermittent low-gradient blackwater stream in Upper Fourmile Creek. Two years of measuring nitrogen in topographically positioned well network indicated rapid transformation and denitrification within the forested wetland valley. Shallow groundwater denitrification in this riparian area reduced more than 90% of excess nitrogen originating from nitrate fertilizer.

Index words: [hydrology, GIS, water quality, stream networks, groundwater modeling]

Topologic and topographic controls on flow networks and transport

by

Scott Raulerson

B.S., Georgia College State University, 2016
M.S., Georgia State University, 2018

A Dissertation Submitted to the Graduate Faculty of the
University of Georgia in Partial Fulfillment of the Requirements for the Degree.

Doctor of Philosophy

Athens, Georgia

2023

Topologic and topographic controls on flow networks and transport

by

Scott Raulerson

Major Professor:	C. Rhett Jackson
Committee:	Nandita Gaur
	Adam Milewski
	Todd Rasmussen

Electronic Version Approved:

Ron Walcott
Dean of the Graduate School
The University of Georgia
August 2023

Dedication

To my wife, Maia. I never would have been able to complete this without you. Your support is what got this dissertation to the finish line.

Acknowledgements

The primary source of financial support for my doctoral education and research was provided through the United States Department of Energy Bioenergy Technologies Office and the United States Forest Service – Savannah River Site Interagency Agreement DE-AI09-00SR22188 and by the United States Department of Agricultural National Institute of Food and Agriculture AFRI Predoctoral Fellowship (2022-67011-36463/1028181).

I thank my advisor, Rhett Jackson, for his support, guidance, and the freedom he gave me to conduct my research and work from start to finish. Your prompt editing of my writing and critical evaluation of my work when I ask that you not pull your punches is something I have very much appreciated throughout this process and I know I will benefit from in the years ahead. Thank you to the rest of my committee: Nandita Gaur, Todd Rasmussen, and Adam Milewski for their support and review of my work throughout my time at UGA.

To my parents, Pat and Don, you both have supported me from the very start, and for that I will always be grateful. You both left it to me to figure out what I wanted to do in life, and have never once questioned those decisions. Thank you to the rest of my family for their support throughout my doctoral program. I wasn't around as much as I know most of you would have liked, but know your support meant the world. I can say with confidence I shocked you all about my decision to continue school after finishing my undergraduate degree not just once, but twice.

Thanks to the many graduate students who have been in the UGA Hydrology Lab and affiliated groups during and before my time working there. There are too many of you to name, and somehow I find myself one of the last standing. I will specifically mention Seth Younger, Jake Bateman McDonald, and Stephen Cooper for all they have done in terms of helping me develop as a scientist and for the camaraderie you all provided outside of work hours. Nathan Melear, Wesley Gerrin, Caleb Sytsma, and Katie Lamp'l you all were always around to provide the optimism or pessimism I might need on a given day.

I thank Doug Aubrey, Kellie Vaché, Menberu Meles, Natalie Griffiths, and Ben Rau for all their guidance and the help they offered. You all acted as quasi-committee members at different junctures throughout the program. I'd also extend thanks to everyone who has been involved with or helped with field or lab work at the Upper Fourmile Creek Experimental Watersheds: Chris Lewis, Kevin Fouts, Tyler McIntosh, and Jordan Horvieth to name just a few.

Contents

List of Figures

List of Tables

Chapter 1

Introduction

1.1 Hydrologic connectivity

Understanding how a watershed is hydrologically connected plays an important in determining how water, solutes, mass, and energy move through a landscape (James and Roulet, 2007; McMillan, 2020). Hydrologic connectivity reflects an integration of many complex processes and influences, from antecedent moisture conditions, geology, climate conditions, surface or subsurface topography, ecological state, to land use, and surface vegetation (Gooseff et al., 2017; Spence and Phillips, 2015). From a hydrology perspective, it influences runoff generation, intermittent stream dynamics, ground and surface water interactions, stream water quality, biogeochemical fluxes, and the travel and residence time of water in a watershed (Hwang et al., 2012; H. J. van Meerveld et al., 2015). Hydrologic connectivity is an important component in the relationship between streamflow generation processes and watershed ecology (Hynes, 1970). The connection between groundwater and surface waters, along with the hyporheic zone serving as a border between the two, serves an important role in helping to maintain the ecological integrity of all the systems (Brunke and Gonser, 1997). The integrity can by threated through reductions in hydrologic connectivity, contamination of one of the systems, or through alteration of the processes that govern the movement of water, solutes, mass, and energy through all three systems (Brunke and Gonser, 1997; Schlosser, 1991).

1.2 Travel times

The distribution of water travel times serves as a fundamental control over the hydrology, solute transport, and biogeochemistry in catchments. It integrates the many hydrologic processes and flow pathways that influence solute fate and transport (McMillan, 2020). This is particularly important for studying the movement of soluble reactive pollutants such as nitrate and phosphate. Transit times are the time that a water particle spends in a system before being discharged at the stream outlet, or leaving the system through groundwater flow paths (McDonnell et al., 2010; McMillan, 2022; H. J. I. van Meerveld et al., 2019). The residence time of a catchment infers the total time spent within all the different transit flow paths (time to reach groundwater, time spent on groundwater flowpath, and time spent in the channel). Stream

discharge and total watershed storage can be linked in the context of the hydraulic turnover time, which is the time it takes to discharge all available water storage (McGuire and McDonnell, 2006; McMillan, 2022). Looking at the distribution of transit times across a watershed can provide insight into how the system stores water, and how these dynamic water flow paths influence preferential water storage and release. This allows transit times to be used as a foundational description of catchment function (Klaus, Chun, et al., 2015).

A key hydrological characteristic that controls the hydrologic connectivity of surface and groundwater and has an influence on groundwater travel times is porosity (M. P. Anderson et al., 2015; Davie, 2019; Fetter, 2001). Total porosity relates to the fraction of pore space within the total volume of a soil plus open spaces (A. Freeze and Cherry, 1979). Effective porosity is the reflection of a medias ability to allow water to flow (Bear, 2018; Davie, 2019). Effective porosity is calculated as the amount of pores that participate in the meaningful flow of water, and is related to the ratio of interconnected interstices to the total volume of soil or rock (Fetter, 2001; A. Freeze and Cherry, 1979; Schwartz and Zhang, 2003). Further, it reflects the volume of pores that will drain after a period of time under the influence of gravity (Davie, 2019). Porosity in either form serves as a key hydrological property in estimating groundwater storage and travel times, while also controlling important surface and groundwater interactions (Edwards et al., 2015; Flinchum et al., 2018). While easy parameter to conceptualize, measuring and quantifying porosity is not an easy process (Anovitz and Cole, 2015). Further, estimates of porosity are often limited in spatial scale due to the need to physically sample across a domain. Methods for estimating porosity span a range of direct, imaging, and geophysical approaches with varying degrees of difficulty (K. H. Adams et al., 2022; Anovitz and Cole, 2015; Buchanan and Triantafilis, 2009). Porosity and other hydrological properties can be measured through borehole pump tests (Ren et al., 2018), x-ray tomography (Anovitz and Cole, 2015), nuclear magnetic resonance (NMR)(Flinchum et al., 2018; Ren et al., 2019; Walsh et al., 2014), electrical resistivity (Binley et al., 2015; Parsekian et al., 2015), ground penetrating radar (GPR)(Harmon et al., 2020), scanning electron microscopes (SEM)(K. H. Adams et al., 2022; Anovitz and Cole, 2015), and seismic refraction (Anovitz and Cole, 2015; Flinchum et al., 2018; Holbrook et al., 2019; Rasmussen et al., 2003).

Beyond transit times, how a catchment stores and exchanges water plays a key role for sediment and solute transport, and the biogeochemistry of the system. Understanding how dynamics change during different periods of water storage is a key factor in understanding and managing for changing regimes. These dynamics can dictate when (and how) old water versus new water is released (Ameli et al., 2017), what concentrations of solutes are going downstream (Botter et al., 2011), and the amount of water available for biological use (Ehleringer and Dawson, 1992). In low-relief, forested watersheds typical of the southeastern United States Coastal Plain, discharge dynamics are further complicated by minimal separation between watershed zones (hillslope, transition, riparian). The relationship between stream discharge and total watershed storage has been used to assess the dynamics of watershed fluxes during different hydrologic regimes(Brauer et al., 2013; Brutsaert and Nieber, 1977; Kirchner, 2009). In low-relief, headwater streams, discharge is often intermittent, incurring a threshold-like behavior between total watershed storage and stream discharge (Haitjema and Mitchell-Bruker, 2005; Jackson et al., 2016). Because of this, traditional recession-based tools for investigating water storage dynamics are not as applicable. An understanding of

when, where, and how different pools of water are being accessed helps to work towards a comprehensive theory of catchment hydrology (Kirchner, 2009).

Approaches to assess the differences between field tracer-based estimates of travel times and the relationships between catchment storage and discharge have taken a turn toward a more stochastic, empirically based approach (Benettin et al., 2017; Botter et al., 2011; Harman, 2015; Kirchner, 2009; Troch et al., 2013). There have been a series of theoretical approaches offered to resolve some of the questions raised from the complex interaction between water storage and its subsequent release. Kirchner (2009) uses the "simple, dynamic systems approach" and stream flow recession concepts introduced by Brutsaert and Nieber (1977) to evaluate time variant catchment fluxes. Berghuijs and Kirchner (2017), Danesh-Yazdi et al. (2018), and Harman (2015) use intricate StorAge Selection (SAS) functions to describe transit times in nonuniform and time-varying terms; dependent upon antecedent storage conditions to decide what the age-selection of discharge is. More recent work has coupled SAS functions at a hillslope scale to predict elucidate hillslope structures such as water table position, travel times, and both saturated and unsaturated solute flow (Kim & Harman, 2022; Kim et al., 2022). SAS functions coupled with tradition field tracer-based estimates of travel times have been used to quantitatively evaluate the Inverse Storage Effect which states that when water storage is high in a catchment, streamflow preferentially mobilizes younger water, as well as to evaluate the Direct Storage Effect, which states that during the wet-up and accumulation of water storage in a catchment that discharge is preferentially older water (Rodriguez et al., 2018; Wilusz et al., 2020). The use of these theoretically based approaches to estimate travel times spatially, across a catchment have had limited applications. Kolbe et al. (2016) used CFC derived groundwater ages, coupled with a 3D numerical modelling to contrast travel times between lowland, transitional, and upland regions. Koh et al. (2018) evaluated two spatially discrete groundwater age models to understand the complexity of nitrate transport through complex hydrogeologic settings. There has been a call to develop better catchment classification system in terms of their structure and function, especially given their role in earth systems models (Fan et al., 2019; Wagener et al., 2007).

1.3 Nutrient transport

There is increasing potential for pollution in our surface and groundwaters due to present and past application of soluble agrochemicals in agricultural settings. Of particular concern here is the application of nitrogen-based fertilizer, in the form of nitrate, and the subsequent role it plays in surface and groundwater contamination. In many agricultural settings, nitrogen is often a limiting nutrient factor in terms of primary production (Gruber & Galloway, 2008). When crop growth is limited due to depleted stocks of reactive nitrogen, nitrogen-rich fertilizers can be applied in order to help with crop growth (Galloway et al., 2004; Pepper et al., 2015). Excess nitrogen-rich fertilizer can be transported into surface waterways by runoff, or leach into groundwater. While a limiting nutrient in most ecosystems, elevated nitrogen concentrations are typically hazardous for aquatic ecosystem, as it can lead to eutrophication of the waterways (Howarth, 2008; Vitousek et al., 2022), and lead to health issues for humans if drinking water is contaminated (Fields, 2004; Robertson & Vitousek, 2009). Further, the natural cycle of removing this

reactive form of nitrogen from the environment, is energy intensive and typically results in incomplete transformations due to the high mobility of nitrate in water (Strauss et al., 2002; Vitousek et al., 1997). Nitrate reduction is primarily completed by anaerobic microbes through the process of denitrification, which use nitrate in anoxic conditions for respiration (Boyer et al., 2006; Payne, 1976; Rivett et al., 2008; Seitzinger et al., 2006). These microbes convert nitrate into gaseous forms of nitrogen (NO, N_2, N_2O), which is then emitted back into the atmosphere (Boyer et al., 2006; Cai et al., 2022; B. Chang et al., 2022; Payne, 1976). While denitrification provides a way to mitigate nitrate concentrations, a byproduct of the process is that when the denitrification process does not come to the end of a full cycle and produce its terminal product (inert N_2 gas), it can release intermediary products, namely nitric oxide (NO) and nitrous oxide (N_2O) , which can be hazardous for the environment (Ravishankara et al., 2009; Welsh et al., 2021). Nitric oxide has contributed heavily to ozone depletion in the atmosphere, while nitrous oxide is a potent greenhouse gas with a warming effect more than 300 times that of carbon dioxide (CO_2) and with a residence time of over 100 years in the atmosphere (Ravishankara et al., 2009; Z. Wang et al., 2017).

It is acknowledged that in most cases, the major of denitrification occurs within the soil of terrestrial environments, but rates of denitrification have been found to be higher in groundwater systems than surface water systems (Seitzinger et al., 2006). Literature reviewing denitrification in the terrestrial environment is extensive (B. Chang et al., 2022; Hill, 2019; Krichels et al., 2022; Sigler et al., 2022), but there are few studies (Groffman et al., 2006; Jahangir et al., 2013; Jahangir et al., 2013; McAleer et al., 2017; Popp et al., 2020; W. Zhang et al., 2022) quantifying groundwater denitrification, especially at a watershed scale. This gap in literature is primarily attributed to the difficulty that comes with measuring denitrification in situ, as the process for dividing observed N_2 concentrations from ambient/background/atmospheric N_2 values is complex (Groh et al., 2019; Lenhart et al., 2021). Groundwater denitrification is known to depend heavily on water chemistry (dissolved oxygen and dissolved organic carbon especially), as these fuel the anaerobic microbial respiration process, but ideal conditions are often site specific due to the complex process that is denitrification and the nitrogen cycle as a whole (Merill & Tonjes, 2014; Rivett et al., 2008). Shallow, subsurface flow pathways through riparian and hyporheic zones provide bacteria potentially ideal conditions for the denitrification process to occur with low dissolved oxygen levels and high dissolved organic carbon in the form of organic matter. There is importance in investigating groundwater denitrification, some studies have found that groundwater denitrification mitigated up to 30% of applied nitrogen (Jahangir et al., 2013), while others report a wide range, from 4% to over 70% (T. R. Anderson, Goodale, et al., 2014; T. R. Anderson, Groffman, et al., 2014). Further studies that quantify denitrification rates in situ will help to understand these site-specific conditions that drive denitrification and nitrate removal, and for us to better understand the importance of denitrification in reducing nitrate loading to our contaminated water bodies.

Watershed nitrogen budgets typically have unaccounted nitrogen, in that the amount of nitrogen added to the system is not reflected in what is measured coming out (Fox et al., 2014; Hester & Fox, 2020). This is especially true in agricultural watersheds that have been heavily fertilized. Denitrification has long be considered a reason for this, but in situ rates have never been quantified at a watershed scale to assess whether it helps to close the nitrogen budget and account for the "missing N" (David & Gentry,

2000). To this aim, our recent multi-year study of the environmental effects of short-rotation woody crop has observed its own gap in the nitrogen budget (Griffiths et al., 2017; Griffiths et al., 2016), and raised questions as to the importance of denitrification and the magnitude with which excess nitrate was leaving the study watersheds.

1.4 Objectives

This dissertation has three distinct objectives which span research objectives in hydrology, hydrogeology, ecology, biogeochemistry, and geography:

1. Provide examples of the benefits of representing watersheds and watershed characteristics like hydrologic connectivity from a longitudinal perspective.
2. Develop and introduce the use of a simple, GIS-based, quasi-two-dimensional water table model based on the 1-D Dupuit equation.
3. Quantify denitrification and determine the fate of elevated groundwater nitrate concentrations caused by leaching of excess fertilizer application.

In Chapter 1, we will investigate how watershed structures and characteristics like hydrologic connectivity are conceptualized and portrayed. We use three case studies that portray watersheds longitudinally and highlight differences in watershed processes that can only be seen when conceptualizing watersheds in this longitudinal space, emphasizing the importance of topography and topographic position in watershed depiction. Chapter 2 introduces a simple, topographically-based, quasi-two-dimensional model that is used to predict water table position and groundwater travel times. We apply the model at Upper Fourmile Creek Experimental Watersheds as proof of concept and use it further to answer questions related to groundwater travel times at the site. Chapter 3 is a two-year study of riparian denitrification potential in Upper Fourmile Creek, which answers further questions at the site related to groundwater nitrate contamination and travel times in Upper Fourmile Creek.

Chapter 2

Watersheds and stream networks viewed longitudinally: Example insights from novel spatial portrayals of watershed characteristics

[1] Raulerson, S.; C. Sytsma, J.R. Webster, and C.R. Jackson. 2023. *River Research and Applications*. 39:819–831.

Reprinted here with permission of the publisher.

Abstract

Longitudinal depictions of watershed structure and characteristics, including topography, stream networks, wetlands, ground water levels, and land use, can provide watershed knowledge and understanding unavailable from standard plan view maps. Three case studies provide examples of knowledge gained by applying longitudinal views of stream networks, watershed hydrologic behavior, and land use distributions. Longitudinal views of mountain stream networks show extreme variability in the slope-area relationships of low Strahler order streams, large discontinuities in drainage area (large parts of drainage area space are absent in networks), and large variations in network curvature. Longitudinal views of a groundwater-dominated headwater watershed increase the inference available from limited groundwater observations and clearly reveal how groundwater connections affect the permanence of surface water features and the distribution of vadose zone storage in the landscape. Plotting land uses longitudinally illuminates and allows a quantitative analysis of how land uses are distributed relative to topographic position. Viewing watersheds and stream networks longitudinally can provide new insights into watershed forms and processes and motivate new questions and research.

2.1 Introduction

Two-dimensional views of watersheds are inherently limited and cannot capture all important aspects of watershed structure. Watersheds are complex three-dimensional structures whose subsurface boundaries may not match surface boundaries in the horizontal directions (Botter et al., 2011; Haitjema & Mitchell-Bruker, 2005; Richey et al., 2015), whose lower flow boundaries and internal hydraulic characteristics are difficult to discern and characterize (Beven, 2006; Hrachowitz & Clark, 2017; Koh et al., 2018; Sayama et al., 2011; Staudinger et al., 2019), and whose surficial boundaries themselves depend on DEM scale and accuracy (e.g. Baker et al., 2006; Lindsay, Francioni, et al., 2019). However, as scientific knowledge is generally communicated through graphs, schematics, and photos published in journals and books, visual representations of watershed characteristics are generally constrained to two dimensions, often using contour lines, colors, or line thickness to provide information on characteristics varying in other dimensions. The large majority of two-dimensional watershed representations use a planform map view, plotting watershed characteristics across the horizontal dimensions. Some alternative graphical means for characterizing watersheds include Torgegrams (Zimmerman & Ver Hoef, 2017), linked micromaps (Silvanima et al., 2018), and hyperscale graphs (Zettler-Mann & Fonstad, 2020). These are useful for displaying statistical results in a meaningful way for geospatial correlations but are not as suitable for depicting data. Representing the multi-dimensionality of watersheds in 2-D graphics is difficult, and alternative graphical means of representing watershed structure should continue to be explored.

Here we propose and provide examples of novel and partly novel longitudinal examinations of watersheds and watershed characteristics. While we often think about watersheds longitudinally, we rarely explicitly plot watershed characteristics that way. We examine three case studies for which viewing a stream network or watershed topography longitudinally illuminates watershed characteristics or behaviors not

revealed through plan views, yielding new insights, and improving watershed understanding. In the first case study we plot and examine the entire stream network of a watershed in longitudinal spaces, and in doing so test aspects of the classic conceptual geomorphic river continuum concept (RCC) of Schumm and Church (Church, 1992; Schumm, 1977). In the second case study, we plot the elevation and flow distance relative to the outlet of every pixel of a watershed along its topographic drain lines (a.k.a. surficial drain lines), stream threads, and wetland water surfaces, along with observed ranges of groundwater elevations. This view amplifies the power of typically limited groundwater observations, illuminating relationships between groundwater levels and the relative permanence of streams and wetlands. The third longitudinal view of watershed characteristics portrays land use variation in terms of each pixel's relative elevation and flow distance to the outlet. This information allows analysts to describe watersheds in terms of the relative position of development and quantitatively relate associated hydrologic and water quality effects of development to watershed position.

All three of these sideview case studies use GIS analysis of standard DEM and hydrography data to reveal new insights into watershed characteristics and behaviors. The methods are simple and accessible to scientists and practitioners of many disciplines. Each case study is presented in its entirety: methods, results, and implications, followed by a summary of findings.

2.2 Example 1: Plotting whole stream networks in longitudinal space

2.2.1 Issues

Longitudinal conceptualizations of how streams change between headwaters and river mouths partially explain large-scale variation in water quality, geomorphology, and aquatic assemblages (Altermatt, 2013; Doretto et al., 2020; Vannote et al., 1980). The River Continuum Concept (RCC, Figure 2.1) is one such approach that explains a substantial amount of longitudinal variability in river characteristics, including slope, average discharge, sediment particle size distributions, and valley alluvial storage (Church, 1992; Schumm, 1977), but large deviations from these trends abound (e.g. Carbonneau et al., 2012; Fonstad and Andrew Marcus, 2010). This theory is commonly portrayed as a conceptual model in which these river properties vary continuously as a function of drainage area (Figure 2.1, Church, 1992, based on concepts of Schumm, 1977). The stream continuum is a useful concept widely used in textbooks, teaching materials, and government reports, but, as we will show, its inherent simplifications ignore the fact that drainage area does not increase continuously along a stream network and that there is extreme variability in elevation, vegetation, slope, and other characteristics of low-order streams in a channel network. At every channel juncture, there is a jump in the drainage area. Consequently, there is no continuum of channel elevations or channel slopes as drainage area increases, as we will illustrate.

Understanding the variability of stream structure throughout stream networks is fundamental to fluvial geomorphology and stream ecology. While physical and biological river continuum theory helps explain many aspects of longitudinal variability in biological and physical characteristics of streams (Doretto

et al., 2020; Vannote et al., 1980), researchers have shown that several landscape factors, such as abrupt changes in geology and topography (stream or valley slope), and geographic shifts in climate and vegetation, affect longitudinal variability in stream power, channel form, and habitat suitability for given taxa (Montgomery, 1999; Pringle et al., 1988; Thorp et al., 2006; Townsend, 1989). Channel confluences have been identified as locations of channel and habitat complexity and particularly high dynamism (Benda et al., 2004; Benda et al., 2003; Church, 1983; Rice et al., 2001). When streams of different sizes come together, there are often temporal mismatches of flood peaks and sediment transport. Discontinuities in channel controls have implications for sediment routing and management (Curran & Hession, 2013; Poeppl et al., 2020; Wohl et al., 2015). Integration of longitudinal approaches with patch-based approaches has been shown to increase model accuracy (Collins et al., 2018; Larsen et al., 2019).

Here we use longitudinal views of complete stream networks in two nearby mountain stream basins differing in basin area and topology to illustrate the variety of forms and connections of low-order streams and to show that river continuum theory hides important channel network complexities, for example the stark discontinuities in relationships between channel elevations and slope as explained by drainage area. Similar longitudinal views of portions of stream networks have been used in knickpoint analyses and to illuminate geologic controls on network profiles (Gallen, 2018; Gallen et al., 2013; Gallen et al., 2011; Schwanghart & Scherler, 2020), but such views have focused on select threads and have not portrayed entire stream networks. As far as we can tell, longitudinal mapping of entire stream networks is novel. Longitudinal projections of entire stream networks may improve understanding of variation in water quality (e.g. Johnson et al., 2019; McGuire et al., 2014) and channel geometry (Carbonneau et al., 2012; Zettler-Mann & Fonstad, 2020) and assist with the experimental and monitoring design (Larsen et al., 2019).

2.2.2 Methods

Using 10 x 10 m DEMs and stream networks generated as a part of the development of the NHDPlus High Resolution (HR) database, we created side views of a stream networks in both elevation-drainage area space, and elevation-distance to outlet space for Cartoogechaye Creek and a portion of the larger Yadkin River, both in the southern Appalachian Mountains of western North Carolina (USGS, 2018)(Figures 2.2 & 2.3). These two mountainous Blue Ridge basins are similar in climate, elevation, vegetation, and topography, differing only in drainage area and network topology, with a dendritic network draining Cartoogechaye and a trellis network draining the Yakdin. The Cartoogechaye Creek basin consists of two HUC12 watersheds (Upper Lower Cartoogechaye Creek) draining a combined 148 km^2 of humid temperate forests and rural residential and agricultural valleys bounded by the eastern Continental Divide and flowing into the Upper Little Tennessee River (confluence 35.15613°, -83.38063°). Elevations range from 580 to 1650 m. Average annual precipitation ranges from 1200 to 2200 mm/yr across the basin, increasing with elevation (PRISM). In short, this is a steep, wet, mostly forested mountain watershed. We also look at the upper portion of the larger Yadkin River basin, upstream of W Kerr Scott Reservoir (36.111963°, -81.313304°). This section of the Yadkin River basin consists of seven HUC12 watersheds which drain into W Kerr Scott Reservoir. This portion of the Yadkin River basin lies predominantly in the

Blue Ridge physiographic region and drains a combined 632 km^2 of mostly humid temperate forests. Elevations range from 313 to 1255m. The Yadkin River joins the Uwharrie River to become the Pee Dee River 222 km downstream from our watershed outlet. Average annual precipitation ranges from 830 to 2100 mm/yr based on PRISM estimates. Neither of these basins includes a reservoir or other direct human modifications to network topography or topology.

Stream networks were created from the NHDPlus HR hydrologically conditioned 10 x 10 m DEM using the 20th percentile of the first order NHDFlowlines as the accumulation threshold. These thresholds were 23 and 22 ha for Cartoogechaye Creek and the Yadkin River respectively. Previous field surveys of first-order southern Appalachian streams found the average contributing area to perennial channel initiation points was 7.5 ha (Rivenbark & Jackson, 2004). We then derived matching flow accumulation and direction rasters, along with vector stream networks which match the original NHDPlus HR streams. We determined the traditional Strahler and Shreve orders using the NHDPlus HR hydrologically conditioned DEM along with the NHDFlowline vector network of streams. This process was followed to ensure a continuous process between stream network delineation and network attribute calculation and to preserve network hierarchy when calculating network position attributes like stream order (Alber & Piégay, 2011). Upstream drainage area, stream order (Strahler and Shreve), slope, and distance from watershed outlet were all calculated from these layers. NHDPlus HR data was downloaded using nhdplusTools package of R (Blodgett & Johnson, 2022; USGS, 2018). Finally, we plotted the pixels of each stream thread by their relative elevation (elevation minus elevation of the basin outlet) and either their drainage area or their distance from the mouth.

2.2.3 Findings and Implications

Elevations and slopes of first- and second- Strahler order streams in these mountain basins vary hugely and show no clustering around a common slope-area relationship (Figures 2.4 - 2.6). The lowest slopes of first-order segments are as small as the lowest slopes of fifth-order segments (Figures 2.7 & 2.8). While average stream slopes decrease with drainage area and increasing stream order as conceptualized by river continuum theory, the variability of slope-area relationships is as important to understanding river networks and associated aquatic ecology as the central tendencies (Figures 2.4 - 2.6; Carbonneau et al., 2012; Fonstad and Andrew Marcus, 2010; Zettler-Mann and Fonstad, 2020; Zimmerman and Ver Hoef, 2017). Even in a mountain environment, low Strahler order streams are not necessarily steep or high (Figures 2.7 & 2.8). The variance of channel elevations and slopes as a function of drainage area collapses as stream order increases (Figures 2.4 - 2.10), similar to variance collapse seen in water quality data across stream networks (Johnson et al., 2019; McGuire et al., 2014). At the scale of the basin analyzed here, the slope-area relationships of the fifth- and sixth- order segments are relatively homogenous.

Alternatively, Shreve stream orders are more tightly correlated with upstream area (Figures 2.9 & 2.10), but they still show very high drainage area variability at small drainage areas. In both the basins analyzed here, this variability reduces substantially at 1000 ha, but the Yadkin drainage still shows substantial variability out to 10,000 ha (Figures 2.9 & 2.10). These drainage area thresholds for variance reduction may be a valuable quantitative watershed characteristic. Again, large portions of the drainage area vs

Shreve order space are empty as the drainage area jumps at each tributary confluence (Figures 2.9 & 2.10). The common RCC conceptualization of a single line portraying channel characteristics as a function of drainage area (Figure 2.1) is misleading, suggesting far more similarity among low order streams than actually exists. The large variances in slopes, elevations, and slope-area relationships in low-order streams are crucial to understanding the ecological and geomorphic variability of low-order streams in channel networks, and this variance is ignored and hidden when plotting average stream slopes or elevations against drainage area.

Plotting channel elevations against flow distance to the watershed outlet suggests questions and hypotheses about network curvature and headwater stream lengths (Figures 2.7 & 2.8). Taking these two basins as case studies, we see far more variability in network curvature in the Yadkin basin than in the Cartoogechaye basin. All the stream profiles in the Cartoogechaye basin are concave, whereas several third- and fourth-order streams in the Yadkin basin have convex profiles, indicating the presence of a particular resistant rock layer running across the northern tributaries of the Yadkin. If we were to calculate stream power down these networks, these convex channel sections would show deviations from the otherwise expected relationships between stream power and drainage area because channel slopes are dropping less steeply at the tops of these profiles and more steeply at the bottom. We also see differences between these watersheds in the density of first-order streams feeding directly into high order streams. These profiles, along with the Shreve-order relationships with drainage area, reveal important differences in the channel networks in these two mountainous Blue Ridge basins that are otherwise similar in climate, vegetation, and mapped surficial geology. Questions that might be motivated by these views include: How does network curvature vary with contributing area, climate, and geology (Horton, 1932; Y. Zhang et al., 2020)? How does network position affect lengths of first and second order streams? How do the biological characteristics of low order streams vary with elevation and slope? Without examining stream networks in this space, the potential importance and utility of such questions would not be apparent.

When channel networks are plotted in their entirety in terms of relative watershed elevation and distance to the outlet, problems with the RCC become apparent, and key aspects of network characteristics become clearer (Figures 2.7 & 2.8). Longitudinal cross-sectional views reveal that channel network attributes differ from the RCC in important ways. Drainage area does not increase linearly along a longitudinal gradient due to the influence of tributary confluences (Figures 2.4 - 2.6; Benda et al., 2004; Benda et al., 2003). Large step increases in drainage area occur at each junction. There are many ranges of drainage area space for which there are no channels (Figures 2.4 - 2.6; Figures 2.9 & 2.10). Surface drainage networks are generally continuous (exceptions may occur in areas of high groundwater flow, particularly in karst environments) but the non-continuous character of drainage area creates discontinuities and disturbances to the trends in stream network characteristics and serves as an example of the types of sudden changes in channel controls hypothesized by the Process Domain Concept (Montgomery, 1999). The discontinuity of drainage area as an explanatory variable has many implications. The large jumps in drainage area, flow, and sediment loads and the frequent mismatch of flood peak arrival times (Figures 2.4 - 2.6; e.g. Meade et al., 1991; Roy and Roy, 1988) at confluences create complex dynamics and behaviors at confluences (e.g. Benda et al., 2004; Boddy et al., 2019), not suggested by the RCC. Thinking about

drainage area as a continuous variable makes sense mathematically and is useful for many hydrological estimates, but the drainage area of stream networks is highly discontinuous.

2.3 Example 2: Plotting surficial drainage threads, groundwater, and water features in longitudinal space

2.3.1 Issues

Knowing the water table position relative to the ground surface is useful for understanding and predicting streamflow and wetland permanence as well as the dominant hydrologic processes across a watershed. We can identify where the water table intersects or approaches the ground surface by the position of streams and wetlands, the presence of hydrophytic vegetation or hydric soils, by areas of high soil moisture, and by "muddy boot" hydrology (Dunne et al., 1975; Hursh, 1936). Most watersheds have no or few wells from which to estimate water table profiles, and this makes it much more difficult to estimate the separation of the land surface and the water table outside of the valleys.

It is a tenet of groundwater hydrology that the water table of a surficial aquifer "forms a subdued replica of the topography" of the hills and intersects with perennial stream elevations in the valleys (A. Freeze & Cherry, 1979). The boundary conditions formed by streams, lakes, valleys, and ridge lines necessarily impose topographic constraints on groundwater behavior resulting in strong topographic influences on water table position (Tóth, 1963). Longitudinal views of surface drainage threads along with stream threads and water table data can elucidate the relationships between groundwater elevations and surface water features.

We define topographic drain lines as the routes water would flow on the land surface if water flowed strictly based on elevation gradients determined from DEMs. This is analogous to a flow direction (D8, MFD, etc.) raster that is commonly used in GIS-based stream delineation, with the distinction that it is a vectorized representation of that surface. We use the term topographic drain line, but there are many analogs for this in literature and colloquially: topographic drain lines, surficial drain lines, surface flow pathways, natural drainage lines (Warburton et al., 2004), natural drainage systems (Altermatt, 2013), natural drainage networks (Petroff et al., 2013), surficial drainage network, flow line network (Zimmermann et al., 2014), and drainage path (Hansen, 2001).

Here we plot the network of surface water bodies (streams and wetlands), all topographic drain lines (for the whole watershed), and the range of observed water table variation in relative elevation/surficial flow length to the outlet space. This simple-to-construct side view provides insight into stream and wetland permanence, water table variability, the distribution of vadose zone storage, and where variable source area runoff or groundwater discharge are likely. We know of no such published representation of watershed hydrologic connections.

2.3.2 Methods

Our study site is a 1.17 km^2 headwater catchment (referred to as Watershed C in previously published papers cited below) within Upper Fourmile Creek watershed, a tributary to Fourmile Creek and the Savannah River. Watershed C is contained within the Savannah River Site, a National Environmental Research Park within the Upper Atlantic Coastal Plain of South Carolina (Figure 2.11). This is a permeable, low-relief, groundwater-dominated watershed (E. Du et al., 2016; Klaus, McDonnell, et al., 2015). The soils consist of loamy sand topsoils over sandy clay loam argillic horizons underlain by unconsolidated sands and clays. Below the stream elevation occurs a dense clay hydrostratigraphic layer, known locally as the Tan Clay, which acts as the base of the surficial aquifer. This site has been previously instrumented with wells, interflow interception trenches, soil moisture sensors, and flumes (E. Du et al., 2016; Ferreira et al., 2021; Griffiths et al., 2017; Griffiths et al., 2016; Griffiths et al., 2018; Jackson et al., 2014; Jackson et al., 2016; Klaus, McDonnell, et al., 2015; Vache et al., 2021). Here we plot the distribution of monthly water levels measured in the wells located in the focal watershed. These monthly water level measurements occurred between December 2011 through July of 2020. Average annual precipitation is 1269 mm and average annual evapotranspiration is 861 mm.

We used a LiDAR-generated 10 x 10 m DEM to delineate topographic drainage lines of Watershed C. All hydrologic conditioning, flow accumulation and direction, topographic drain line extraction, network distances, and network geometry were completed in MATLAB using the TopoToolbox add-in (Schwanghart and Scherler, 2014) (Figure 2.11). Topographic drainage lines were routed down to the valley edges, where the landscape becomes flat and lumpy, and water table position is near the surface. The valley is defined in this flat, low-relief landscape as the regions with hydric soils, mostly-permanent wetlands, and within 10 m of the ephemeral stream. Perennial, intermittent, and ephemeral streams were defined from USGS 7.5-minute DLG and from USFS reports (Hiergesell, 1998; Hiergesell and Jones, 2004).

2.3.3 Findings and Implications

Plotting water table positions relative to topography, stream lines, and wetlands in relative elevation and distance-to-outlet space increases the inferential power of limited groundwater observations. Water table variation is low in the valleys just above the start of perennial streamflow and becomes much larger higher in the watershed (Figure 2.12). The valleys essentially act as grade control for the water table and limit groundwater variation near the valleys. Data from six well locations show high water table variability near the intermittent stream segments and reveals that the permanent wetland C and the nearly-permanent wetland A (referred to regionally as Carolina bays) are often perched above the water table near ephemeral stream locations. We can thus infer that deposition of fine sediments and organic matter in these wetlands (e.g. C. Craft et al., 2018; C. B. Craft and Casey, 2000) helps them hold water for long periods when the water table is well below the bottom of the wetland. The ephemeral stream channels are located well above the mean plus standard deviation of nearby groundwater levels. Two of the well locations in this catchment feature a shallow and a deep well, and we can see that there are strong downward vertical gradients high in the watershed. In this longitudinal space, even a limited set of wells allows us to visualize

the general water table configuration relative to the land surface, and thus allows us to quantify vadose zone storage throughout the watershed and to identify locations where the water table is near the ground surface and thus are likely to act as variable source areas.

2.4 Example 3: Plotting land use distributions in longitudinal space

2.4.1 Issues

Landscape position is a fundamental driver of ecological processes. Alexander von Humboldt created the field of biogeography by observing that landscape position, including elevation, slope, and proximity to streams, strongly controls microclimate, resource availability, and the spatial distribution of plants and animals (Humboldt et al., 2008). Landscape position also controls the suitability of land for agriculture and building and thus affects human settlement patterns (Boerner, 2006; LaGro, 2005; Živković, 2019), particularly at lower rural densities. The interactions of human land uses and biogeographic controls affect ecosystem responses to climate change (Elsen and Tingley, 2015).

In mountainous rural landscapes, people tend to farm and build houses on the valley floors where the land is more suitable for farming. Living in the valley also avoids the need to drive roads in the steeper and high elevation parts of the watershed where road maintenance costs are higher, and hazards increase. Accordingly, impervious surface cover is more concentrated close to streams across most of the US (Wickham et al., 2014).

The location and pattern of development in a watershed is known to affect its impacts on peak flow magnitude. Many studies have found that development location can significantly alter the magnitude of peak streamflows (S. Du et al., 2015; Yang et al., 2011; Yeo and Guldmann, 2006). Basin size, impervious surface connectivity, and flow timing have been found to have significant impacts on peak flow as well, which may explain the differing conclusions of which basin position is best for development (Dan-Jumbo and Metzger, 2019; S. Du et al., 2015; Mejía and Moglen, 2010).

Here we look at the distribution of land uses across mountainous rural watersheds as a function of distance from the watershed outlet and relative elevation from the outlet. This view provides insight into the interactions between human land use and the biogeographic controls that affect how ecosystems respond to that land use. A simpler, less complete, version of this graphical methodology was used by Webster et al., 2012, but we have not seen it elsewhere.

2.4.2 Methods

We look at two rural mountainous watersheds, the South Fork Skeenah Creek (35.110539°, -83.413636°) and Watauga Creek (35.1124704°, -83.4068468°) outside of Franklin, North Carolina. Both watersheds flow into the Upper Little Tennessee River. South Fork Skeenah watershed drains 6.49 km^2 and ranges in elevation from 629 to 1114 m. Watauga Creek watershed drains 17.06 km^2 and ranges in elevation from

615 to 1232 m. Annual precipitation in both watersheds ranges from 840 to 2120 mm based on PRISM estimates.

For each watershed, we plot land use in the planform, and as a longitudinal profile in the relative elevation/flow distance to outlet space. Land uses for North Carolina were obtained through the 2019 National Land Cover Database (NLCD) at a 30 x 30 m resolution (Dewitz and USGS, 2021). A 10 x 10 m DEM was obtained from the NHDPlus HR database (Blodgett and Johnson, 2022; USGS, 2018). We plot the 30 x 30 m NLCD rasters in the planform figure, along with land use and watershed/geographic centroids with basic watershed features (elevation contours and NHDPlus HR streams (Figures 2.13 - 2.14). We plotted each 10 x 10 m DEM pixel as a point in relative elevation/flow distance to the outlet space, and we color-coded the dots by land use. For the purposes of plotting land use with elevation (Figures 2.15 - 2.16), each 30 x 30 m NLCD land use pixel was split into nine, 10 x 10 m pixels, each with the same land use but different elevation values. Flow distance to the watershed outlet was calculated using the TopoToolbox add-in of MATLAB (Schwanghart and Scherler, 2014).

We calculate two types of centroid points in each watershed, a geographic and watershed centroid. The geographic centroid is a commonly estimated physical characteristic in watershed hydrology. It is defined as a point within the watershed that represents the weighted center for the watershed in geographic space (X, Y coordinates). It is simply the mean X and Y coordinates of the watershed, adjusting for the area that falls outside the watershed when represented as a grid (Razavi and Coulibaly, 2017). The watershed centroid is defined within the longitudinal space rather than planform. The watershed centroid is calculated similarly to the geographic centroid but uses relative elevation and flow distance to the outlet instead of X, Y coordinates. For clarity, we have excluded from the maps land uses that contribute < 2% to the overall area.

2.4.3 Findings and Implications

By plotting land uses of all pixels in relative elevation/flow distance to the outlet space, differences in land use distributions that are suggested in plan view become distinct and also quantifiable (Figures 2.13 - 2.16). Such a plot clearly reveals that agriculture and development in the South Fork Skeenah watershed are concentrated in the valleys, with little to no development above the watershed centroid (Figure 2.13; Figure 2.15). The only developed areas above the watershed centroid in the South Fork Skeenah consist of roads crossing the watershed divides. Conversely, development and forest conversion occur high in the Watauga Creek watershed, with substantial amounts of development above the watershed centroid and extending to the watershed divide in some places (Figure 2.14; Figure 2.16). Agriculture is concentrated within the valley of Watauga Creek, with few locations in higher relief regions.

In this space, we can calculate the centroid (and variability) of each land use and compare it to the centroid of the watershed itself (Figures 2.13 - 2.16). In this way, we can put watersheds on a continuous gradient of watershed position and use this gradient to design hydrological, ecological, and water quality studies and to compare responses across watersheds as a function of development position. Otherwise, evaluating watersheds with respect to land use locations must be done categorically (e.g. Jackson et al., 2017; Schoonover et al., 2006) which can be difficult when land use distributions vary continuously. The

high natural variability in local precipitation, geomorphology, and other natural controls make it difficult to discern if land use, or another process is driving hydrological, ecological or water quality change.

2.5 Summary

Simply turning a watershed on its side and viewing it longitudinally can provide new insights into the spatial distribution of watershed characteristics and allow expanded inference about the hydrology, geomorphology, ecology, and water quality of watersheds. Here we provide examples of non-traditional longitudinal watershed views that we have not seen in the literature. These longitudinal views are not traditional cross-sections, which examine watershed characteristics in horizontal and vertical coordinates along a specific transect. Instead, these longitudinal views encompass the entirety of a watershed like a planform map does, but with vertical dimensions and longitudinal dimensions. These views are easy to create with GIS and DEMs, and they can inform our understanding of watersheds.

These longitudinal views have descriptive powers that planform maps do not. The first example reveals extreme variance of low order stream slopes and elevations in stream networks and that much of drainage area space is unpopulated in stream networks. The second example shows that plotting surficial topographic drainage threads with stream drainage threads and groundwater data as functions of elevation and flow distance to the outlet can help us understand groundwater connections to streams and wetlands, the duration of flows in streams, and the distribution of vadose zone storage in a watershed. In this case, a longitudinal view of watershed topography and surface water features increases the information power of a low number of groundwater wells. In the third example, we show that sideviews can be used to quantify the relative watershed position of different land uses and to design and interpret ecological and water quality studies that examine development position as a control of watershed hydrology and water quality.

Longitudinal analyses of stream networks, watersheds, and groundwater-surface water connectivity are currently uncommon. We suggest they should be part of our standard tool set for describing and characterizing watersheds. We should be mixing traditional and longitudinal representations into our watershed characterization efforts, and the examples shown here demonstrate how this could be helpful to watershed scientists and managers.

Figures

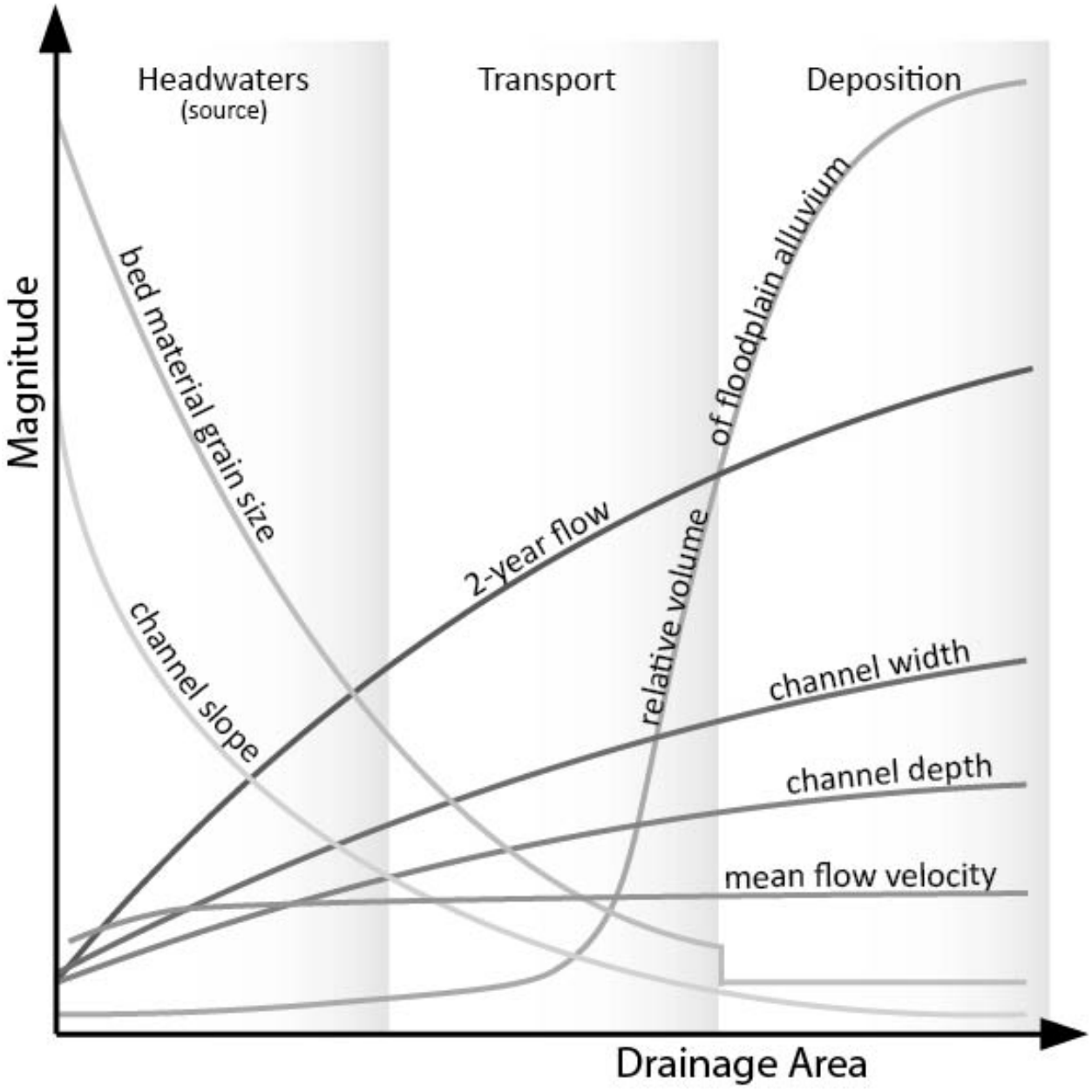

Figure 2.1: The physical stream continuum (based on Church 1992 from concepts of Schumm 1977) hypothesizing a predictable continuum of channel and valley characteristics as a function of drainage area.

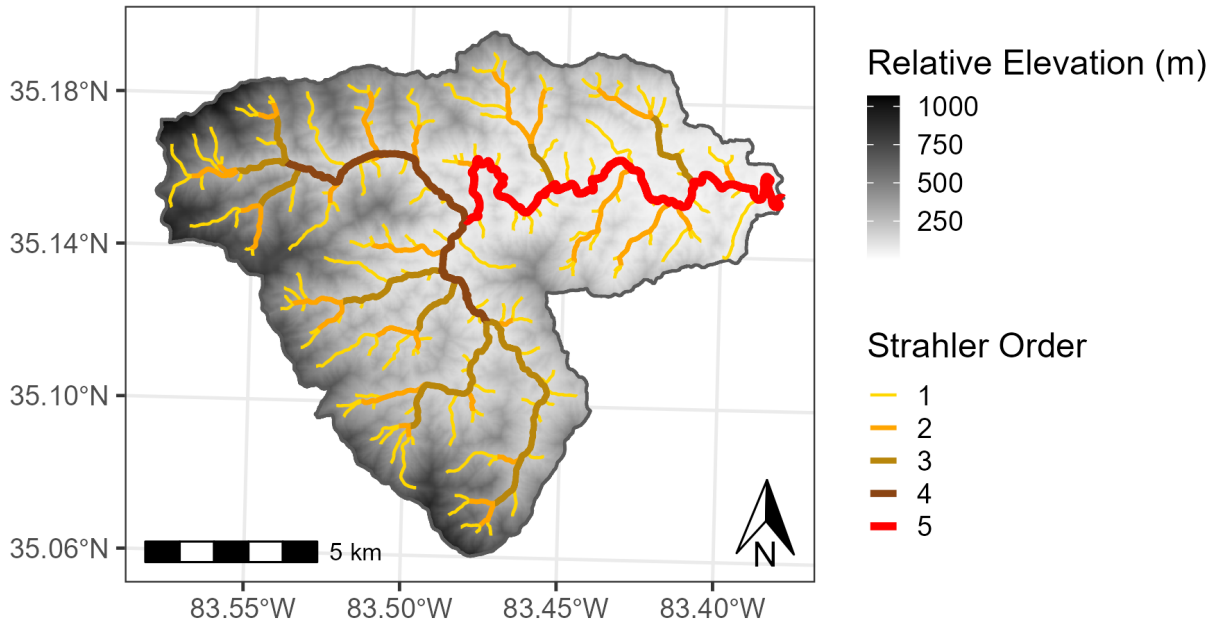

Figure 2.2: Planview stream network color coded by Strahler stream order in the Cartoogechaye Creek basin. Even with elevation information and color-coding of stream orders, a planform network map cannot convey the network lessons revealed by plotting channel thread elevations against drainage area

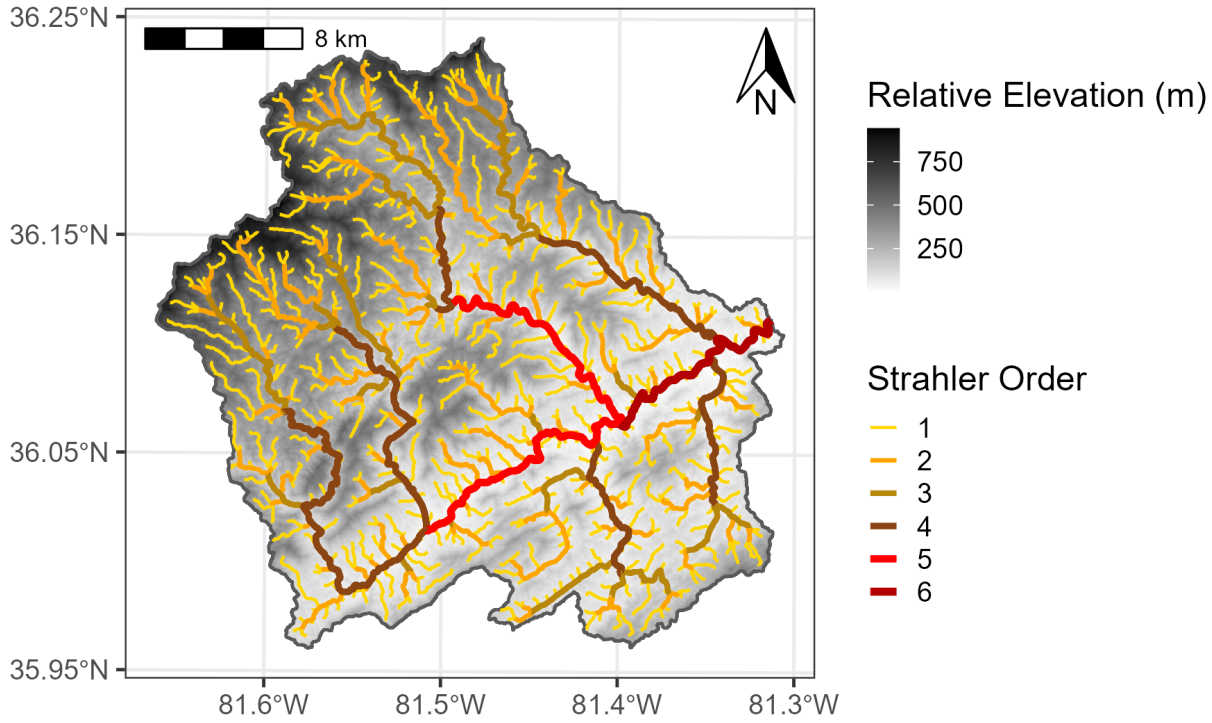

Figure 2.3: Planview stream network color coded by Strahler stream order in Yadkin River basin. Even with elevation information and color-coding of stream orders, a planform network map cannot convey the network lessons revealed by plotting channel thread elevations against drainage area

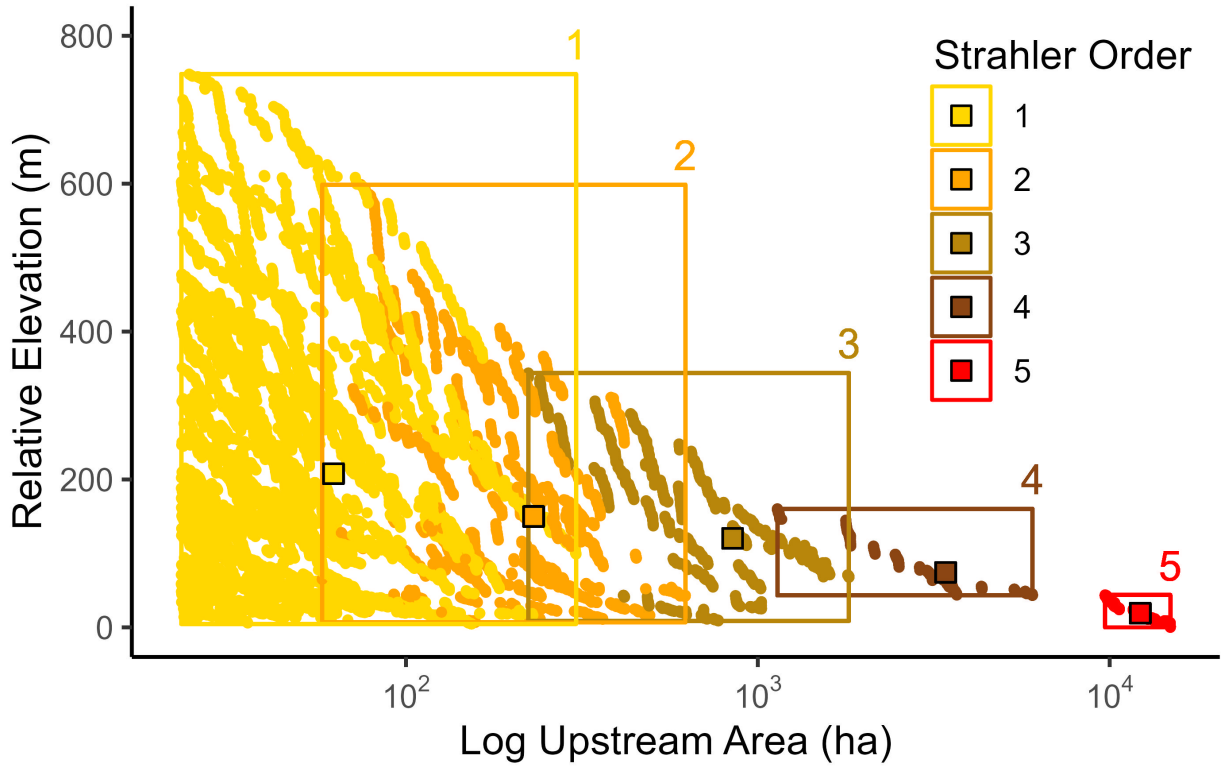

Figure 2.4: Channel thread elevations in the Cartoogechaye Creek basin as a function of drainage area coded by Strahler stream order. Log drainage area scale. Bounding boxes indicate the maximum, and minimum elevation drainage area for each stream order. Squares within each bounding box indicate the mean drainage area and elevation of that stream order. Large regions of drainage area space are empty as drainage area jumps at each tributary confluence

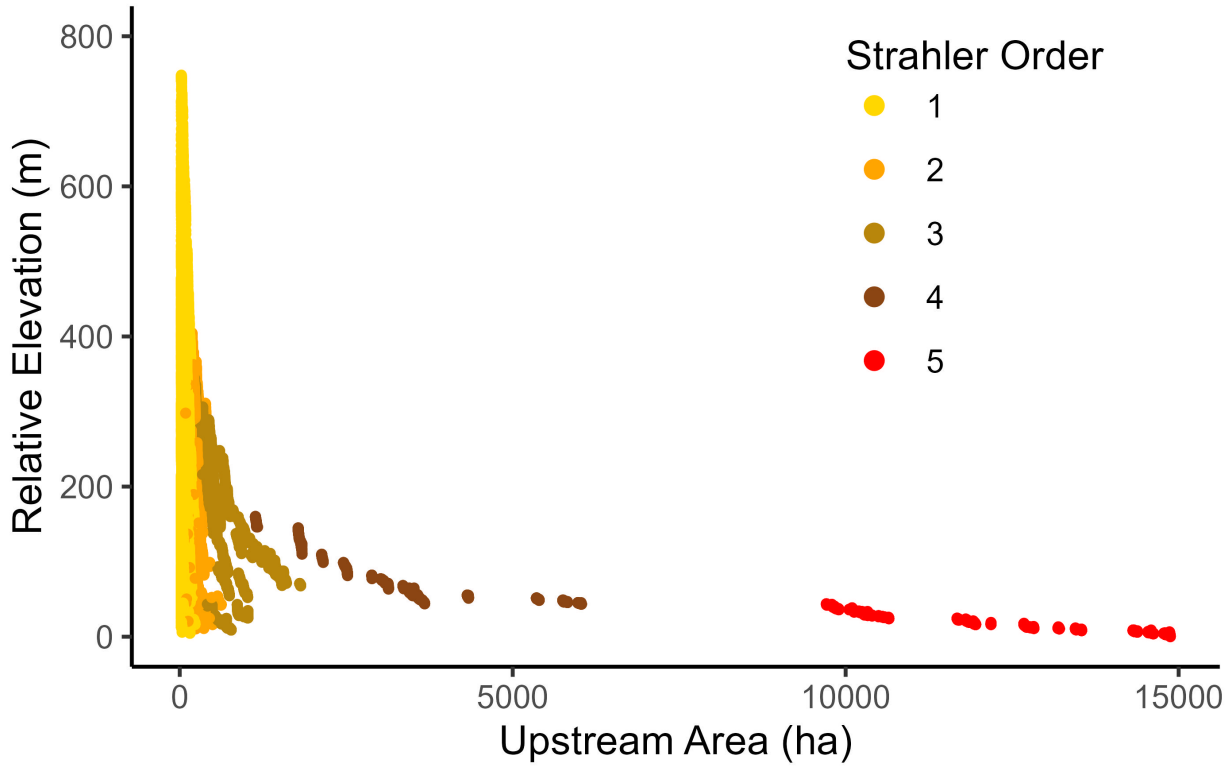

Figure 2.5: Channel thread elevations in the Cartoogechaye Creek basin as a function of drainage area coded by Strahler stream order. Arithmetic drainage area scale. Large regions of drainage area space are empty as drainage area jumps at each tributary confluence

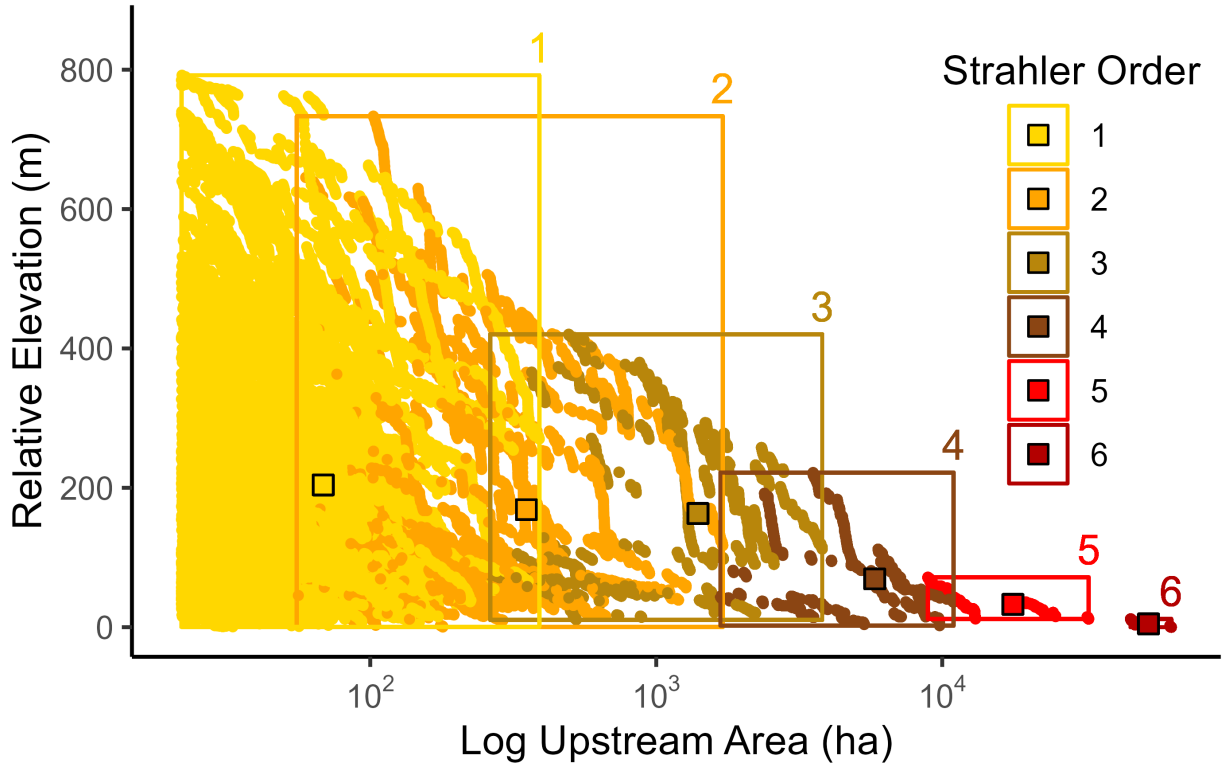

Figure 2.6: Channel thread elevations in the Yadkin River basin as a function of drainage area coded by Strahler stream order, drainage area shown at a log scale. Bounding boxes indicate the maximum, and minimum elevation drainage area for each stream order. Squares within each bounding box indicate the mean drainage area and elevation of that stream order.

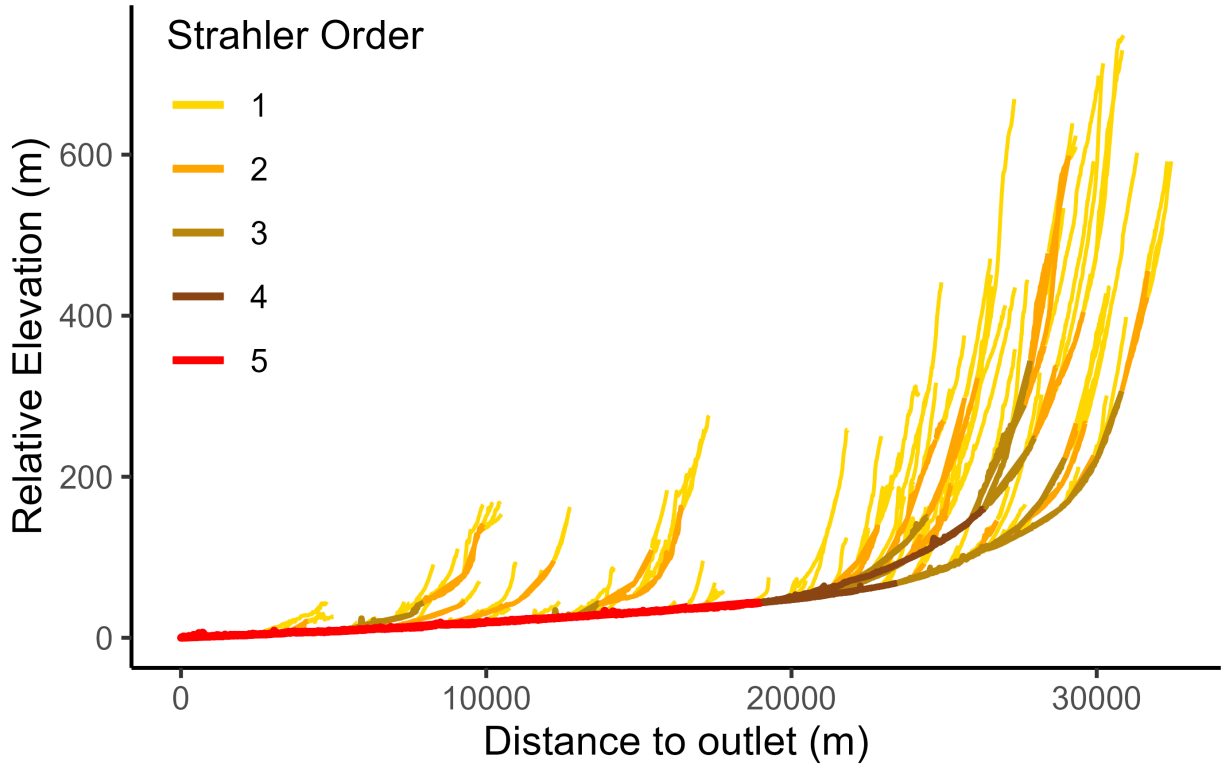

Figure 2.7: Channel thread elevations as a function of distance upstream from watershed outlet in the Cartoogechaye Creek basin. Flow distance from the outlet is a continuous variable. For Cartoogechaye Creek, mapping in this space illustrates not that first- and second-order streams differ dramatically from fourth- and fifth-order streams, but that the characteristics of first- and second-order streams differ based on watershed position.

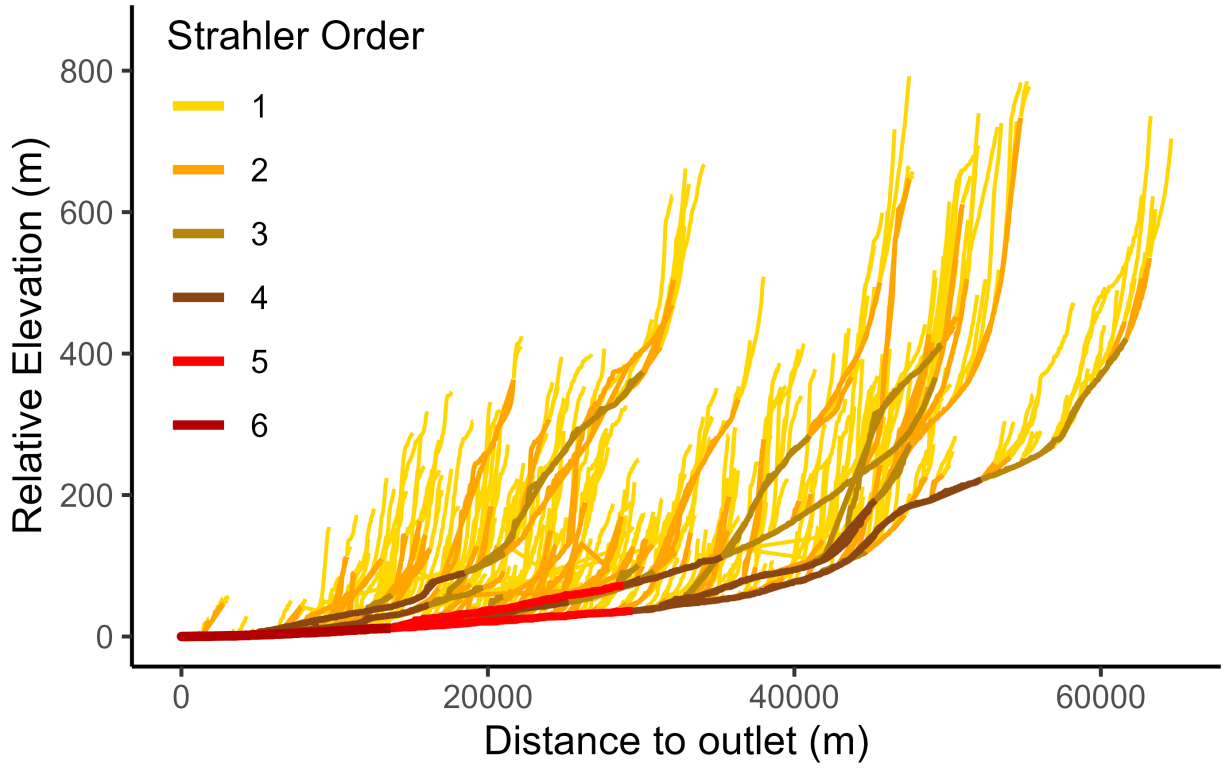

Figure 2.8: Channel thread elevations as a function of distance upstream from watershed outlet in the Yadkin River basin. Flow distance from the outlet is a continuous variable. In the Yadkin River basin, mapping in this space illustrates not that first- and second-order streams differ dramatically from fifth- and sixth-order streams, but that the characteristics of first- and second-order streams differ based on watershed position.

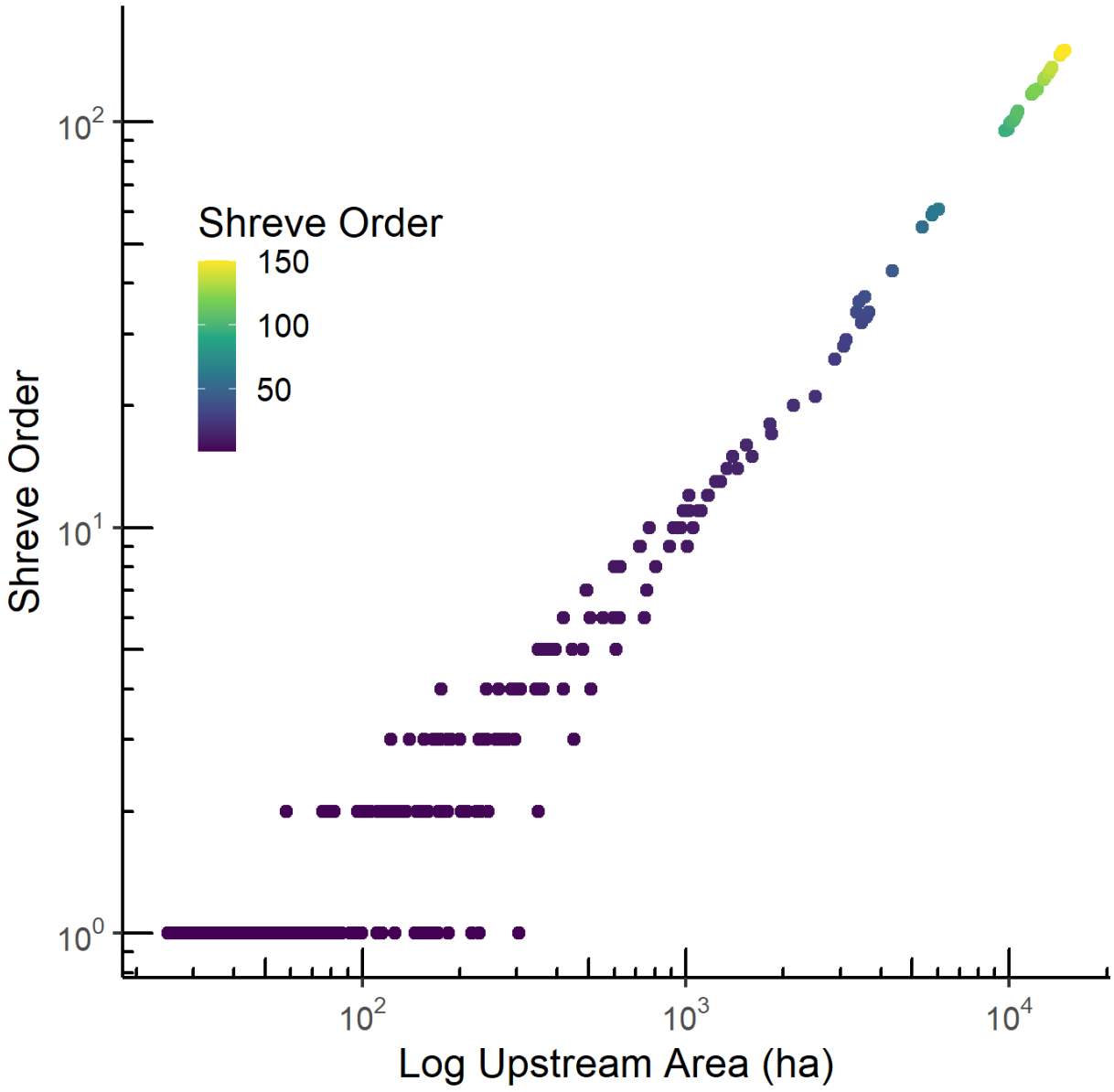

Figure 2.9: Shreve stream order and drainage area, coded by Shreve order for each stream segment in Cartoogechaye Creek. Upstream area reflects the drainage area at the bottom of each segment. Drainage area and Shreve order are both at a log scale. Shreve order is tightly correlated with upstream area. Large regions of drainage area space are empty as drainage area jumps at each tributary confluence

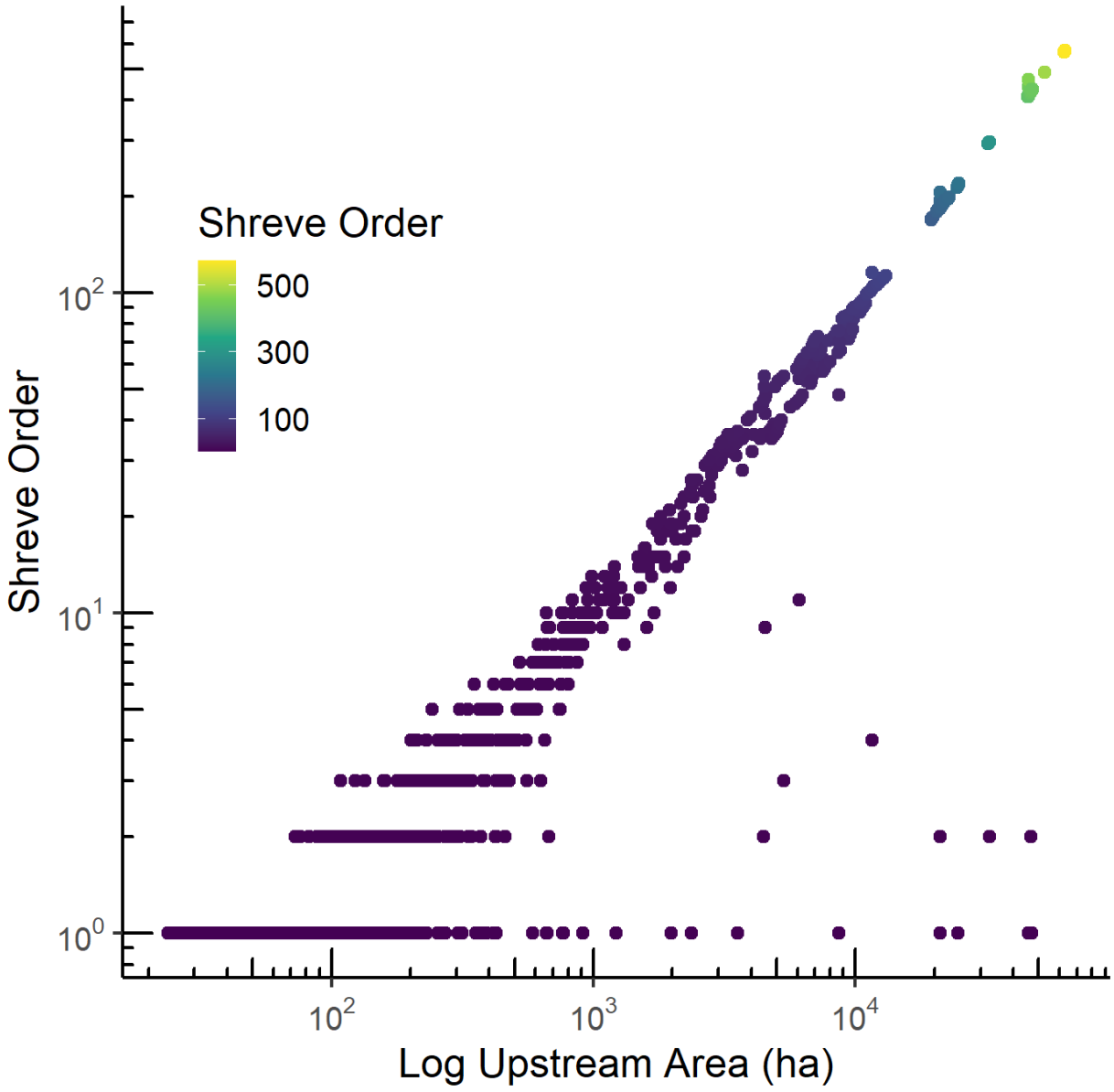

Figure 2.10: Shreve stream order and drainage area, coded by Shreve order for each stream segment in Yadkin River. Upstream area reflects the drainage area at the bottom of each segment. Drainage area and Shreve order are both at a log scale. Shreve order is tightly correlated with upstream area. Large regions of drainage area space are empty as drainage area jumps at each tributary confluence

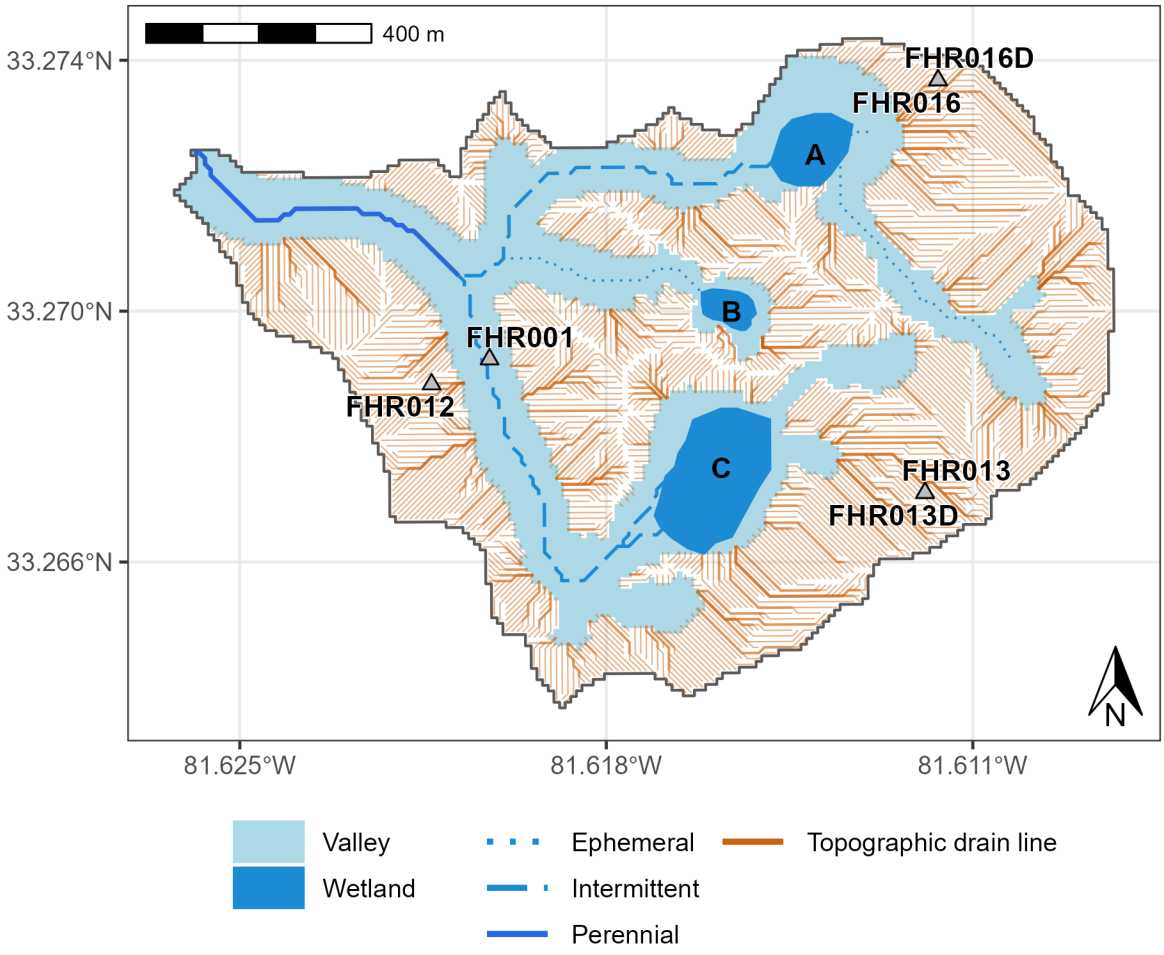

Figure 2.11: Surficial drainage threads and groundwater wells in planform view, Upper Fourmile Creek Basin, Savannah River Site, SC. Wells are displayed as bounded gray triangles, with accompanying well identification labels adjacent.

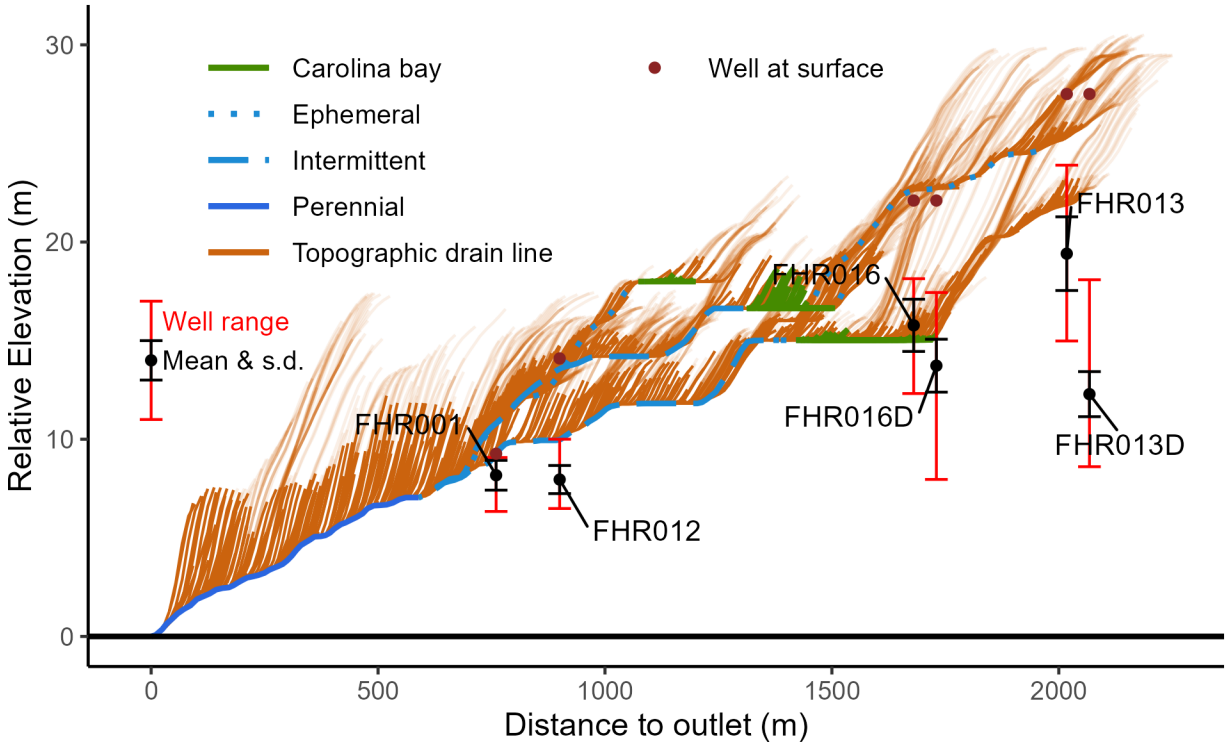

Figure 2.12: Surficial drainage threads and water table elevations relative to flow distance to perennial stream valley floor, Upper Fourmile Creek Basin, Savannah River Site, SC. Line thicknesses of topographic drain lines reflect the Strahler order for the surficial networks.

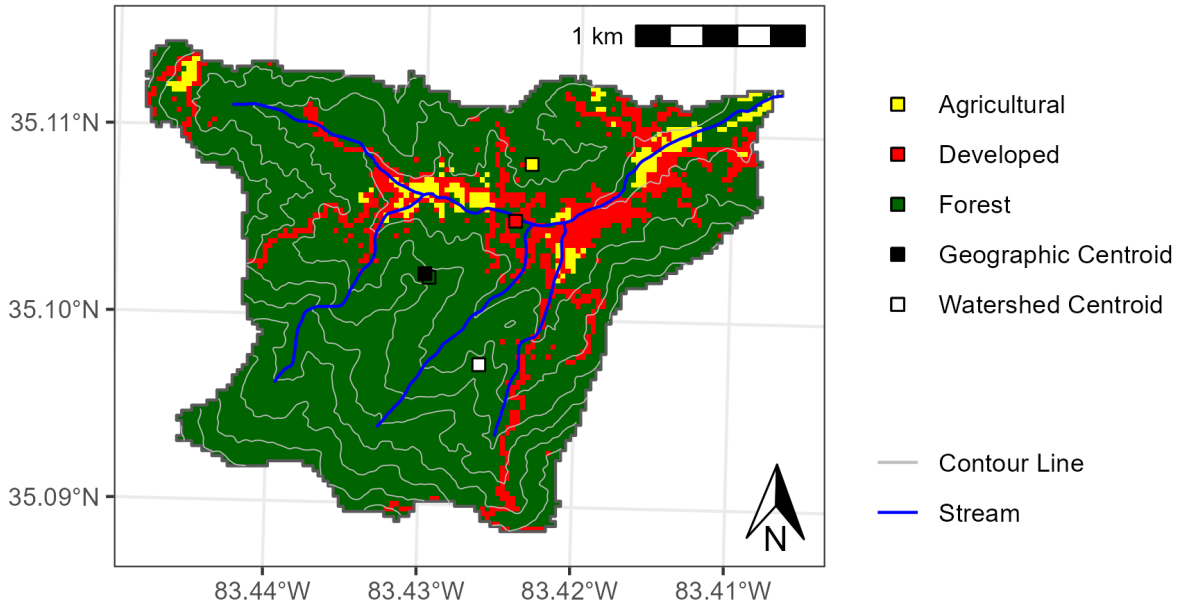

Figure 2.13: Planform map of South Fork of Skeenah Creek watershed. The maps show the NLCD land use across each watershed, as well as the NHD-defined streams within these watersheds. Elevation contours are shown at a 50 m scale. Note the contours reflect actual, not relative, elevation. Colored squares reflect the centroids of each land use in the outlet distance and relative elevation space. Geographic centroid reflects the weighted center of the watershed in geographic space (X, Y coordinates), and the watershed centroid reflects the weighted center of the watershed in the outlet distance and relative elevation space.

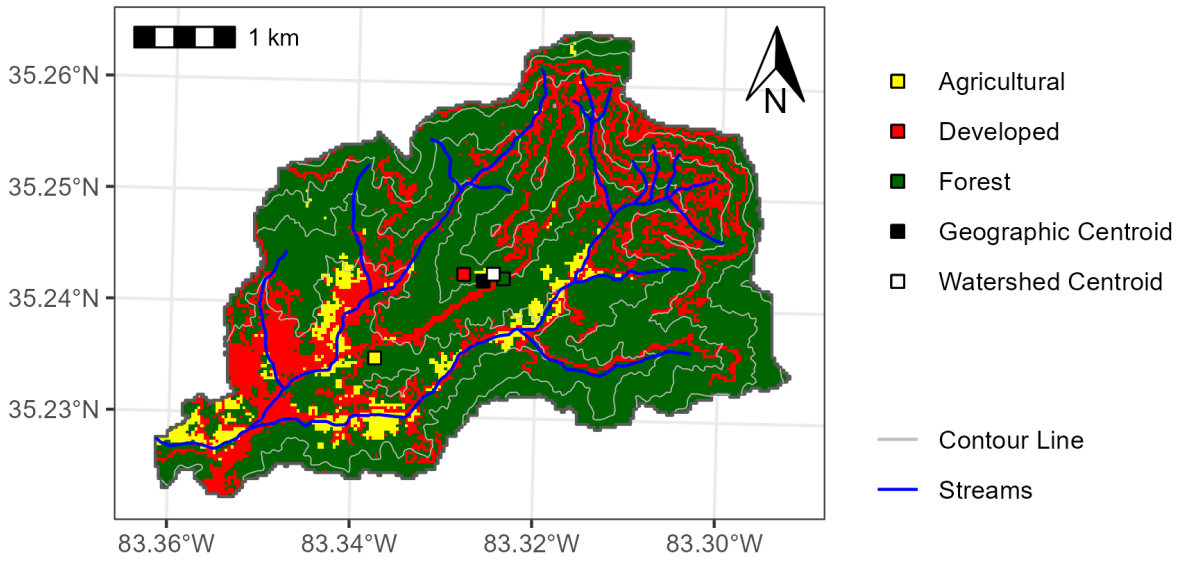

Figure 2.14: Planform map of Watauga Creek watershed. The maps show the NLCD land use across each watershed, as well as the NHD-defined streams within these watersheds. Elevation contours are shown at a 100 m scale for the Watauga Creek watershed. Note the contours reflect actual, not relative, elevation. Colored squares reflect the centroids of each land use in the outlet distance and relative elevation space. Geographic centroid reflects the weighted center of the watershed in geographic space (X, Y coordinates), and the watershed centroid reflects the weighted center of the watershed in the outlet distance and relative elevation space.

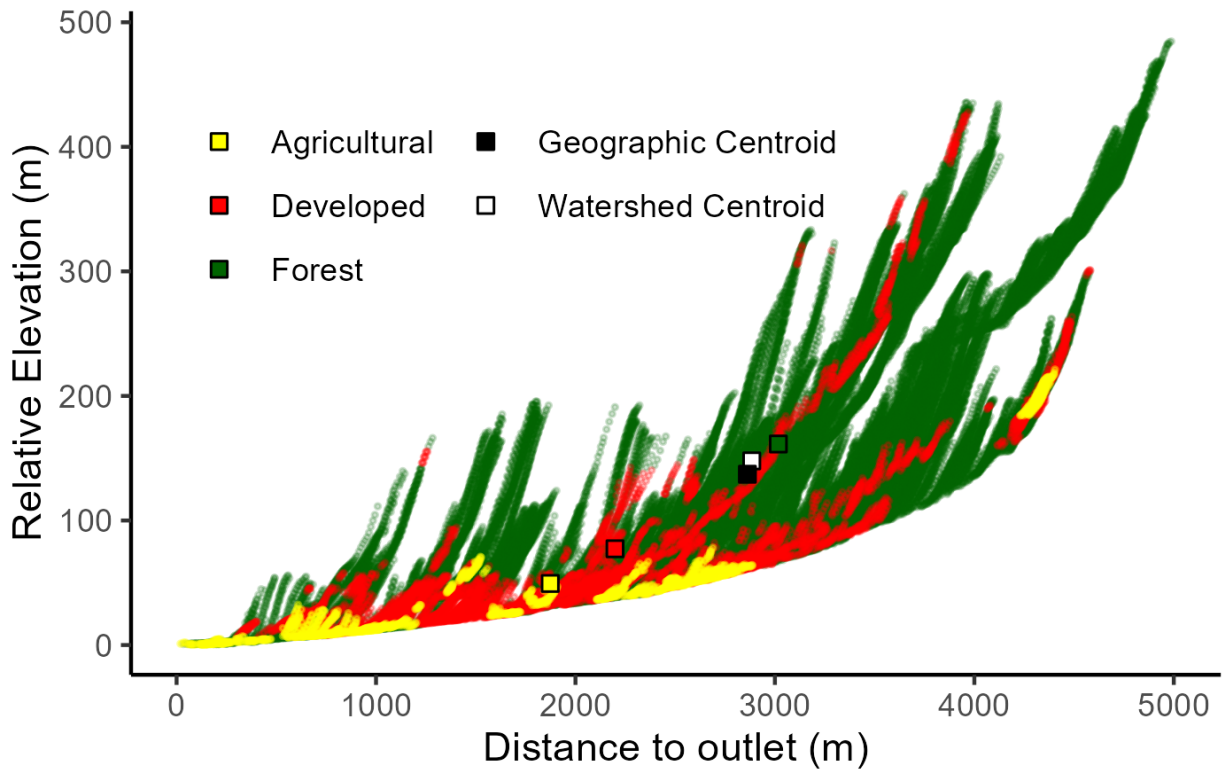

Figure 2.15: Side view of land use distribution in South Fork of Skeenah Creek, a rural mountainous watershed with only valley development. Each dot represents a 10 x 10 m DEM pixel color coded by the NLCD land use class of that pixel and placed with respect to flow distance to outlet and relative watershed elevation. Colored squares reflect the centroids of each land use in the outlet distance and relative elevation space. Geographic centroid reflects the weighted center of the watershed in geographic space (X, Y coordinates), and the watershed centroid reflects the weighted center of the watershed in the outlet distance and relative elevation space.

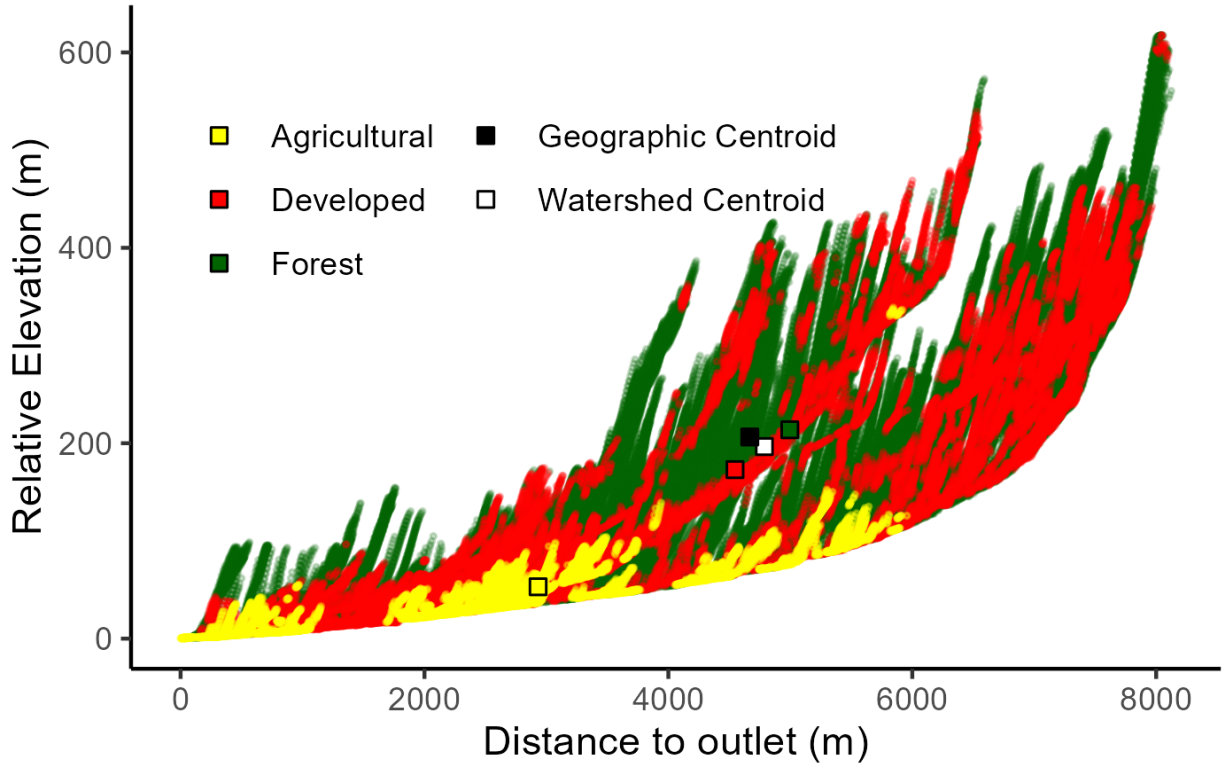

Figure 2.16: Side view of land use distribution in Watauga Creek, a rural mountainous watershed with both valley and mountainside development. Each dot represents a 10 x 10 m DEM pixel color coded by the NLCD land use class of that pixel and placed with respect to flow distance to outlet and relative watershed elevation. Colored squares reflect the centroids of each land use in the outlet distance and relative elevation space. Geographic centroid reflects the weighted center of the watershed in geographic space (X, Y coordinates), and the watershed centroid reflects the weighted center of the watershed in the outlet distance and relative elevation space.

Chapter 3

A topographically based, GIS-driven, two-dimensional water table model built on the one-dimensional Dupuit equation

[1] Raulerson, S.; C.R. Jackson, K. Vache, M.M. Bitew, S.E. Younger. To be submitted to *Hydrological Processes*.

Abstract

Groundwater transit times and water table position serve as foundational controls of how catchments function. The distribution of each influences the movement of solutes through the landscape and the subsequent biogeochemistry of the system as a whole. Understanding the fate and transport of soluble pollutants, like nitrate and phosphate (common in most agricultural and silviculture settings) is an important consideration in land management. For land managers who seek to understand the groundwater hydrology of the catchments, the time, resources and expertise needed to model groundwater behavior are consistent barriers. Here we present a 2-D, topographically based, GIS-driven model of water table position that can be used by resource managers to estimate water table position and provide support for analysis of solute transport. This 2-D model is based on Dupuit's equations for one-dimensional horizontal flow in a phreatic aquifer between two parallel rivers. Water table elevation along each point on topographically defined drainage pathway is calculated, and the resulting water table profiles are statistically smoothed. The resulting flow paths and pore velocities are used, along with a detailed set of field-based measurements, to address questions of the fate and transport of nitrate from fertilized pine plantations in three adjacent low-relief, groundwater driven headwater streams in the Upper Atlantic Coastal Plain. We use the proposed water table model to estimate catchment-wide transit times and subsurface water storage as mechanisms to evaluate these lingering questions of nitrate transport from the plantations.

3.1 Introduction

Understanding groundwater flow is a consistent barrier to workers seeking to understand the hydrology of the systems in which they work. Watershed-wide estimates of water table position, flow direction, travel times, and groundwater storage are often limited in their evaluation by the time, resources, and expertise needed to understand groundwater flow (Baalousha, 2009; Bronstert, 1999; Condon et al., 2021; Rahmati et al., 2018). There are many approaches to investigate groundwater at a watershed scale, but most typically utilize complex 2- or 3-D forms of Richards equation to serve as the driving equation in groundwater models that are typically computationally expensive to iteratively solve, time consuming to develop, and only approximate solutions due to the nature of solving a 3-D partial differential equation (R. A. Freeze, 1971; R. A. Freeze & Witherspoon, 1966, 1967; Kumar, 2012; Troch et al., 2013). These types of models have their purpose, and the varying degrees of complexity for them is driven in part by their intended use and needed outcomes (K. H. Adams et al., 2022; Kumar, 2012; Litwin et al., 2020; Paniconi & Putti, 2015).

These limitations have spurred modelers and resource managers alike to push for simplified water table models, which can be used by non-experts to make generalizations about system hydrology (K. H. Adams et al., 2022; Elshall et al., 2020; Kolbe et al., 2020; Kolbe et al., 2016; Wagner et al., 2014). Further, they can be used to answer questions regarding water table position, groundwater travel, solute transport, and receiving water quality. A landscape-wide model of water table positions could be used to estimate the

travel time of water from different portions of the landscape. Water transit times serve as a foundational control over the hydrology, solute transport, and biogeochemistry of watersheds and are of particular importance when considering the transport and fate of soluble reactive pollutants such as nitrate and phosphate (Klaus, Chun, et al., 2015; Klaus, McDonnell, et al., 2015). Looking at distributions of transit times across a watershed can give insight into how the system stores water and how these dynamic water flow paths can influence the preferential storage and release of water and subsequent solutes (Benettin et al., 2022; McDonnell et al., 2010; H. J. I. van Meerveld et al., 2019). Groundwater transit time distributions are generally right-skewed with long tails, speaking to the problems of legacy contaminants gradually accumulating in streams(Benettin et al., 2022; Scher et al., 2002). Excess nitrate from historical fertilizer use is slowly being transported along longer groundwater flow pathways, and due to the timescale of the transport, concentrations will continue to rise as water from these slow-moving pathways gradually accumulates into regional aquifer systems (Cooper et al., 2020; Lürling & Mucci, 2020; Paerl et al., 2020; Vitousek et al., 2022). Quantifying the time it takes these pollutants to move towards riparian zones is of particular interest, as this is the zone where there will be the greatest likelihood of permanent removal of nitrogen from the riparian aquifer through denitrification (Cooper et al., 2020; Lürling & Mucci, 2020; Lutz et al., 2020).

Here we outline the use of a topographically based, GIS driven, steady-state 2-D model of water table position. We use a one-dimensional form of Dupuit's equation for horizontal flow in a phreatic aquifer between parallel rivers to estimate water table position. This solution is physically based and allows for a direct solution without numerical approximation. In this case, the model is run from valley to ridgeline, simply assuming a symmetrical hillslope on the other side of the ridge. The model has easy-to-constrain site-specific input parameters and is applied to a GIS-derived network of surface flow paths across an entire watershed. We apply this model at two experimental headwater catchments of Fourmile Watershed at the Savannah River Site (SRS) within the state of South Carolina. These watersheds were experimentally manipulated to investigate the effects of intensively managed short-rotation pine (*Pinus taeda*) production on water quality (Griffiths et al., 2017). Heavy fertilization at the site resulted in elevated NO_3^- – N within shallow groundwater, but no distinct changes in deep groundwater, riparian groundwater, or streamwater. One explanation for the perceived lack of nitrate transport in groundwater at the site was longer than expected groundwater travel times. Previous studies and research on site (Aadland et al., 1995; E. Du et al., 2016; Flach et al., 1999; Gellici et al., 1995; Jackson et al., 2014; Rasmussen et al., 2003; Rasmussen & Mote, 2007; Vache et al., 2021) point toward median groundwater travel times that are in the range of 8 – 10 years, with near stream areas closer to 1 – 2 years, suggesting that the more than 7 years from the initial fertilizer application has been a sufficient time has passed for the contaminated groundwater to reach the streams. Our objectives were to introduce our topographically based and GIS driven model of water table position and use the model to calculate groundwater travel times for saturated and unsaturated flow to understand the processes and controls that govern the transport and fate of nitrate fertilizer that have leached away from a short rotation pine plantation.

3.2 Methods

3.2.1 Modeling approach

We estimate water table position using Dupuit's equation for one-dimensional groundwater flow in an unconfined aquifer. This solution (Equation 3.1) estimates horizontal flow in a phreatic aquifer between two parallel rivers (Bear, 1972; Dupuit, 1848), by averaging Boussinesq equation over a long period, which results in steady-state prediction of water table position (Boussinesq, 1904; Brutsaert & Nieber, 1977; Guérin et al., 2019; Leray et al., 2019).

$$K(h_x^2 - h_0^2) - Nx(L - x) + K\frac{x}{L}(h_0^2 - h_L^2) = 0 \tag{3.1}$$

With this solution, we assume that the Dupuit-Forcheimer assumption holds, and that flow is dominantly horizontal above the stream elevation, recharge to the aquifer is steady at a long-term scale, and the aquifer is symmetrical and uniform in extent. h_x is the water table position over a boundary layer, h_0 is the initial water table height over the boundary layer, N is annual recharge, x is distance along a drain line, K is hydraulic conductivity, and L is the total length of drain lines upstream of that drain line. By imposing a symmetry assumption, $h_0 = h_L$, Equation 3.1 simplifies to:

$$h_x = \sqrt{h_0^2 + \frac{Nx}{K}(2L - x)} \tag{3.2}$$

Equation 3.2 provides a direct solution of water table position above a boundary condition. By applying this equation to all topographic drain lines in a watershed, we create a quasi-2D model. The major difference with Dupuit's formulation is that this formulation must account for increases in drainage area as topographic drain lines come together.

Annual recharge and aquifer hydraulic conductivity (N and K) are estimated based on available site-specific records. Drainage network distance (x and L) are calculated using GIS flow routing and distance algorithms applied to digital elevation models. Initial water table position (h_0) is estimated based on available site geologic and hydrostratigraphic data. Schematically, we visualize Equation 3.2 as a cross section of the aquifer in Figure 3.1.

We solve this equation along individual surface flow pathways, as well as across the entire watershed drainage network. This gives an estimate of the water table position across the entire landscape. This formulation of Dupuit's equation is used to estimate water table position on a single surface flow pathway that had no branching pathways by Guérin et al. (2019). We depart from the approach of Guérin et al. (2019) by iteratively solving Equation 3.2 across the full network of branching surface flow pathways. Parameterization is relatively straightforward when looking at a single, non-branching flow pathway (Figure 3.2; Example A).

In this scenario, a cross section of the aquifer looks largely like Figure 3.1. When larger, branching, and more complex networks of surface flow pathways are considered, conceptualization and parameterization of Equation 3.2 becomes more complex (Figure 3.2; Example B). Water table position must be calculated in

the correct sequence, starting at the branch outlet moving upslope towards the ridgeline. Considerations for initial water table height (h_0), appropriate network distance (x and L) are required at branch junctions.

We take approaches from graph and network theory that have become of recent interest in hydrologic sciences to apply Equation 3.2 across the full network of surface flow pathways and resolve the sequencing and parameterization concerns (Heasley et al., 2019; Heckmann et al., 2015; Lindsay, Francioni, et al., 2019; Lindsay, Yang, et al., 2019; Phillips et al., 2015; Rinaldo et al., 2006; Rinaldo et al., 2014; K. Wang et al., 2020; Zaliapin et al., 2010). We conceptualize the surface drainage network as a directed acyclic graph, where every internal sub-network routes to a downstream outlet. In most cases of stream network analysis and graph theory, the stream network of a watershed is considered a "tree", with all "branches" (tributaries) draining to the tree "root" (watershed outlet), with first order headwater tributaries being considered the tree "leaf" (Fang et al., 2017; Fürst & Hörhan, 2009; Rinaldo et al., 2006; Schwanghart & Scherler, 2014; Schwanghart & Kuhn, 2010; Zaliapin et al., 2010). Because we are interested in internal drainage structures, we route all surface flow to the edges of the near-stream valley zones, resulting in a "forest" of "trees". This forest represents all the sub-networks that contribute to flow within the watershed. With this conceptualization, we are able to sequentially (based on stream order) solve Equation 2 from the root at the valley edge, up to the ridge line for each sub-drainage network, while also updating key parameters at branch junctions.

3.2.2 Study site

We highlight the use of this model in the context of an extensive watershed experiment originally designed to evaluate the effect of silviculture treatments and best management practice on short-rotation loblolly pine plantations, with an emphasis on understanding the soil, water quality, and biomass production. Greater detail on the site description, experimental design, and sampling protocols have previously been established elsewhere (E. Du et al., 2016; Ferreira et al., 2020, 2021; Griffiths et al., 2017; Griffiths et al., 2019; Griffiths et al., 2016; Griffiths et al., 2018; Jackson et al., 2014; Jackson et al., 2016; Klaus, McDonnell, et al., 2015; Klaus & Jackson, 2018)(Meles et al., 2020; Meles Bitew et al., 2020; Ruzol et al., 2022; Vache et al., 2021; Younger et al., 2023). Our sites are two adjacent first order, headwater catchments that are tributaries to Fourmile Creek and the Savannah River (Figure 3.3). These watersheds are contained within the Savannah River Site, a National Environmental Research Park and located within the Atlantic Coastal Plain of South Carolina. Watershed C is 117 ha in area and Watershed B is 169 ha in area.

Both catchments have typical geology and climate for the region. Permeable, low-relief (2 – 3% slope) and groundwater-driven catchments. Soils on site are mapped as Dothan and Fuquay series (Rogers, 1990). Sandy A and E horizons overlie more clay-rich sandy clay loam Bt horizons. A horizons vary in thickness but are generally 80 – 90% sandy with limited amounts of accumulated organic matter. E horizons are sandy to sandy loam, typically around 10 – 60 cm in thickness, and found around 10 – 25 cm. Transitional EB horizons are sandy loam to sandy clay loam and are found at 25 – 45 cm. Bt horizons are found in all soil profiles at varying depths, they are typically sandy clay to clay in texture with clay contents of > 35% (Younger et al., 2023). More generally, the soils on site consist of loamy sand topsoils overlaying sandy clay loam argillic horizons, over unconsolidated sands and clays (Kilgo & Blake, 2005). The bottom boundary

for our model is well defined with a dense clay hydrostratigraphic layer, known locally as the Tan Clay. This serves as the base of the surficial aquifer, and the basis for parameterizing h_0 in Equation 2. Annual precipitation on site ranges from 992 to 1538 mm, and annual evapotranspiration ranges from 304 to 1448 mm (Table 3.1) (Caldwell et al., 2018; E. Du et al., 2016; Griffiths et al., 2019; Kilgo & Blake, 2005; Ruzol et al., 2022; Vache et al., 2021). Average annual precipitation at the site averages 1209 mm and average annual evapotranspiration is 866 mm (Table 3.1).

Heavily instrumented, the site has 8 wells installed with screening depths varying from 3.9 to 43.6 m (Figure 3.3). These monitoring wells are located at varying topographic and landscape positions within the watershed. Wells FHR013 – 16D are pairs of co-located wells, one with a shallow screening depth and the other much deeper (Figure 3.3). Grab measurements of water table position in these wells were taken on a monthly basis from December 2011 for the deep wells (ending in a "D" designation) and from September 2012 for the shallow wells, all ending in July of 2020. There are a total of 948 monthly groundwater observations spanning December 2011 to July 2020.

3.2.3 Model parameters and selection

Recharge (N) was estimated from published records of climatic data for the region, as well as from data collection on site (Table 3.1) (Aadland et al., 1995; Caldwell et al., 2018; E. Du et al., 2016; Ferreira et al., 2020, 2021; Griffiths et al., 2019; Kilgo & Blake, 2005; Ruzol et al., 2022; Vache et al., 2021; Younger et al., 2023; Younger et al., 2020). Annual aquifer recharge ranged from 147 mm to 839 mm, with an average of 351 mm (Table 3.1 – 3.2). Recharge (N) in the model was defined as 0.4 m/yr.

Initial water table depth (h_{0i}) was determined using available literature of the surficial aquifer in the region (Table 3.2). Most sources identify the locally known Tan Clay hydrostratigraphic layer as a common bottom boundary for the surficial aquifer (Aadland et al., 1995; E. Du et al., 2016; Mathes et al., 2001; Prowell, 1996; Rasmussen et al., 2003; Rasmussen & Mote, 2007). The Tan Clay aquitard divides the Upper Three Runs Aquifer into the surficial aquifer and the semiconfined Barnwell-McBean Aquifer underlain by the Green Clay Aquitard (Aadland et al., 1995; Flach et al., 1999; Gellici et al., 1995; Hiergesell, 1998; Hiergesell & Jones, 2004; Prowell, 1996; Rasmussen et al., 2003; Rasmussen & Mote, 2007; Wells, 2009). We assume the Tan and Green Clay aquitard layers are impervious layers with zero losses that are laterally expansive across our model domain, but it is known that there is some amount of downward leakage to the lower Barnwell-McBean and Gordon Aquifer systems (Figure 3.4). This lateral groundwater movement through the unconfined and semiconfined flows to the southeast, toward Fourmile branch (Bruns, 2000; Rasmussen & Mote, 2007). Records indicate a thickness of between 3 and 12 m for the surficial aquifer, but note some exceptions where it can be found up to 25 m below the surface (Aadland et al., 1995; Rasmussen et al., 2003). The initial water table depth (h_{0i}) in the model is defined as 10 m.

Available literature on surficial aquifer properties at the site were used to bound hydraulic conductivity (K) estimates and determine an initial K value. Hydraulic conductivity investigations in different portions of the Upper Three Runs Aquifer determined an average K of 923 m/yr (Table 3.2). The top of the surficial aquifer K ranged 27.8 to 556 m/yr with an average of 233 m/yr (Flach et al., 1999). Other investigators report average hydraulic conductivity between 4,339 – 17,355 m/yr for the combined upper and lower surficial

aquifer (Aadland et al., 1995; Gellici et al., 1995). Irrigation and dye tracer experiment at our application site found that topsoil on site range from 876 – 24,528 m/yr and the argillic horizon from 8.76 to 43.8 m/yr (E. Du et al., 2016; Jackson et al., 2016; Meles Bitew et al., 2020). Plot-scale estimates of surficial conductivities from these same experiments estimate a hydraulic conductivity of 4,029 m/yr (Jackson et al., 2016). Hydraulic conductivity (K) is defined in the model as 4,000 m/yr.

Estimates of porosity are used in subsequent groundwater travel time calculations. We use aggregated measures of porosity found in more detailed hydrogeologic studies as our basis. Total porosity (η) is well studied in the Aadland et al. (1995) and Gellici et al. (1995) reports as 35%, with further studies estimating it between 25% – 41%, with an average of 35% (Meles Bitew et al., 2020)(Table 3.2). Aadland et al. (1995) reports an effective porosity (η_e) of 25%. Total porosity (η) is defined as 40% and effective porosity (η_e) 25% in travel time estimates.

3.2.4 Parameter sensitivity

The model uses only two variables that describe the hydraulic properties of the aquifer. h_{0i} and K are the two parameters within the model which allow for optimization based on the range of feasible values presented in Table 3.2. We use Monte Carlo techniques to investigate the uncertainty and sensitivity of h_{0i} and K estimates. This process is meant to show how model parameters characterizing subsurface conditions impact water table position calculations and to evaluate the relative influence of h_{0i} and K on model predictions. Root mean squared error (RMSE) between well records and predicted water table position is used to evaluate parameter sensitivity across the full range of values described in Table 3.2 for h_0 and K from 100 generalized Monte Carlo realizations (Robinson & Metternicht, 2006).

3.2.5 Comparison to simple USGS model predicting surficial aquifer positions across CONUS

We compared the predicted depth to groundwater (DTW) predictions with the CONUS-wide prediction generated from Zell and Sanford (2020). Their estimates were generated from a series of 75 different MODFLOW-6 simulations, which were intended to estimate surficial groundwater systems across the United Stations, at a long-term, steady-state scale. The result of that modeling is an estimate of depth to groundwater across CONUS, at a 250 m scale.

3.2.6 Implementation

To investigate the influence of DEM resolution on model output and subsequent travel time estimates, we calculate water table position and groundwater travel times at 10 m, 20 m, and 30 m resolution from LiDAR generated DEM's. These DEM's are hydrologically conditioned using a constrained regularized smoothing (CRS) algorithm to address pits and flats in the landscape. This process ensures a monotonic downstream decrease in elevation for the watershed, meaning all gradients in the network point

towards the watershed outlet. Hydrologic conditioning was completed using the TopoToolbox add-in of MATLAB (Schwanghart & Scherler, 2014; Schwanghart & Kuhn, 2010).

Flow direction, accumulation, vector flow network extraction, network distances, and geometry were all completed through TopoToolbox. Attributes for each node on the network branches needed for graphing or for use in Equation 3.2 included: distance along line (x; Equation 3.2), accumulating downstream distance (L; Equation 3.2), distance to watershed outlet, elevation, Strahler stream order, and sub-network ID. Drainage networks were routed down to the valley, where the landscape is flat, and the water table is near the surface. Valley areas for our region are identified as regions of the watershed which consist of hydric soils, delineated wetlands, Carolina bays, and near stream zones within 10 m of delineated streams. Manual cleaning of the network was required at some connection points (Carolina bays/wetlands to perennial/intermittent stream network) as an artifact of DEM noise.

We assume the water table is at, or near the surface for all locations within the valley and stream zone. For all regions upslope of the valley, we sequentially solve Equation 3.2 for each separate sub-network starting at the largest Strahler stream order for each branch, moving sequentially higher to the first-order branches. h_x is calculated for each node on a branch, with an initial h_0 value set at the branch root along the valley edge. This initial h_0 value is determined based on site geologic data and is updated for each subnetwork. h_0 is updated at branch junctions, reflecting the maximum h_x value from the immediate downstream branch that it intersects. h_x and h_0 values for each node are stored as the algorithm crawls through the network of surficial drainage lines. L is similarly updated as h_0 at each tributary junction to reflect the total length of drain lines upstream of that drain line.

We use two representations of the lower no-flow boundary. First we define the aquifer bottom using the traditional formulation as a uniform, flat layer that spans the horizontal lateral extent of the watershed (Equation 3.3). We compare that with a second formulation, that allows for a sloped aquifer such that the lower boundary parallels the longitudinal position of the valley, and remains the same distance from the valley floor from the bottom to the top of the watershed (Equation 3.4). We present results using both conceptualizations ho presented in Equations 3.3 and 3.4, which reflect differences in how the aquifer bottom boundary conditions are defined.

$$h_{0f} = h_{0i} + (z_{to} - z_{wso}) \tag{3.3}$$

$$h_{0s} = h_{0i} + z_{to} \tag{3.4}$$

3.2.7 Travel times

Using the water table position estimated from Equation 3.2, we calculate watershed-scale estimates of unsaturated, saturated, and total transit times (Equations 3.5 - 3.7). We use the derived water table surface from the Dupuit model (h_x, Equation 3.2) and constrained estimates of aquifer characteristics (hydraulic conductivity, K; effective porosity, η_e; total porosity, η; recharge, N).

$$t_t = t_{unsat} + t_{sat} + t_{ch} \tag{3.5}$$

$$t_t = \frac{\eta_e d_{gw}}{N} + \sum \frac{\eta L^2}{\Delta h_x K} + \frac{L_{ch}}{M S^{1/2} R^{2/3}} \tag{3.6}$$

$$t_t = \frac{\eta_e d_{gw}}{N} + \sum \frac{\eta L^2}{\Delta h_x K} \tag{3.7}$$

Channel transit times (t_{ch}) are ignored due to their relatively short travel times (hours) in comparison to unsaturated and saturated travel times (months to years) for the small, headwater catchment of interest here. Removing t_{ch} from Equation 3.5 and Equation 3.6 simplifies calculating total travel time t_t, to Equation 3.7. t_{unsat} is the cumulative time to reach groundwater along a directed flow pathway, based on the depth to groundwater (d_{gw}) that can be calculated based on the calculated water table position of Equation 3.2 (h_x) and the surface elevation. t_{unsat} depends on the thickness of the unsaturated zone which decreases with distance to the near-stream zone (valley). t_{sat} is the cumulative travel time in the groundwater flow path based on the change in hydraulic head Δh_x as water and solutes travel along a flow pathway, moving some distance, L, between measurements. t_{sat} depends on the flowpath length, hydraulic head and assumes a straight flow pathway between nodes. (i.e. calculated node to node based on flow direction).

To investigate the influence in our modeling approach that effective and total porosity have on calculations of unsaturated and saturated travel times, we calculate travel times using the full range of porosity values outlined in Table 3.2.

3.3 Results

3.3.1 Water table surface

Unless otherwise stated, all model results presented are from a 10 m DEM and flat bottom boundary conditions.

The water table surface generated from Equation 2 using a 10 m DEM in Watersheds B and C are displayed longitudinally (Figure 3.6) and in the planform view (Figure 3.7). Water table depth (WTD) in Watershed C ranges from at the land surface in the valley and adjacent riparian zones to around 13.5 m at watershed divides, with mean and median depths of 2.24 m and 1.23 m respectively (Figure 3.7). WTD in Watershed B ranges from the land surface in the valley and adjacent riparian zones to upwards of 18 m at watershed divides and internal drainage boundaries, with mean and median depths of 3.41 m and 2.67 m (Figure 3.7). Maximums occur in upper portions of the watersheds, near both watershed boundaries and internal drainage divides, as well as in areas where there are dense networks of surface flowpaths.

The water table surface shown in Figure 3.7 is compared with the water table surface generated from the Zell and Sanford (2020) in Figure 3.5. Water table position in the upslope landscape positions and in

the areas that serve as internal drainage divides between networks of surface flowpaths show differences of ± 10 m. The upper portions of both watersheds generally show that Zell and Sanford (2020) estimates of water table depth are greater than our model estimates. In Watershed C, the Zell and Sanford (2020) predictions tend to be better, clustering around the stream elevations. The higher up in Watershed C, the predictions become more high-bias. In Watershed B, the Zell and Sanford (2020) predictions are generally very high-biased throughout the watershed.

3.3.2 Travel times

In Watershed B, total travel times (t_t) outside of the valley ranged from under a day in the riparian zones to upwards of 73 years near drainage divides, with mean and medians of 10.96 and 6.06 years respectively. Unsaturated flow travel times (t_{unsat}) ranged from less than a day near riparian zones to 7.75 years, with a mean of 1.84 years and median of 1.57 years. Saturated flow travel times (t_{sat}) ranged from 0 to 70.97 years with a mean of 7.43 years and median of 2.63 years (Table 3.3).

In Watershed C, total travel times (t_t) ranged from 0 to 74.73 years, with mean and median of 9.43 and 4.9 years respectively. Unsaturated flow travel times (t_{unsat}) ranged from 0 to 5.84 years, with a mean of 1.36 years and median of 1.08 years. Saturated flow travel times (t_{sat}) ranged from 0 to 73.35 years with a mean of 8.07 years and median of 3.23 years (Table **??**).

3.3.3 Model sensitivities

The sensitivity of the model is based on the choice of h_0 and K, where K essentially adjusts the bend in the water table profile and h_0 dictates the initial water table height the model starts with. Increasing h_0 and K will both flatten the resulting water table surface, with h_0 to a much higher degree. Error related to initial water table height (h_0) ranged from 2.7 m, to upwards of 16.8 m (Figure 3.10). Error associated with h_0 had a local minimum between h_0 = 5 and h_0 = 10. h_0 values greater than that range increased RMSE linearly. In contrast with the initial water table height (h_0), output of the model was relatively insensitive to changes in hydraulic conductivity (K)(Figure 3.10). There is no global error minimization associated with using a particular K value from the range described in Table 3.2.

Increasing effective (η_e) and total porosity (η) in the calculation of unsaturated (t_{unsat}) and saturated (t_{sat}) travel times in Equation 3.7 resulted in longer travel time distributions (Figure 3.11). Mean t_{unsat} times increases from 0.97 years at η_e = 0.125, to 1.95 years at η_e = 0.25, to 3.12 years at η_e = 0.4. Mean t_{sat} times increases from 2.52 years at η = 0.125, to 5.04 years at η = 0.25, to 8.07 years at η = 0.4 (Figure 3.11).

Use of a sloped bottom boundary condition in Watershed C resulted in shorter travel time calculations (Figure 3.12; Table 3.3). Median t_t was reduced from 4.9 to 2.86 when using a sloped bottom boundary. Median t_{unsat} travel times were reduced from 1.08 to 1.02 respectively, and t_{sat} was reduced from 3.23 to 1.38 (Figure 3.12; Table 3.3).

Coarser DEM resolution (> 20 m) resulted in water table profiles that are artificially inflated as a reflection of changes to network distances used in Equation 2 (Figure 3.13). These distances change in relation to DEM resolution. In Watershed C, median unsaturated flow travel times (t_{unsat}) changed little

with respect to DEM resolution (Table 3.4). As DEM resolution becomes coarser, median saturated travel times (t_{sat}) increased from 3.23 to 4.37 years at 20 m resolution and 4.95 years at 30 m resolution. Similarly, total travel times (t_t) increased from 4.90 to 6.0 years at 20 m resolution, to 6.30 years at 30 m resolution. Cumulative distributions of travel times in Watershed C shift towards longer travel times with increasing resolution (Figure 3.14).

3.4 Discussion

3.4.1 Model function

This simple and parsimonious GIS-driven model easily estimates water table position, vadose zone thicknesses, and groundwater travel times without the need for mesh generation and training in traditional groundwater modeling techniques, eliminating the consistent barrier to access in groundwater hydrology (Arora et al., 2019; Buttle, 2016; Kong et al., 2015; Staudinger et al., 2017). The thickness of the vadose zone and saturated groundwater are important in many subsurface processes from groundwater quality, susceptibility to contamination, solute transport, water travel times, denitrification potential, and estimating water storage (Brauer et al., 2013; Kobayashi & Yokoo, 2013; Richey et al., 2015). Typically characterizing the subsurface in such a way is accomplished through point scale geophysics measurements like ground penetrating radar (GPR), resistivity, or nuclear magnetic resonance (NMR) to name a few, all of which are prohibitive to implement at a watershed-scale from financial and labor-cost perspective (Binley et al., 2015; Walsh et al., 2014).

We can see the high variability in groundwater levels in both watersheds by representing them in a longitudinal space, which also allows us to view the watershed's hydrography, topography, and model results in a space that gives context to the model output (Figure 3.6). The variability in groundwater levels is low in the valleys and substantially increases upslope in Watershed C. In the valley and adjacent riparian areas of both watersheds, the water table is at or within 1.5 meters of the surface (Figures 3.7 - 3.9). At internal drainage divides and near watershed divides, the model estimates a much deeper water table ranging from 5 m to upwards of 17 m in some regions where there are dense networks of surface flowpaths. We can see that depending on where in the landscape there can be up to 30 m of vadose zone storage below the surface (Figure 3.6). When considering a simple water balance approach to estimating hydraulic turnover in a watershed where the turnover is the total storage divided by watershed discharge, a difference of 30 m in depth makes a large difference in the starting volume of water being considered (McGuire & McDonnell, 2006; Schwientek et al., 2009).

The variability in water table position from our model output as you move upslope in either watershed is comparable to the variability in water table position from the Zell and Sanford (2020) estimates of WTD (Figure 3.5; Figure 3.6). Compared to the water table surface of Zell and Sanford (2020) , our model results in a much lower prediction of water table position in the upper portions of the watershed, as well as within the internal drainage divides (Figure 3.5). The two surfaces are most similar in the regions adjacent to the valley, which could in part be due to those areas having more of a simple network geometry for

parameterizing and solving Equation 2 than the upslope regions have. This distributed estimate of water table position across the landscape is useful for incorporation into site indices, where WTD can be a key factor in determining survival and growth of species in agroforestry settings (Somarriba et al., 2001; G. G. Wang & Klinka, 1996).

3.4.2 Travel time estimates

Calculated total groundwater travel times (t_t) in the riparian areas were generally < 2 years (Figure 3.9). Areas near ridgelines with internal drainage divides exhibited higher total travel times. Across Watershed C, there were mean groundwater travel times of 9.43 years and median times of 4.9 years. The distributions of groundwater and vadose zone travel times decay exponentially, with long tails that are associated with longer groundwater flow paths. These distributions range from less than a day near riparian zones, to upwards of 75 years. In comparison to groundwater travel times, vadose zone travel times are much shorter, and are much more constrained in their distributions. In Watershed C, mean t_{unsat} was 1.36 years, while t_{sat} was 8.07 years, while the distribution of t_{unsat} was much more constrained with a range less than a day near the riparian areas, to 5.84 years. This shows the influence that t_{sat} plays in estimates of total groundwater travel times compared to vadose zone travel times.

Streamwater residence times from previous study analyzing natural occurrences of stable isotopes have indicated residence times > 5 years, and supported that much of the flow in these watersheds is groundwater driven (E. Du et al., 2016; Griffiths et al., 2016; Klaus, Chun, et al., 2015). Initial estimates from previous studies indicated travel times within the range of 8 – 10 years, with near stream riparian areas being on the order of 1 – 2 years.

3.4.3 Model sensitivities

DEM resolution is an important consideration in the calculation of WTD and in travel time calculations. As resolution of the DEM increased, the overall estimate of groundwater travel times increased. This is likely due to the scaling of network distances as resolution increases a, resulting in changes to the network distances used in Equation 3.2 (x and L) to calculate water table position, and in Equation 3.7 when calculating t_{sat}. DEM resolution is a long known concern in many aspects of hydrological modeling (K.-t. Chang & Tsai, 1991; Munoth & Goyal, 2019; Saksena & Merwade, 2015; Schoorl et al., 2000), and has been studied already at our site when evaluating perform of a GIS-based topographic model of wetness (Meles et al., 2020). Similar relationships were found between DEM resolution and prediction of flood inundation areas, where coarser resolution DEMs produced larger flood areas, over predicting the flood area (Saksena & Merwade, 2015). Other work has shown the importance of DEM resolution, and processing (smoothing and aggregating), in stream and watershed delineation, with particular consideration to the impacts changes to either of those characteristics will have on resulting water budgets (Erdbrügger et al., 2021). We observe a similar scenario, where with increased DEM resolution, the model produces over-inflated estimates of water table positions in areas of dense drainage (Figure 3.6; Figure 3.13). In these dense areas, the change in DEM resolution causes more pronounced changes to network distances as the

topography is becoming more generalized. This is a topic that has been identified when applying the 2 - and 3D form of Dupuit's equation (Bresciani et al., 2014; Loáiciga, 2020).In those cases, they have found there to be an idealized ratio of water table depth to hillslope length where a topographically implemented water table model has the ability to best perform (Bresciani et al., 2014).

Similar considerations need to be made in determining an appropriate bottom boundary condition. Traditional applications of Equation 3.2 conceptualize the aquifer in an idealized way, homogenous, uniform K, with a constant lateral extent. A sloped bottom boundary condition results in lower t_t estimates because of reduced groundwater storage in both the vadose zone and saturated zone. There is a reduction in overall storage within both zones, meaning the hydraulic turnover time at a fixed discharge rate will be decreased.

3.4.4 Similar models

Similar efforts supporting more simplified topographically based water table models generally still utilize numerical methods, sophisticated finite element/volume schemes, or 3D mesh grids which iteratively solve Richards equations or other comparable solutions forward in time. Litwin et al. (2020) presents a model which has similar goals as us, but uses a 2D form of Dupuit's equation that is solved numerically using a finite volume technique and is based in the Python framework of LandLab (J. M. Adams et al., 2017; Barnhart et al., 2020; Hobley et al., 2017; Litwin et al., 2020; Litwin et al., 2022). Guérin et al. (2019) uses the same 1D form of Dupuit's as us, and intends to use it as a long-term, steady state estimate of water table position. One key difference is that they only solve this over a single hillslope transect, and mean to use their implementation to validate co-located well records location on that transect, and estimate total aquifer storage based on that single transect (Guérin et al., 2019). Most comparable studies implementing a similar formulation of Dupuit's equation are either not distributed solutions at a watershed scale (i.e. Guérin et al. (2019)), use integrated land surface models (LSMs) used in Earth Systems Modeling (ESMs) for modeling Earth's physical processes on near geologic timescales (i.e. Fan et al. (2019), Litwin et al. (2020), and Picourlat et al. (2022)), or are otherwise coupled models not intended to calculate water table position explicitly.

3.4.5 Model considerations and limitations

There are clear dangers in use of groundwater models by non-experts, from incorrect use, violation of underlying assumptions, to misinterpretation of results. Here we have presented use of a physically-based, GIS driven, topographically based, and relatively parsimonious water table model, which doesn't require the labor and financial costs required to set up numerical solutions to groundwater flow that usually are used to answer more complex problems than relative water table position in a landscape.

The model was sensitive to DEM resolution in both the resulting water table surface, and in the delineation of surface flow pathways. The model operates as an essentially steady state representation of the surficial aquifer based on long-term aquifer recharge information. The sensitivity of the model is entirely dictated by the choice of h_0 and K, where K essentially adjusts the bend in the water table profile and ho

dictates the initial water table height the model starts with, and is a topic studied in previous theoretical evaluations of Dupuit's equation (Bresciani et al., 2014; Leray et al., 2019) where it is acknowledged as a limitation to its use. We have similarly shown the sensitivity of both parameters when comparing model results with long-term groundwater records (Figure 3.10). Model performance is most sensitive to h_0, while adjusting K minimally changes the resulting water table surface at a watershed-scale. Appropriately estimating porosity in the calculations of is a similarly important when calculating t_{unsat} and t_{sat}. Evaluating the resulting travel time distributions from the full range of porosity estimates found in literature (Table 3.2), we find mean t_{unsat} times ranging from 0.97 years at the lower end of porosity estimates, to 3.13 years at the upper end. Comparably, mean t_{sat} times ranged from 2.52 years at the low end of porosity estimates to 8.07 years at the upper end of the range of porosity values

3.5 Conclusion

This topographically-based, GIS-driven two-dimensional model of steady-state water table position, based on the one-dimensional solution to Dupuit's equation for flow in a phreatic aquifer requires minimal parameterization and no mesh-generation. The only required variables are the hydraulic conductivity (which can be varied spatially) and the depth of the aquifer below the stream valley. This model is intended to be used as another tool in groundwater hydrology, and not as an alternative to more sophisticated and complex mesh-based groundwater models that are typically used to determine more than just predicting water table position across a landscape. It can serve as a tool that academic, industry, and government workers with a baseline background in GIS, hydrology, and geology can use to guide further investigations into groundwater flow and to understand solute transport and watershed function.

Context is key in application of this model. We show that it can work well in most of the watershed but the resulting water table becomes unrealistically high when you a dense drainage network comes together (i.e. WS B and portion of WS C), and also when coarser resolution DEMs are used. Considerations must be made to a number of parameters to appropriately use this model. DEM resolution can alter network distances used to drive water table calculations and that can alter subsequent calculations of groundwater travel times. Differences in how bottom boundary conditions are conceptualized will influence groundwater travel time estimates, as well as any potential application to use this model to estimate groundwater storage in the vadose and saturated zone due to changes in storages and hydraulic turnover time.

We utilize the model output to estimate groundwater travel times and answer questions related to solute transport at two long-term research watersheds which have been used to evaluate the environmental impacts of short rotation woody crop plantations. Using the outlined model, we estimated median total groundwater travel times of 4.9 years, which is within the time frame of our monitoring of groundwater and stream NO_3^-– N concentrations. The distribution of total groundwater travel times for both Watershed C and B were long-tailed and decayed exponentially. These distributions of total travel times range from less than a day near riparian zones, to upwards of 75 years for portions of each watershed near internal drainage divides, or in upper sections of catchments.

Figures

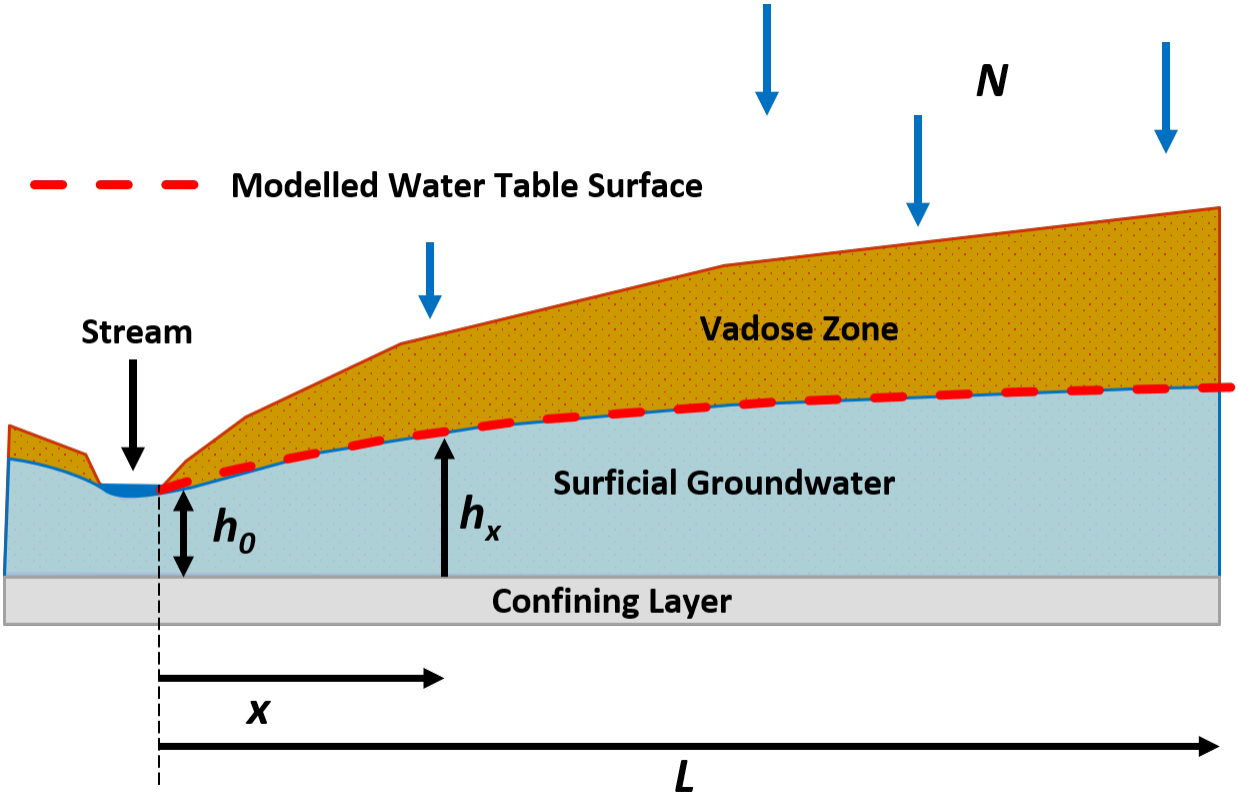

Figure 3.1: Hillslope slice depicting Dupuit formulation used in Equation 2.

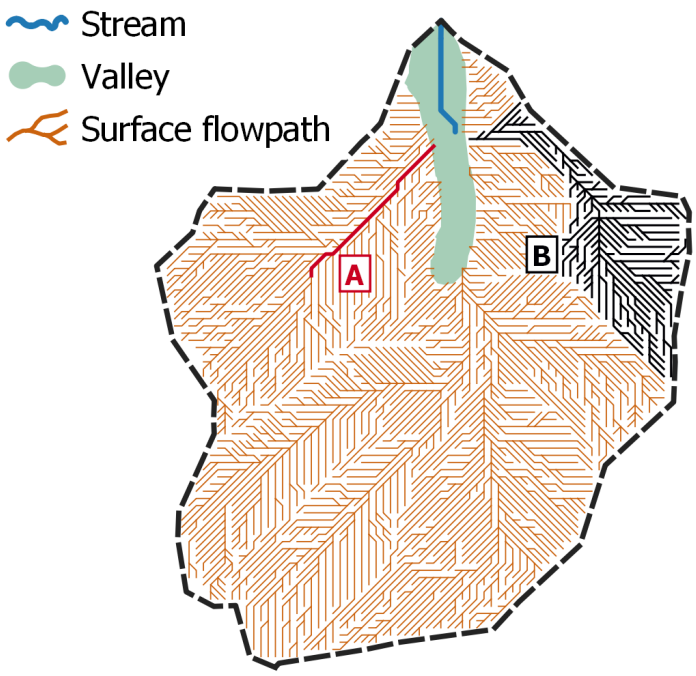

Figure 3.2: Planform of watershed drainage network, highlighting a simple subnetwork in A, and more complicated subnetwork in B.

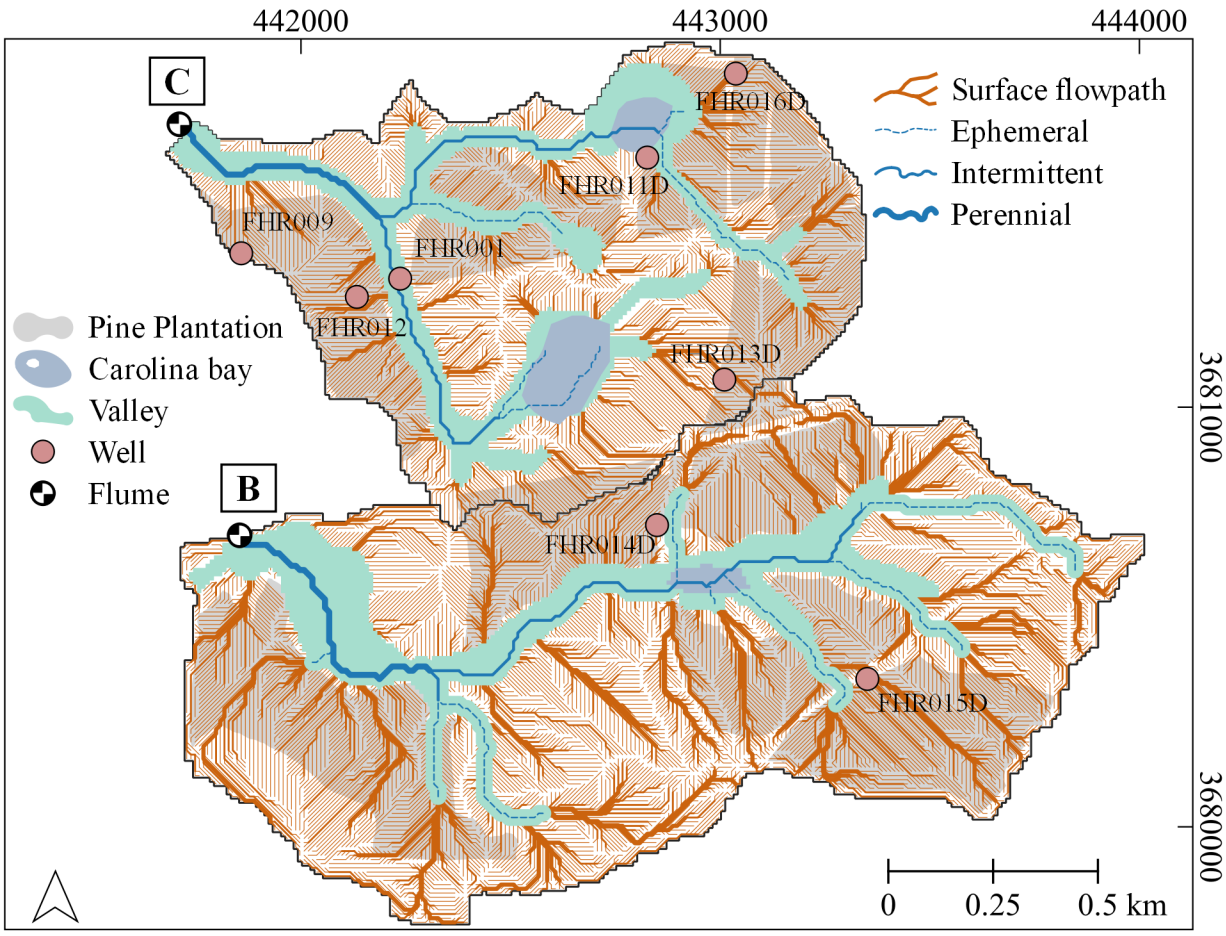

Figure 3.3: Planform view of Watersheds C and B, displaying the valley, Carolina bay wetlands, wells, and managed young pine plantations. Streams in the water and the surface flowpaths describing the topographic flow of water on site are also displayed.

<table>
<tr><th>Age</th><th colspan="3">Lithostratigraphy</th><th colspan="3">Hydrostratigraphy</th></tr>
<tr><td>Miocene</td><td>Hawthorn</td><td colspan="2">Altamaha (Upland Unit)</td><td rowspan="4">Surficial Aquifer</td><td rowspan="8">Upper Three Runs Aquifer</td><td rowspan="11">Floridan Aquifer System</td></tr>
<tr><td rowspan="10">Eocene</td><td rowspan="4">Barnwell</td><td colspan="2">Tobacco Road</td></tr>
<tr><td rowspan="3">Dry Branch</td><td>Irwinton Sand</td></tr>
<tr><td>Twiggs Clay</td><td>Tan Clay Aquitard</td></tr>
<tr><td>Griffins Landing</td><td rowspan="3">Barnwell-McBean Aquifer</td></tr>
<tr><td colspan="2">Clinchfield</td></tr>
<tr><td rowspan="3">Orangeburg</td><td colspan="2">Tinker/Santee</td></tr>
<tr><td colspan="2">Warley Hill</td><td>Green Clay Aquitard</td></tr>
<tr><td colspan="2">Congaree</td><td rowspan="2">Gordon Aquifer</td></tr>
<tr><td rowspan="3">Black Mingo</td><td colspan="2">Fishburne/Fourmile</td></tr>
<tr><td>Paleocene</td><td colspan="2">Snapp/Williamsburg</td><td rowspan="2">Crouch Branch Aquitard</td><td rowspan="2">Meyers Branch Confining System</td></tr>
<tr><td rowspan="2">Cretaceous</td><td colspan="2">Ellenton</td></tr>
<tr><td rowspan="2">Lumbee</td><td colspan="2">Steel Creek/Peedee</td><td rowspan="2">Crouch Branch Aquifer</td><td rowspan="2">Dublin-Midville Aquifer System</td></tr>
<tr><td colspan="2">Black Creek</td></tr>
</table>

Figure 3.4: Lithostratigraphic and hydrostratigraphic units at the Savannah River Site, South Carolina, adapted from Aadland et al. (1995), Gellici et al. (1995), and Rasmussen and Mote (2007).

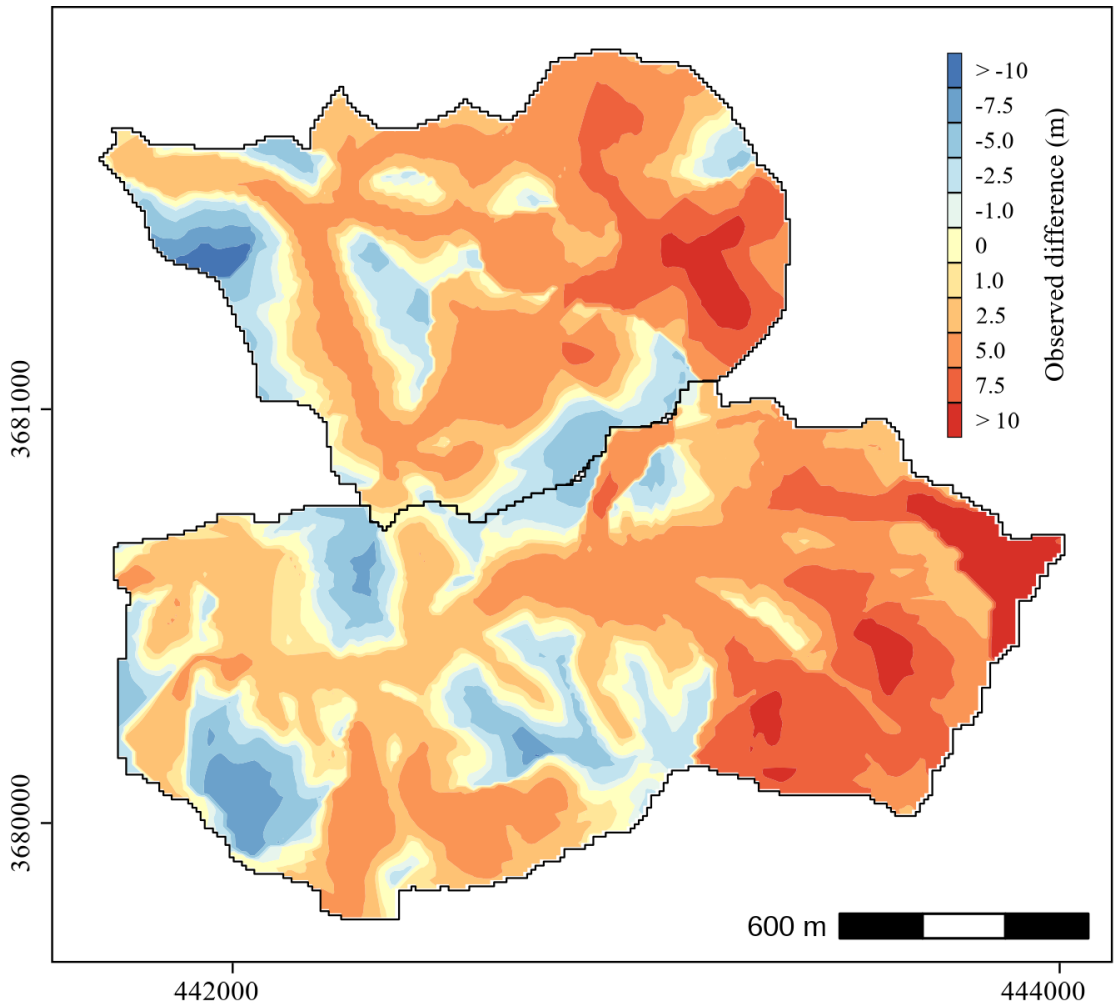

Figure 3.5: Comparison of simulated WTD from Zell and Sanford (2020) and the Dupuit model. Observed difference is between the simulated water table surface from Zell and Sanford (2020) compared with our simulated water table surface using standard model conditions. Negative values indicate our predicted water table position is lower than Zell and Sanford (2020), positive values indicate our predicted water table is higher than Zell and Sanford (2020).

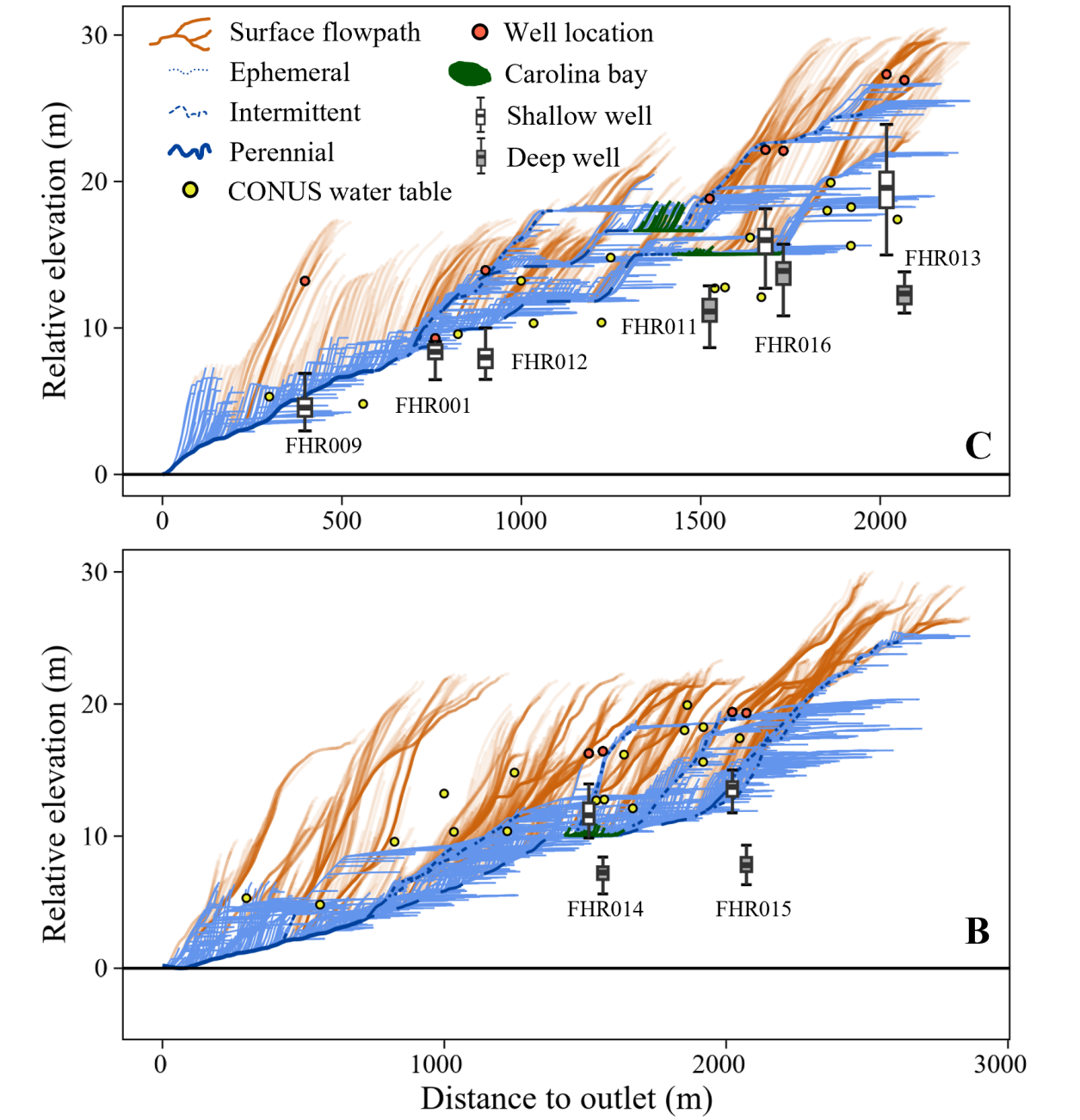

Figure 3.6: Longitudinal profile of Watershed C and Watershed B. Surface flow pathways are displayed, with the predicted water table surface from equation (4) shown beneath those pathways. Perennial, intermittent and ephemeral stream reaches are displayed, as are Carolina bay/wetlands within the landscape. Well positions on the surface are shown as red circles. Boxes represent the interquartile range (IQR) for each well, with the bar indicating the median. Whiskers represent 1.5 times the upper and lower limits of the IQR. Estimates of water table position for each pixel generated by the Zell and Sanford (2020) CONUS water table model are displayed as yellow circles.

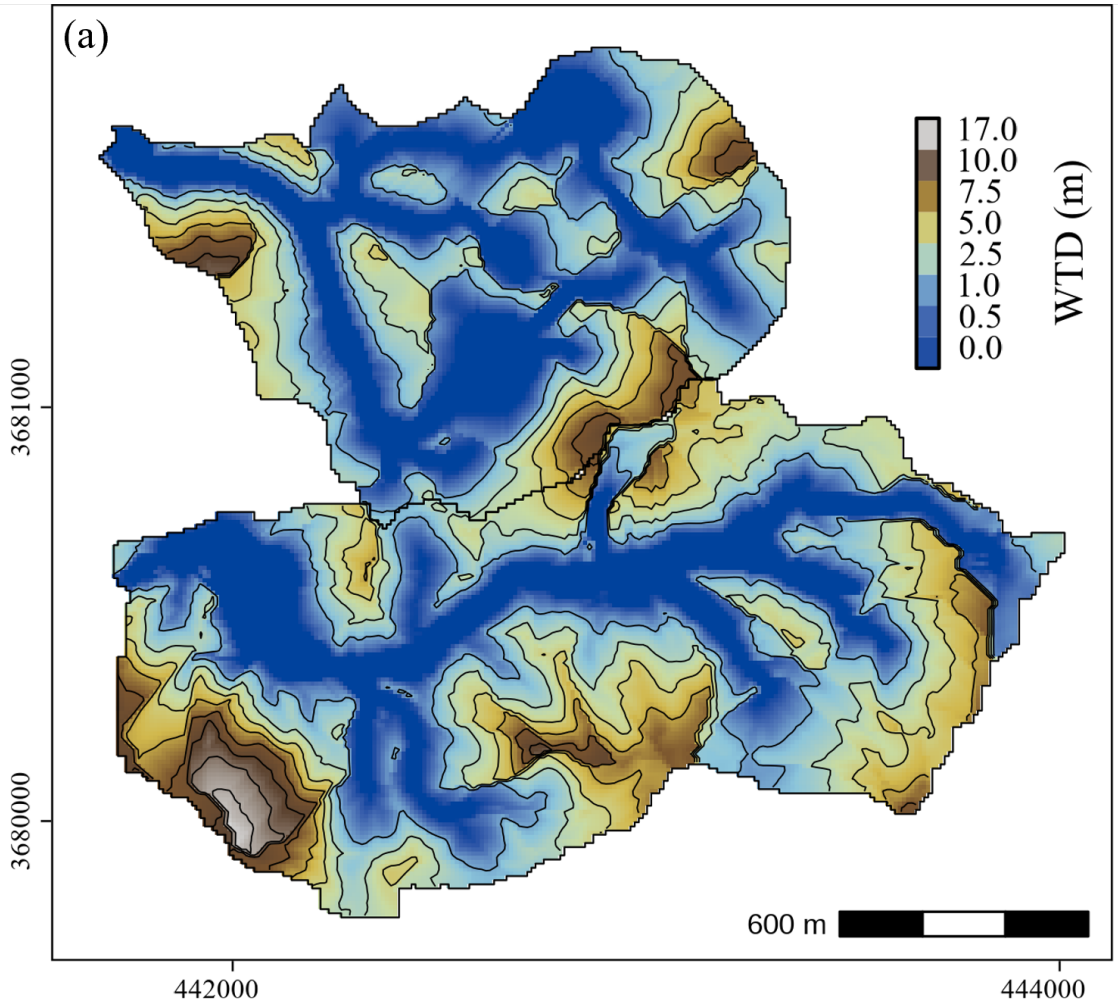

Figure 3.7: Planform maps of Watersheds B and C showing (a) Predicted water table depth (WTD) (m) using a 10 m resolution DEM and a flat bottom boundary condition.

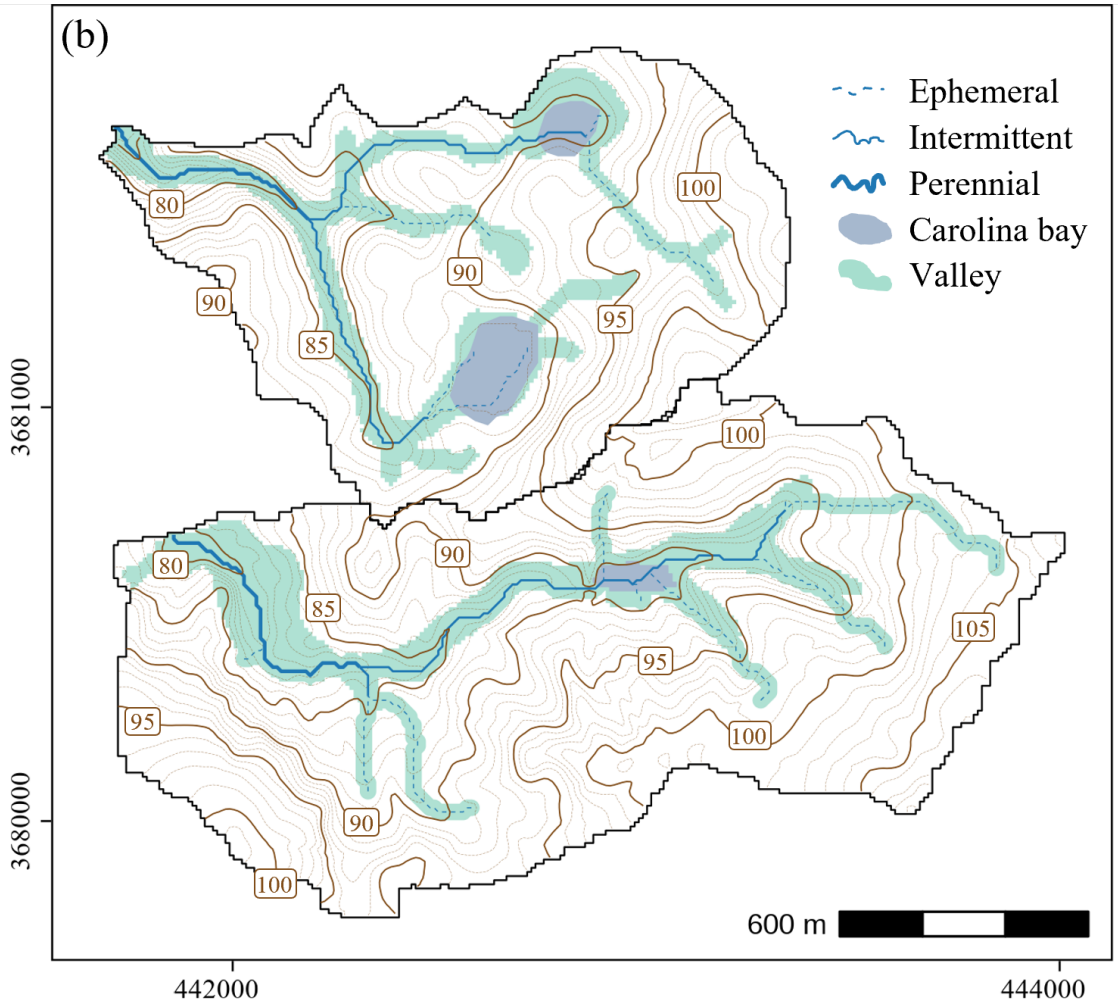

Figure 3.8: Planform maps of Watersheds B and C showing (b) topographic map showing hydrography and elevation contours at 5-m intervals

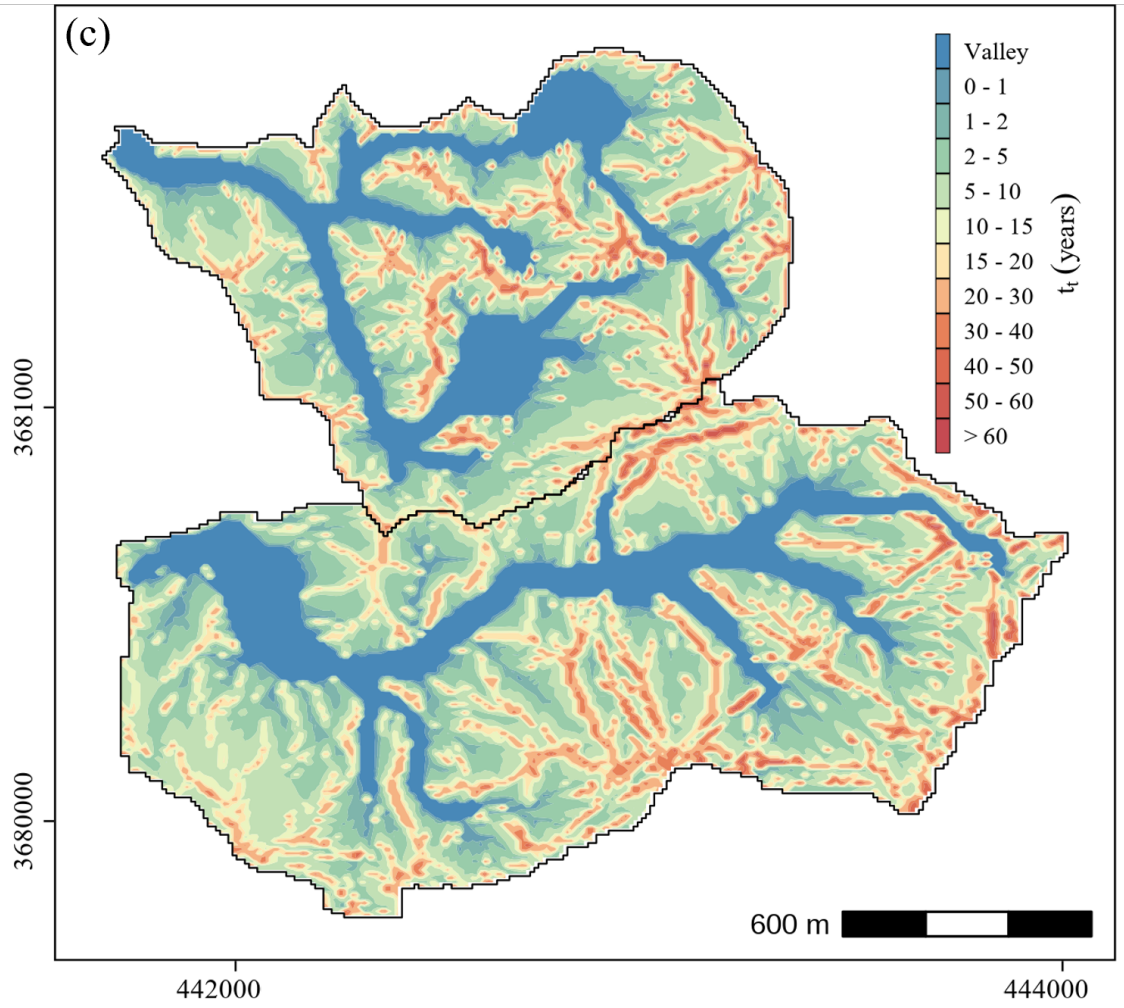

Figure 3.9: Planform maps of Watersheds B and C showing (c) predicted total travel times t_t in years.

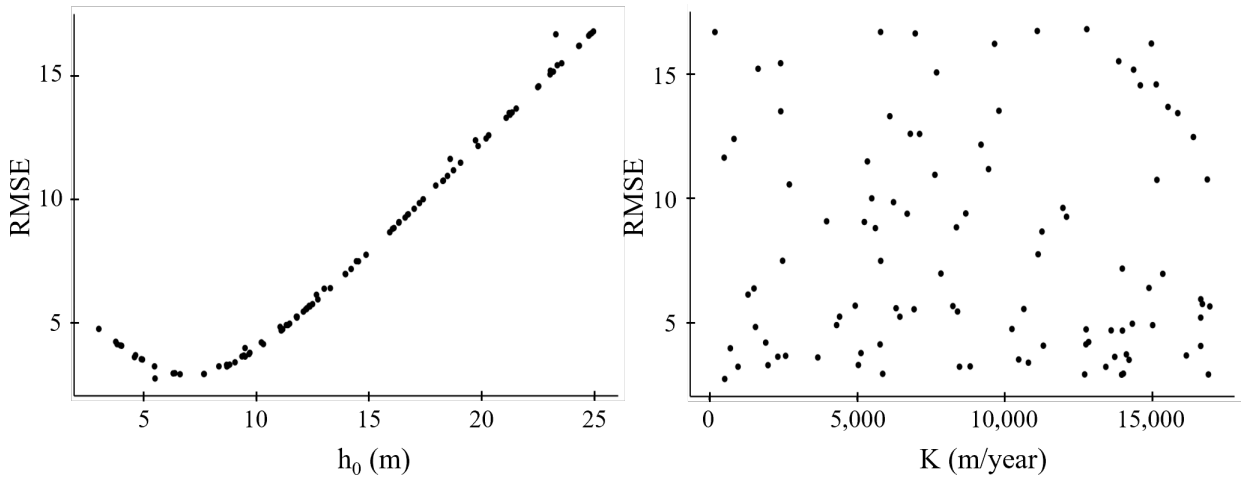

Figure 3.10: Sensitivity of model parameters to initial water table height (h_0) and hydraulic conductivity (K). Difference between long-term groundwater records model realizations using unique combinations of K and h_0 generated through Monte Carlo techniques are displayed. Differences between long-term groundwater records and model output are presented as root-mean-squared error (RMSE).

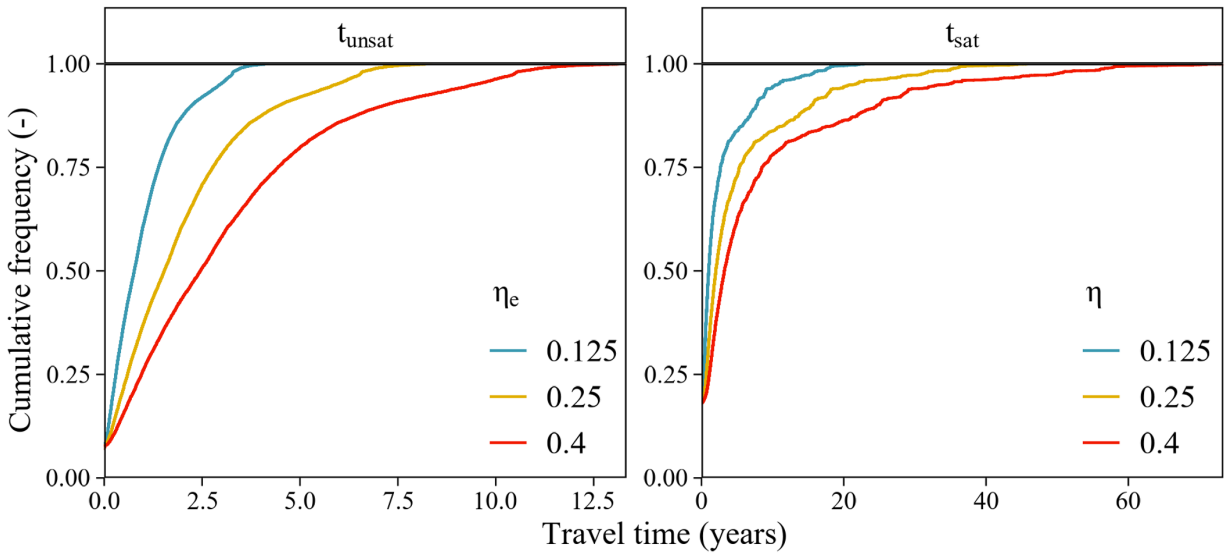

Figure 3.11: Cumulative travel time distributions in Watershed C are shown for a variety of effective (η_e) and total porosity (η) estimates.

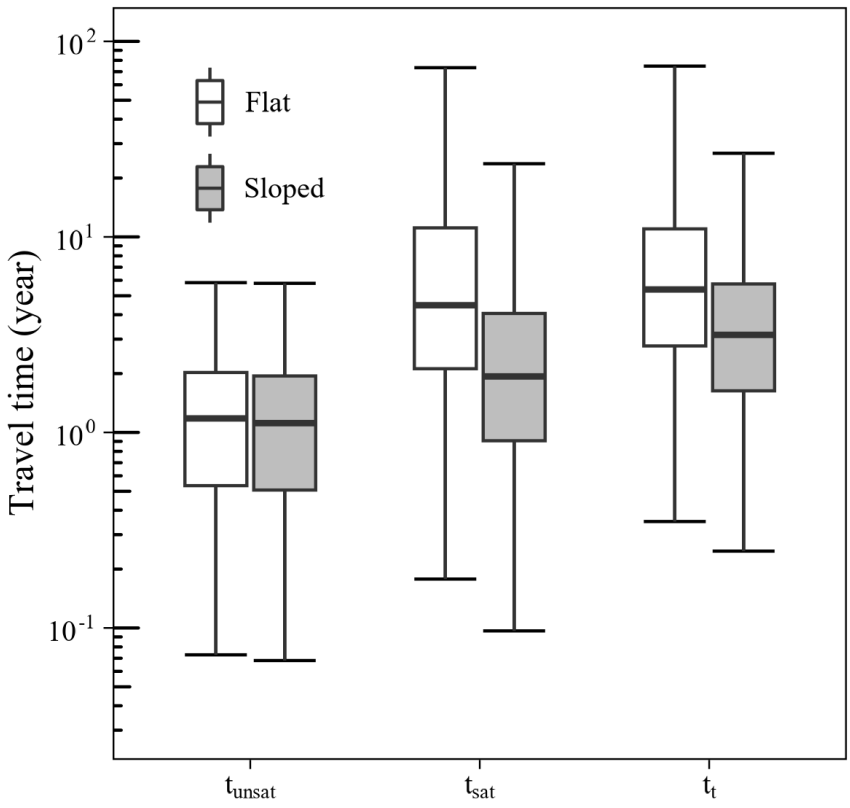

Figure 3.12: Travel time estimates in Watershed C using a 10 m resolution DEM under the two different representations of bottom boundary conditions, flat and sloped valley bottoms.

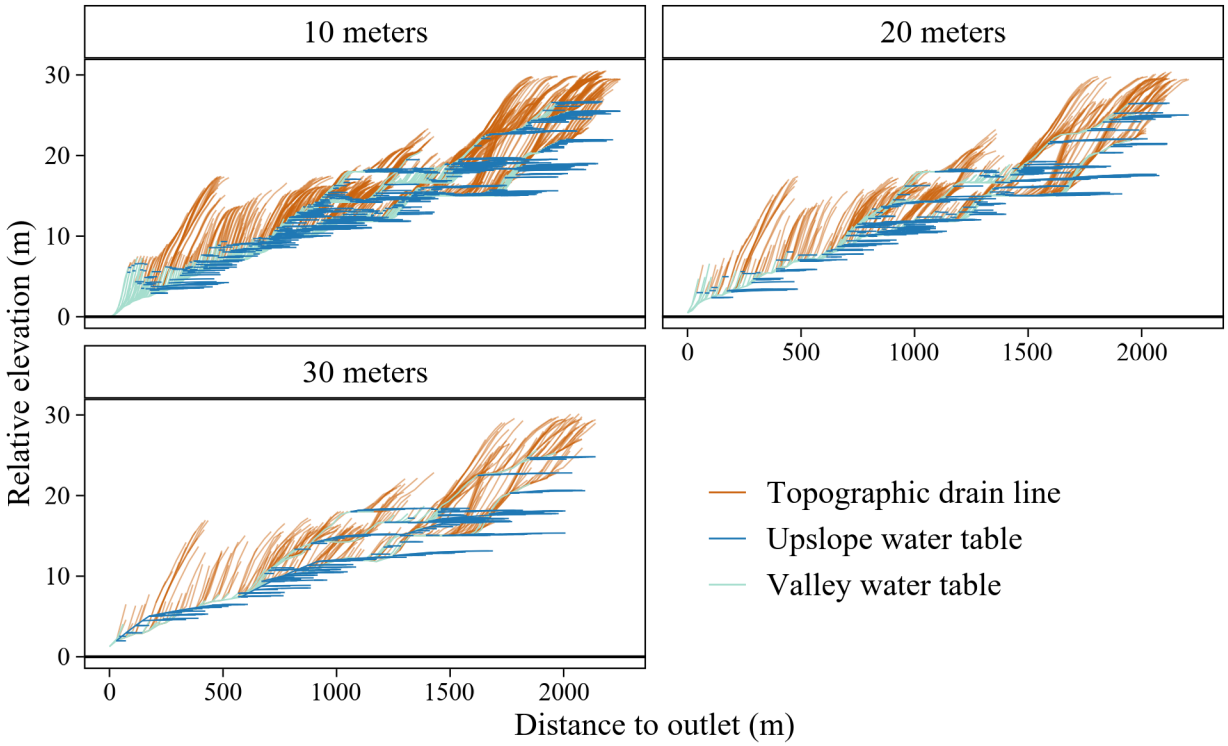

Figure 3.13: DEM resolution impacts on surface flowpath delineation and Dupuit model output using a flat bottom boundary condition in Watershed C.

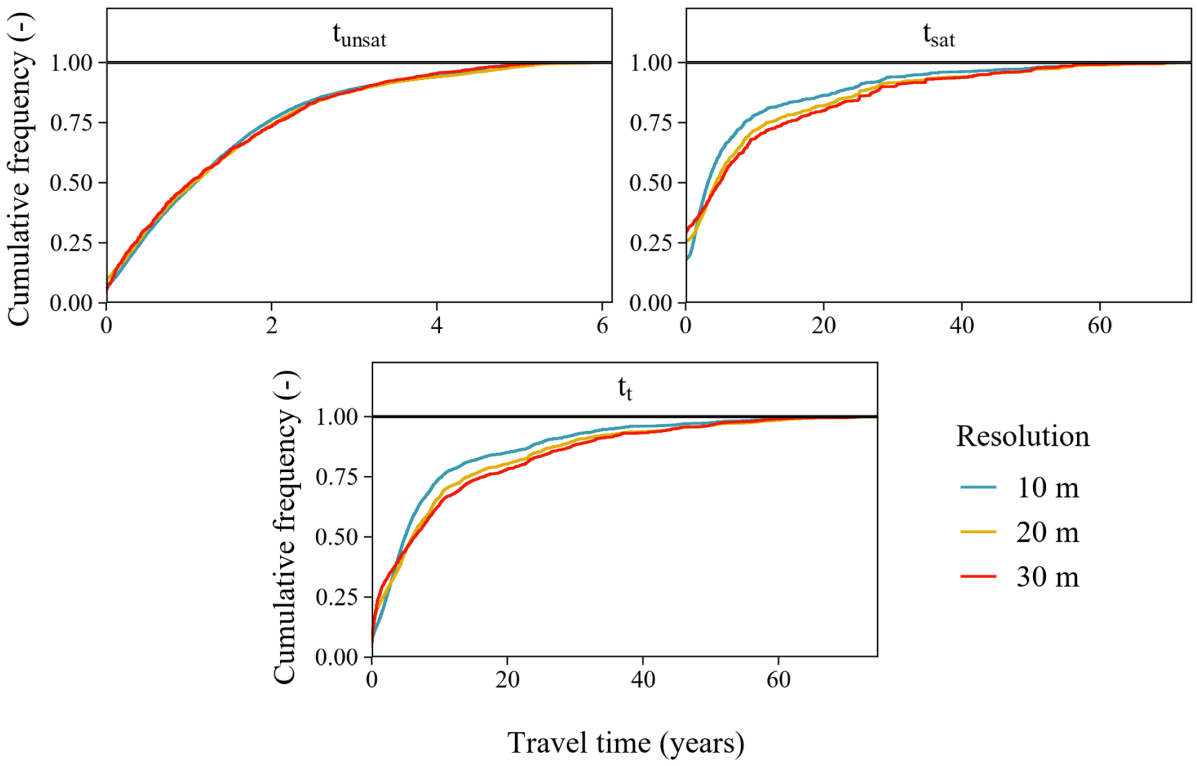

Figure 3.14: Cumulative travel time distributions in Watershed C are shown for 10, 20, and 30 m DEM resolutions.

Tables

Table 3.1: Estimates of precipitation (P), evapotranspiration (ET), and recharge in Upper Fourmile Creek on an annual scale.

	P (mm/yr)	**ET** (mm/yr)	**N** (mm/yr)
Kilgo and Blake (2005)	1225	1448	-
Caldwell et al. (2018)	1143	304; 996; 698; **(666)**	839; 147; 445; **(477)**
Aadland et al. (1995)	1194	813	381
Haitjema and Mitchell-Bruker (2005)	1220	1400	-
Griffiths et al. (2019)	992; 1109; 1088; 1538; 1205; 1280; 1187; 1415; **(1227)**	540 – 794 **(667)**	-
Vache et al. (2021)	1225	800	-
Mean	**1217**	**866**	**351**

Table 3.2: Estimates and variability of model parameters used in Equation 3.2 and Equation 3.7.

Parameter	Notation	Unit	Range	Source	Model Parameter
Aquifer characteristics					
Hydraulic Conductivity	K	m/yr	8.76 – 17,355	Aadland et al. (1995) Gellici et al. (1995) Flach et al. (1999) Rasmussen et al. (2003) Haitjema and Mitchell-Bruker (2005) Jackson et al. (2016) Meles Bitew et al. (2020)	4,000
Effective Porosity	η_e	–	0.125 – 0.25	Aadland et al. (1995) Gellici et al. (1995) Meles Bitew et al. (2020)	0.175
Total Porosity	η	–	0.25 – 0.41	Aadland et al. (1995) Gellici et al. (1995) Meles Bitew et al. (2020)	0.35
Aquifer recharge	N	m/yr	0.15 – 0.84 (0.35)	Aadland et al. (1995) Haitjema and Mitchell-Bruker (2005) Kilgo and Blake (2005) Caldwell et al. (2018) Griffiths et al. (2019) Vache et al. (2021))	0.4
Initial water table depth	h_0	m	3 – 25	Aadland et al. (1995) Rasmussen et al. (2003) Rasmussen and Mote (2007)	10
Drainage network characteristics					
Flowpath length	x	m	Variable	–	–
Total upstream flow pathways	L	m	Variable	–	–

Table 3.3: Range, mean ($\bar{x}$), and median (η) estimates of unsaturated (t_{unsat}), saturated (t_{sat}), and total travel times (t_t) in Watershed C and Watershed B from a 10 m resolution DEM and flat boundary condition.

Watershed	t_{unsat} (years)				$_{sat}$ (years)				t_t (years)			
	Min	Max	$\bar{x}$	η	Min	Max	$\bar{x}$	η	Min	Max	$\bar{x}$	η
C	0	5.84	1.36	1.08	0	73.35	8.07	3.33	0	74.73	9.43	4.9
B	0	7.75	1.84	1.57	0	70.97	7.43	2.63	0	72.13	9.27	4.84

Table 3.4: Range, mean ($\bar{x}$), and median (η) estimates of unsaturated (t_{unsat}), saturated (t_{sat}), and total travel times (t_t) in Watershed C at different DEM resolutions and flat boundary conditions.

Resolution	t_{unsat} (years)				t_{sat} (years)				t_t (years)			
	Min	Max	$\bar{x}$	η	Min	Max	$\bar{x}$	η	Min	Max	$\bar{x}$	η
10	0	5.84	1.36	1.08	0	73.35	8.07	3.23	0	74.73	9.43	4.9
20	0	6.12	1.89	1.06	0	72.99	9.87	4.37	0	74.41	11.26	6
30	0	6.13	1.35	1.01	0	69.59	10.4	4.95	0	71.81	11.75	6.3

Chapter 4

Rapid denitrification of nitrate-contaminated groundwater in a low-gradient blackwater stream valley

[1] Raulerson, S.; J.B. Jeffers, N.A. Griffiths, B.M. Rau, C. Matteson, and C.R. Jackson. Accepted by *Biogeochemistry*.

Reprinted here with permission of the publisher.

Abstract

Leaching of excess nitrogen (N) to groundwater in fertilized landscapes can overwhelm natural biogeochemical processes and cause long-term eutrophication of aquatic systems. We investigated N fate and transport from an intensively managed short-rotation woody crop (*Pinus taeda*) plantation through the riparian zone of an intermittent, low-gradient blackwater stream. Fertilization of the *P. taeda* plantation on the uplands resulted in contamination of groundwater with nitrate concentrations between 0.9 – 1.9 mg N L^{-1}. No corresponding increase in nitrate was observed in stream water or shallow groundwater in the riparian zone. Groundwater travel-time modeling predicted that N from near-stream, upland plantation areas should have reached streams during the monitoring period. Two years of measuring N species in well water in contrasting landscape positions (within the plantation, swale, riparian edge, forested hillslope, and valley), indicated rapid nitrate transformation and denitrification within the forested wetland valleys. Denitrification in the shallow groundwater system within the toeslopes and the riparian zone was estimated to have removed >90% of nitrate. These results highlight the importance of riparian zones as pathways for the removal of N and for controlling downstream N loads.

4.1 Introduction

Excessive and inefficient fertilization of managed lands is polluting groundwaters and surface waters and contributing to river, lake, and estuarine eutrophication (Howarth, 2008; Robertson & Vitousek, 2009; Withers et al., 2014; Wurtsbaugh et al., 2019). Of particular concern is the application of inorganic nitrogen (N) fertilizer, and the subsequent role of highly mobile nitrate in surface and groundwater contamination. In many agricultural settings, N is often a limiting nutrient for crop primary production (Gruber & Galloway, 2008). When crop growth is limited due to depleted stocks of reactive nitrogen, N fertilizers can be applied in order to increase crop growth (Galloway et al., 2004; Pepper et al., 2015). When applied in excess, N fertilizer can be transported into surface waterways by groundwater or surface runoff pathways. These elevated N concentrations can lead to eutrophication of waterways, particularly estuaries (Howarth, 2008; Vitousek et al., 2022), and lead to health issues for humans if drinking water is contaminated (Fields, 2004; Robertson & Vitousek, 2009).

The N cycle in terrestrial and aquatic ecosystems includes a denitrification pathway in which heterotrophic bacteria in the presence of organic carbon under anoxic conditions convert dissolved inorganic nitrogen, primarily nitrate, into gaseous forms of N that escape to the atmosphere (Schlesinger & Bernhardt, 2013). Promoting denitrification in riparian zones, wetlands, and small streams is a key aspect of strategies to mitigate N pollution from managed lands (Cooper et al., 2020; Lowe & Keenan, 1997; Lowrance et al., 1997; Lürling & Mucci, 2020; Paerl et al., 2020) and reduce the spatial extent of coastal hypoxia (Rabalais et al., 2007; Rabalais & Turner, 2019; Rabalais et al., 2002). While denitrification provides a way to mitigate elevated nitrate concentrations, when the denitrification process does not come to the end of a full cycle and produce its terminal product (inert N_2 gas), it can release intermediary products, namely nitric oxide (NO) and nitrous oxide (N_2O), which can be hazardous for the environment (Rav-

ishankara et al., 2009; Welsh et al., 2021). A better understanding of riparian denitrification, including identifying spatial "hot spots" and temporal "hot moments", would help in the development of strategies to mitigate N pollution in waterways (McClain et al., 2003; Musolff et al., 2016; Senbayram et al., 2012; Senbayram et al., 2022; Vidon et al., 2010).

Literature reviewing denitrification in the terrestrial environment is extensive (B. Chang et al., 2022; Hill, 2019; Krichels et al., 2022; Sigler et al., 2022), but there are few studies (Groffman et al., 2006; Jahangir et al., 2013; Lowrance, 1992; Lowrance et al., 1995; McAleer et al., 2017; Popp et al., 2020; W. Zhang et al., 2022) quantifying groundwater denitrification, especially at a watershed scale but we know that denitrification rates are often higher in deep groundwater than in surface water, making it important to quantify when assessing impacts at a watershed scale (Seitzinger et al., 2006). This gap in the literature is primarily attributed to the difficulty that comes with measuring groundwater denitrification in-situ, as the process for attributing observed N_2 concentrations to ambient/background/atmospheric vs. denitrification-derived N_2 is complex (Groh et al., 2019; Lenhart et al., 2021).

Groundwater denitrification is driven by multiple factors that are reflected in measures of water chemistry (dissolved oxygen and dissolved organic carbon especially). Shallow, subsurface flow pathways through C-rich, low-oxygen riparian and hyporheic zones, such as those in blackwater systems, provide bacteria potentially ideal conditions for denitrification to occur. However, in-situ studies often find that denitrification rates are site specific (Merill & Tonjes, 2014; Rivett et al., 2008), likely due to differing importance of denitrification drivers from site to site. For example, some studies have found that groundwater denitrification mitigated up to 30% of applied N (Jahangir et al., 2013), while others report a wide range, from 4% to over 70% (T. R. Anderson, Goodale, et al., 2014; T. R. Anderson, Groffman, et al., 2014). Further studies that quantify groundwater denitrification rates in-situ will help to understand these site-specific conditions that drive denitrification and nitrate removal, and the extent to which denitrification can reduce nitrate concentrations in groundwater before reaching surface waters.

Watershed N budgets typically have unaccounted N, in that the amount of N that enters or is added to the system is not reflected in what is measured coming out (Hester & Fox, 2020; Meding et al., 2001; Thompson Tew et al., 1986). This is especially true in watersheds that have been heavily fertilized. Denitrification has long been considered partially responsible, but in-situ rates have not been quantified at a watershed scale to assess whether it helps to close the N budget and account for the "missing N" (David & Gentry, 2000). To this aim, a recent multi-year, watershed-scale study of the environmental effects of a fertilized short-rotation pine plantation observed a similar gap in the N budget (Griffiths et al., 2017; Griffiths et al., 2016), and raised questions as to the importance of denitrification in mediating losses of excess nitrate from the study watersheds.

Here we quantify denitrification rates and monitor water chemistry within an experimental headwater catchment of the Fourmile Watershed at the Savannah River Site (SRS) in the state of South Carolina, USA. This catchment is one of two that were experimentally manipulated to investigate the effects of intensively managed short-rotation pine (*Pinus taeda*) production on water quality (Griffiths et al., 2017). High fertilization rates led to elevated levels of NO_3^- – N within the shallow groundwater for at least 7 years after treatment. In contrast, corresponding increases in streamwater or riparian groundwater nitrate

were never observed within the treatment watersheds, and no clear changes in groundwater, riparian groundwater, or streamwater nitrate were observed in an adjacent reference (unmanaged) watershed. There are three possible explanations for this lack of increase in stream and riparian groundwater nitrate: 1) longer than expected groundwater travel times; however, previous studies (E. Du et al., 2016; Jackson et al., 2014; Vache et al., 2021) indicate median groundwater travel times are 8-10 years, with near stream areas closer to 1-2 years, suggesting that sufficient time has passed for the contaminated groundwater to reach the streams; 2) denitrification in groundwater reduced nitrate concentrations before reaching the stream; 3) nitrate resides in the porewater of the vadose zone. Our objectives were to measure concentrations of gaseous and dissolved nitrogen species including N_2, N_2O, NO_3^-, and total N along the groundwater flow path from the upland plantation, through a topographic swale, to the toeslope, and into the valley, and also compare measurements under an unmanaged forest stand on the other side of the valley.

4.2 Methods

4.2.1 Study site

The study hillslope transect is along a first-order, low-gradient, intermittent blackwater stream that is tributary to Upper Fourmile Creek, Fourmile Creek, and the Savannah River. The basin is contained with the Savannah River Site, a National Environmental Research Park located within the sandhills region of the Upper Atlantic Coastal Plain, South Carolina, USA (Figure 4.1). The study watershed (Watershed C) is one of 3 adjacent experimental watersheds (Watersheds R, B, and C) that have been extensively studied as part of a paired watershed investigation of intensive woody biomass production (Ferreira et al., 2020; Griffiths et al., 2019; Ruzol et al., 2022; Vache et al., 2021). These streams are groundwater-dominated (E. Du et al., 2016; Jackson et al., 2014; Klaus, McDonnell, et al., 2015) and feature low nutrient concentrations (Griffiths et al., 2017) typical of blackwater streams in the region (Jager et al., 2011). Soils are highly permeable, consisting of loamy sand topsoils overlaying sandy clay loam argillic horizons above unconsolidated sands and clays. Annual precipitation on site ranged from 992 to 1538 mm over the long-term study, with an average of 1225 mm (Kilgo & Blake, 2005). Annual evapotranspiration ranges from 304 to 1448 mm over the long-term study, with an average of 866 mm (Caldwell et al., 2018; Kilgo & Blake, 2005). Average annual precipitation during this 2-year denitrification study was 995 mm, with the first sampling year receiving 947 mm and second sampling year receiving 1043 mm.

During 2012, approximately 50% of Watersheds C and B were harvested of mature pines, while Watershed R was left undisturbed. Surrounding the intermittent, low-gradients streams, a minimum 12.5 m undisturbed riparian buffer, but usually wider, was left intact on both sides of the stream channels. Buffer boundaries were marked at the transition from planted pines to bottomland hardwoods, so the buffers included a lowland hardwood overstory with a dense woody and herbaceous understory. Hydric soils characterized the riparian buffer.

Following site preparation and planting of loblolly pine seedlings in February - March 2013, the first fertilizer treatment was applied in April 2013. This first application consisted of 281 kg ha^{-1} of diammo-

nium phosphate (50.6 kg N ha^{-1} and 56.2 kg P ha^{-1}). A second fertilizer treatment occurred in March 2014 using 241 kg ha^{-1} of urea (110.9 kg N ha^{-1}). A third treatment of blended urea and diammonium phosphate was applied in February 2015. The blend consisted of urea at 179.2 kg ha^{-1} (82.4 kg N ha^{-1}) and diammonium phosphate at 134.4 kg ha^{-1} (24.2 kg N ha^{-1} and 26.9 kg P ha^{-1}). The final fertilizer treatment occurred in September 2016 and consisted of 425 kg ha^{-1} of urea (196 kg N ha^{-1}). These fertilizer applications were well in excess of timber industry standards and were designed to push the envelope for assessing best management practice (e.g., riparian buffer) effectiveness. Fertilizer application is summarized in Table 4.1.

4.2.2 Instrumentation

4.2.3 Watershed nitrate measurements

Starting in 2011, 13 separate groundwater wells were installed across Upper Fourmile Creek (Figure 4.1). Watershed R had 3 groundwater wells, Watershed B had 4 groundwater wells, and Watershed C had 6 groundwater wells. These 13 wells were installed in the uplands. Paired shallow (screened sections 13.0 – 19.3 m below soil surface) and deep (screened sections 25.6 – 43.6 m) wells were installed at 2 locations in both Watersheds B (FHR014 and FHR015) and C (FHR013 and FHR016). An additional deep well was installed in Watershed C (FHR011), but without a paired shallow well. Deep wells are identified with a 'D' suffix. All other wells had screening depths between 2.7 to 13.1 m.

Riparian groundwater wells were installed around May 2010. Two wells were installed per watershed near the watershed outlet. Riparian wells were installed in the riparian soils adjacent to stream channels (< 5 m on either side of stream) and screened to collect water 1.7 to 2.0 m below the surface.

Streams were sampled at the outlet of each watershed. Samples were taken adjacent to instrumented H flumes that were monitoring discharge at a 15-minute interval

4.2.4 Denitrification wells

From October 2016 through March 2017, 21 shallow wells were installed at 17 locations in Watershed C for water and gas sampling to estimate denitrification rates (Figure 4.1). These wells were sampled monthly, except when dry, from March 2017 to March 2019 for water chemistry (temperature, pH, specific conductivity (SPC), dissolved oxygen (DO), oxidation-reduction potential (ORP)), dissolved gas concentration (N_2, Ar, and N_2O), and nutrients (total nitrogen (TN), nitrate (NO_3^-–N), dissolved organic carbon (DOC), and ammonium (NH_4^+–N)). Shallow wells consisted of 0.6 m screens attached to a 1.5 m riser and deep wells consisted of a 1.5 m screen attached to 3 m risers. All wells were backfilled with filter packs and the top 20 cm sealed with bentonite. Paired deep wells were installed at 4 locations: W02, W03, W11, and W12. Depth to groundwater and groundwater elevation was recorded at each sampling event (DTG, GW_Z, respectively), and the change in depth to groundwater between sampling events was calculated (ΔDTG).

Wells were placed in transects along different landscape positions of a likely groundwater flow pathway (Figure 4.1). These locations included: on a hillslope within a 4-year-old (at the time of initial sampling) short rotation pine stand ('plantation'), along a drainage swale ('swale'), the boundary edge between the streamside management zone (SMZ) and plantation ('edge'), within the hyporheic zone of an intermittent stream valley ('valley'), and along a forested hillslope within the SMZ ('forest') (Figure 4.1).

Wells were purged 24 – 48 hours before each sampling event to ensure fresh and representative groundwater samples. Three groundwater samples were taken at each well: for N_2 and Ar, N_2O, and for nutrient and dissolved organic carbon (DOC) concentrations. All dissolved gas samples were taken using a peristaltic pump at a rate of 90 mL min^{-1} to minimize ebullition.

4.2.5 Collection and measurement of dissolved gases

Collection and measurement of dissolved gases followed the protocol of comparable studies measuring denitrification (Groffman et al., 2006; Jahangir et al., 2013; McAleer et al., 2017; Weymann et al., 2008; W. Zhang et al., 2022; Zhou et al., 2018). N_2 concentrations were determined using the N_2:Ar method for measuring dissolved N_2 in solution using high-precision Membrane-Inlet Mass Spectrometry (MIMS). N_2O concentrations were determined using gas chromatography.

N_2 and Ar samples were collected by overflowing 12 mL exetainers with sampled groundwater, preserved with 0.2 mL of 50% $ZnCl_2$ solution, and capped with zero headspace. These vials were then inverted in 50 mL centrifuge tubes and stored in ice until returned to the lab. N_2 and Ar samples required no lab processing and were refrigerated between 4 - 7 °C until shipped for analysis.

N_2O samples were collected by overflowing 160 mL glass serum bottles. Serum bottles were then capped with butyl rubber septa and aluminum crimp caps, with zero headspace and stored on ice until sample processing. All N_2O samples were processed in preparation for analysis the next day following each sampling event. An inert headspace equilibration technique (3:1, He:H_2O) as outlined by Jahangir et al. (2012) was used to extract representative headspace samples for each sample to be analyzed for N2O. Two, 2-inch hypodermic needles with stopcocks and silicone tubing attached, were inserted through a rubber septa into the serum bottle. Helium (He) was injected through one needle at 15 – 20 psi, while sample water flowed out the second needle and tubing into a graduated cylinder. As soon as a headspace formed in the bottles, stopcocks were closed and the serum bottles were then placed on a horizontal shaker (140 oscillations per minute) and left for 13 minutes. The sample bottles were then removed from the shaker and left to stand at room temperature for 60 minutes. 15 mL samples of the headspace were then extracted with a 20 mL syringe and injected into evacuated 12 mL exetainers. Until shipment to the analytical lab, headspace samples were stored at room temperature.

4.2.6 Hydrogeochemistry

Following the sample collection for dissolved gases in the denitrification wells, a 500 mL water sample was taken with the peristaltic pump for nutrient analysis. These samples were stored in an acid-washed HDPE bottle and placed on ice for processing and filtration. Immediately after sample collection and

prior to placing samples on ice, all water chemistry parameters (temperature, pH, SPC, DO, and ORP) were measured in-situ using a handheld probe (YSI Quadrocapble ProPlus).

Deep and shallow groundwater wells across each watershed were sampled monthly beginning in September 2011 and riparian wells monthly beginning in May 2010. A bailer was used to fill 500 mL acid-washed HDPE bottles from both the groundwater and riparian wells and immediately placed on ice for processing and filtration. In contrast to other sampling regimes, stream water was sampled weekly for nutrient analysis starting in January 2010. 500 mL acid-washed HDPE bottles were used to sample stream water.

Three samples were taken from each 500 mL aggregate sample: 60 mL sample stored in a HDPE bottle for total nitrogen (TN); 60 mL sample for NO_3^-– N and NH_4^+– N stored in an HDPE bottle; and a 40 mL sample for DOC stored in an amber glass vial. The sample for TN analysis was left unfiltered. The NO_3^-– N and NH_4^+– N sample was vacuum filtered (0.7 μm filter pore size; 45 mm GF/F GE Healthcare Whatman). The DOC sample was filtered and then preserved with 0.1 mL (2 drops) of 6N hydrochloric acid (HCl). TN, NO_3^-– N, and NH_4^+– N samples were frozen (-20 °C) until analysis, and the DOC sample was refrigerated until analysis (4 - 7 °C).

4.2.7 Plantation vadose water

At 3 locations (PV1 - PV3; Figure 4.1) within the plantations of Watershed C, soil sampling below the argillic Bt horizon every meter down to 5.1 m was conducted for the sampling of plantation vadose zone water from December 2019 to January 2020. Soil samples were collected using a combination of hand augers with extensions and through the use of a Giddings Machine 15-SCT GSRPST drill rig with a bucket auger attachment. Soil samples were immediately placed into Ziploc® double zipper freezer bags and stored in ice-filled coolers. In the lab, 12 mL Exetainer® vials (Labco Ltd, Lampeter, UK) were filled with the stored soil samples. Depending on water content, between 7 and 19 vials were filled for each depth sample to ensure enough water was cryogenically extracted for nutrient analysis. Cryogenic vacuum distillation of the residual pore water was completed using an extraction setup based on the design of Koeniger et al. (2011) and Millar et al. (2018). Samples were placed in an aluminum heating block and connected to a second Exetainer vial via a stainless-steel capillary (2.00 × 0.95 mm). This second vial was set in a liquid nitrogen cold trap, and the aluminum block heated to 200 °C, keeping the samples under a baseline vacuum pressure of between 75 - 100 mTorr. Residual pore water was vaporized out of the sample vials and distilled into the collection vial within the cold trap. Samples were then placed back in the freezer until analysis for TN and NO_3^-– N.

4.2.8 Sample analysis

Unfiltered TN samples were analyzed using the combustion oxidation and chemiluminescence detection method (Shimadzu TOC-L CHS/CSN analyzer and Shimadzu TOC-V). Filtered samples were analyzed for NO_3^-– N using the cadmium-reduction method (SEAL Analytical AA3 autoanalyzer and Astoria Pacific AA2), and for NH_4^+– N using the phenol-hypochlorite method (SEAL Analytical AA3 autoana-

lyzer). Filtered and preserved samples were analyzed for DOC concentrations using the high-temperature combustion catalytic oxidation method (Shimadzu TOC-L CSH/CSN analyzer). N_2:Ar samples were analyzed using MIMS as described in Kana et al. (1994) and N_2O samples were analyzed using automated gas chromatography (GC) on a Shimadzu GC-14 GC system for greenhouse gas analysis.

4.2.9 N_2O and excess N_2 calculations

Dinitrogen produced from denitrification was calculated as N_2 in excess of the expected solubility of N_2 in water equilibrated with the atmosphere (Weymann et al., 2008). Dissolved N_2 in excess of water equilibrated with the atmosphere was assumed to be from denitrification occurring in groundwater (Jahangir et al., 2013; McAleer et al., 2017; Weymann et al., 2008). This formulation of $Excess_{N_2}$ (Equation 4.1) was originally derived by Weymann et al. (2008) and has been used in previous in-situ denitrification studies.

$$Excess_{N_2} = Total_{N_2} - EA_{N_2} + EQ_{N_2} \tag{4.1}$$

In Equation 4.1, $Excess_{N_2}$ reflects N_2 in excess of water in equilibrium with the atmosphere, $Total_{N_2}$ reflects the total amount of N_2 that was within the sample, EA_{N_2} reflects the N_2 from the dissolution of excess air, and EQ_{N_2} reflects the amount of N_2 in equilibrium with the atmosphere. Excess N_2 and Ar can dissolve into infiltrating water through the entrapment and dissolution of gas bubbles as water percolates through the unsaturated zone into the saturated zone (Heaton & Vogel, 1981). We estimated the excess N_2:Ar using the known ratios of N_2:Ar ratios present in the atmosphere, compared that with the Ar concentrations within our sample, and then compared that with the measured Ar concentration with water in equilibrium with the atmosphere at the sampling temperature (Equation 4.2) (Heaton & Vogel, 1981; Weymann et al., 2008). EA_{N_2} is calculated from Equation 4.2:

$$EA_{N_2} = (Total_{Ar} - EQ_{Ar}) * \frac{(Atm_{N_2})}{(Atm_{Ar})} \tag{4.2}$$

where $Total_{Ar}$ reflects the total Ar concentration in the sample, EQ_{Ar} reflects the Ar concentrations of water in equilibrium with the atmosphere at a given sampling temperature, and the ratio of Atm_{N_2} to Atm_Ar reflects the known ratio of N_2 to Ar in the atmosphere. Units for all parameters in Equation 4.1 and Equation 4.2 are molar concentrations. $Excess_{N_2}$ was converted to mg N L^{-1} for all subsequent equations.

All forms of N presented below (Equation 4.3 - Equation 4.3) are in units of mg N L^{-1}. We use the combined intermediary (N_2O) and terminal ($Excess_{N_2}$) end products of denitrification (EP) (Equation 4.3), plus the measured amount of NO_3^- in groundwater to estimate the initial amount of nitrate in the system available for denitrification as outlined by Böhlke et al. (2002) and Weymann et al. (2008)(Equation 4.4).

$$EP = Excess_{N_2} + N_2O \tag{4.3}$$

$$N_{initial} = NO_3^- + EP \tag{4.4}$$

Reaction progress is a measure of the progress of the denitrification reaction or the extent to which nitrate is lost via denitrification and is estimated by comparing the products of denitrification to the estimate of initial nitrogen concentrations $N_{initial}$ (Jahangir et al., 2013; McAleer et al., 2017; Weymann et al., 2008). This formulation of RP is outlined by Weymann et al. (2008) and Zhou et al. (2018), and is based on Böhlke et al. (2002).

$$RP = \frac{EP}{N_{initial}} \tag{4.5}$$

Finally, we estimated the amount of incomplete denitrification using Equation 4.6. We compared the ratio of the intermediary denitrification product (N_2O), with the sum of the combined end products of denitrification (EP; Equation 4.3) (Jahangir et al., 2013; McAleer et al., 2017; Weymann et al., 2008).

$$Ratio_{N_2O} = \frac{N_2O}{EP} \tag{4.6}$$

4.2.10 Statistics

We analyzed for differences in nutrients, dissolved gases, and denitrification parameters by landscape position and by sampling event (month). All collected data were tested for normality using a Shapiro-Wilks test. All datasets violated the assumptions of normality ($p > 0.05$), and as a result, only non-parametric statistics were used. Seasonality of dissolved gas, nutrients, and denitrification parameters was tested using a Kruskal-Wallis H test. Seasons were defined as Fall (September - November), Winter (December - February), Spring (March - May), and Summer (June - August). We compared the ranked sums between each landscape position using a Kruskal-Wallis H test. Annual changes of dissolved gases, nutrients, and denitrification parameters were tested using a Kruskal-Wallis H test. In cases where a statistically significant difference occurred ($p \leq 0.05$), we further analyzed relationships using a Dunn test for multiple comparisons.

To analyze relationships between water chemistry parameters, nutrient concentrations, dissolved gas concentrations, denitrification measures, landscape characteristics, and hydrological characteristics, a Spearman correlation analysis was completed. Water chemistry parameters (temperature, ORP, pH, SPC, and DO), nutrient concentrations (DOC, NO_3^-, NH_4^+, TN), and hydrological plus landscape characteristics (DTG, ΔDTG, and GW_Z) were defined as site-specific environmental factors. Denitrification measures consisted of dissolved gas concentrations ($Excess_{N_2}$ and N_2O) and denitrification parameters (EP, RP, and $Ratio_{N_2O}$).

A principal component analysis (PCA) was conducted to investigate the driving factors of denitrification and the importance of denitrification parameters in the variability and correlations of the different drivers of denitrification and how these varied by landscape position. We used all measured and calculated parameters in this analysis and ran separate PCAs by year.

We report adjusted p-values for any post-hoc analysis (i.e., Dunn test). Only complete observations where there were records of all measured parameters were used in statistical tests.

4.3 Results

4.3.1 Watershed nitrate

Prior to the fertilization, a regional drought caused the streams in the reference and both treatment watersheds to go dry. Treatment Watershed B and C were dry from mid-2011 through the summer of 2012 and reference Watershed R was dry from mid-2011 through the spring of 2013. Following the first application of fertilizer in April 2013, nitrate increased in shallow groundwater wells down slope of the application sites in both treatment Watersheds C and B (Figure 4.2). In contrast, groundwater nitrate concentrations in the unmanaged Watershed R decreased or remained at background levels of < 0.5 mg N L^{-1}. In the treatment watersheds, nitrate concentrations increased one to two orders of magnitude to just under 2.0 mg N L^{-1}, still under the EPA drinking water limit of 10 mg N L^{-1}. In contrast, there was no increase in nitrate concentration in riparian groundwater or in stream water in the treatment watersheds over the 7-year period after fertilization (Figure 4.2).

4.3.2 Hydrology and hydrogeochemistry of denitrification wells

Water levels in the denitrification wells were at or near the surface within the valley for most of the study (Figure 4.3). Depth to groundwater and variability thereof increased upslope (Figure 4.3). The temperature of shallow groundwater across all landscape positions varied seasonally and ranged from 9.9 to 22.2 °C, with a median temperature of 16 °C. Groundwater in the swale was cooler than the other positions (Table 4.2). The forest, the only south-facing landscape position, had the highest measured groundwater temperatures. Groundwater in the catchment was relatively acidic, with the pH ranging from 3.7 to 6.9, with a median of 4.54. There was no significant variation in pH by landscape position (α = 0.05).

Groundwater dissolved oxygen varied substantially throughout the year, ranging from <1 mg L^{-1} to 10.18 mg L^{-1}, with a median of 2.03 mg L^{-1}. Median concentrations in the valley (0.92 mg L^{-1}), were significantly lower than concentrations in all other landscape positions (p < 0.001). The highest median DO occurred in the plantation (3.43 mg L^{-1}). Specific conductivity ranged from < 10 μS cm^{-1} to as high as 140.7 μS cm^{-1} with a median of 31.6 μS cm^{-1}. Median conductivity was highest in the swale (39.4 μS cm^{-1}) and plantation (33.4 μS cm^{-1}). Oxygen reduction potential (ORP) ranged from 49.6 to 412 mV with a median of 266.9 mV. ORP was significantly lower (median of 198.2 mV) in the valley than any other landscape position (p < 0.001; Table 4.2).

4.3.3 Nutrient chemistry in denitrification wells

Groundwater NO_3^- – N varied seasonally (χ^2 = 8.39, p = 0.039, df = 3). Concentrations during the Spring were higher than the Fall (p = 0.08), and significantly higher than Winter (p = 0.04).

NO_3^-– N concentrations varied significantly across landscape positions ($\chi^2 = 144.55$, $p < 0.001$, df = 4). NO_3^-– N concentrations in the stream side management zone (SMZ) (valley + forest) were significantly lower than any of the other locations (Figure 4.4a). Median NO_3^-– N concentrations in the valley and forest were relatively similar (0.005 and 0.014 mg L^{-1}, respectively) (Table 4.2). Similarly, NO_3^-– N concentrations in groundwater in the plantation, edge, and swale were similar as well (0.807, 1.261, and 1.123 mg L^{-1}, respectively). However, NO_3^-– N concentrations varied from month to month and well to well, and NO_3^-– N concentrations were observed above the US EPA standard of 10 mg N L^{-1} three times in the plantation (10.5, 10.1, and 10.1 mg L^{-1}) and twice in the edge (16.7 and 11.3 mg Lv). There was a statistically significant reduction ($p < 0.001$) in NO_3^-– N concentrations from Year 1 to Year 2 of monitoring in all topographic locations outside of the SMZ (Figure 4.4a). NO_3^-– N concentrations of depth-integrated samples of plantation vadose water during Year 2 plotted between NO_3^-– N concentrations in groundwater in the edge and valley locations (Figure 4.4a).

Groundwater TN concentrations also varied seasonally ($\chi^2 = 7.884$, $p = 0.0485$, df = 3). TN concentrations during the Spring were higher ($p = 0.1$) than in the Winter. TN concentrations within the forest and valley were significantly lower than all upslope locations ($\chi^2 = 134.62$, $p < 0.001$, df = 4) (Figure 4.4b). Median concentrations in the valley (0.134 mg N L^{-1}) and forest (0.096 mg N L^{-1}) did not differ. There was a significant reduction ($p < 0.001$) in TN concentrations from Year 1 to Year 2 in all locations outside of the SMZ, as was the case for NO_3^-– N (Figure 4.4b). Like NO_3^-– N, plantation vadose water concentrations of TN plotted lower than the edge wells, but more similar to valley TN concentrations than was the case with NO_3^-– N.

Groundwater NH_4^+– N varied seasonally ($\chi^2 = 10.06$, $p = 0.018$, and df = 3), with concentrations in Spring lower than in the Fall ($p = 0.07$) and Summer ($p = 0.07$).

NH_4^+– N concentrations varied significantly across landscape positions ($\chi^2 = 20.65$, $p < 0.001$, df = 4). NH_4^+– N concentrations in the plantation and valley were significantly greater than in the swale or forest (Table 4.2). NH_4^+– N concentrations were significantly greater in Year 2 than in Year 1 of monitoring at all locations.

Groundwater DOC varied seasonally ($\chi^2 = 12.78$, $p = 0.005$, df = 3). DOC concentrations in the Fall were significantly higher than in the Summer or Spring. DOC concentrations also varied significantly across landscape positions ($\chi^2 = 90.51$, $p < 0.001$, df = 4). DOC was significantly higher in the valley (2.87 mg L^{-1}) than in any other location (Table 4.2). There was no significant change in shallow groundwater DOC from Year 1 to Year 2.

4.3.4 Dissolved gases and denitrification products

Valley and forested hillslope locations had significantly lower concentrations of N_2O than other landscape positions ($p < 0.001$, Table 4.3, Figure 4.5). N_2O was the primary form of reduced nitrogen within Watershed C when compared to N_2 (Table 4.3). Median measures of the Ratio_{N_2O}(Equation 4.6) ranged from 0.56 and 0.64 in the forest and valley respectively, to 0.92 and 0.90 within the plantation and edge respectively. Reaction progress (RP) varied by landscape position (Table 4.3). Median measurements of RP in the valley and forest were high, 0.986 and 0.97 respectively. Measurements outside the SMZ

ranged from 0.58 in the swale, to 0.69 and 0.75 in the edge and plantation. RP outside of the SMZ was significantly lower than inside of the SMZ ($p < 0.001$, Table 4.3)

N_2O was the primary denitrification end product across all topographic positions (Figure 4.5). Median N_2O production in upslope locations was much greater in Year 1 (2.9 – 4.9 mg N L^{-1}) than in Year 2 (1.5 – 2.5 mg N L^{-1}) (Figure 4.5). Median $Ratio_{N_2O}$ increased in the forest from Year 1 (0.45) to Year 2 (0.73) (Figure 4.5).

4.3.5 Correlations and principal components: gases, nutrients, hydrogeochemistry, and hydrology

N_2O concentrations were positively correlated with ORP (0.53), DTG (0.45), and GW_Z (0.55) negatively correlated with DOC (-0.44) and has a strong positive correlation with TN (0.7) and NO_3^-– N (0.78). EP similarly was positively correlated with ORP (0.55), DTG (0.45), and GW_Z (0.56), and negatively correlated with DOC (-0.45), and had strong positive correlations with TN (0.70) and NO_3^-– N (0.79). NO_3^-– N was positively correlated with GW_Z (0.59) DO (0.44), SPC (0.44), ORP (0.59), DTG (0.44), and had a negative correlation with DOC (-0.56). RP was positively correlated with DOC (0.57) and had a negative correlation with DO (-0.47), SPC (-0.44), GW_Z (-0.57), and ORP (-0.53). Looking at scatter plots of N_2O with NO_3^-– N and NH_4^+– N (Figure 4.7), as well as NO_3^-– N with DTG (Figure 4.3), we can see distinct groupings based on landscape position.

During Year 1, the two largest principal components together explained 54.5% of the variation in denitrification and associated parameters (Figure 4.8a). RP, SPC, NO_3^-, and N_2O contributed significantly to PC1 (40.6% of variation), while DO, DOC, NH_4^+, and DTG contributed significantly to PC2 (13.9% of variation). There were distinct differences in landscape position, with the valley and forest separated from the areas outside the SMZ, with similar orientations. The patterns in Year 2 varied from Year 1 (Figure 4.8b). The two largest principal components together explained 41% of the variation between water chemistry, hydrology, and denitrification parameters. RP, NO_3^-, $Ratio_{N_2O}$, and DTG contributed significantly to PC1 (25.9% of variation), while $Excess_{N_2}$, pH, and temperature contributed significantly to PC2 (15.1% of variation). There were again distinct differences by topographic position, with the valley and to a lesser extent the forest grouped away from the positions outside the SMZ. We see that in both years DOC, NH_4^+, and RP differentiate the separation between the SMZ and the rest of the landscape.

4.4 Discussion

4.4.1 Nitrogen gradients along a hillslope

Nitrogen concentrations, speciation, and dynamics differ substantially across topographic positions reflecting differences in biogeochemical controls. In particular, the valley and forest locations are similar to one another and distinct from the fertilized and upslope locations (plantation, swale, and edge). Reductions in nitrogen concentrations from Year 1 to Year 2 could be due to a decrease in the overall fertilizer

signature, though we don't see that in the long-term monitoring (Figure 4.2). Differences in moisture conditions between the years is another possibility to explain the interannual variability of nitrate, though here we have comparable precipitation year to year (947 vs 1043 mm). NO_3^- – N concentrations in valley groundwater (median = 0.807 mg N L^{-1}) were three orders of magnitude less than in groundwater below the plantation (median = 0.005 mg N L^{-1}), and TN in the valley groundwater (median = 0.134 mg N L^{-1}) was one order of magnitude less than in the plantation (median = 0.964 mg N L^{-1}), indicating a substantial loss of N as groundwater moves through the toe slopes and valley. The reduction in NO_3^- – N is likely higher than the reduction in TN because one component of TN is dissolved organic matter which is greater in the valley than upslope positions. We know that nitrate availability is one of the primary drivers in differentiating among landscape positions and is an important component in driving incomplete denitrification (Figures 4.6 - 4.8). Upland locations where fertilizer was applied had higher DO and lower DOC, with much higher ORP values when compared to the valley (Table 4.2). This further supports the observed gradient of nitrate and net denitrification processing across the hillslope and indicated that these parameters are strongly controlled by site-specific environmental factors (e.g., DO, DOC, temperature, pH).

4.4.2 Inhibition of complete denitrification

Nitrous oxide (N_2O), the intermediate product of denitrification, was the dominant form of reduced nitrogen within our study area. High N_2O concentrations may reflect coupled nitrification-denitrification processes or environmental conditions (low DOC, high dissolved oxygen, low pH, low conductivity, short residence times) unsuitable for complete denitrification. We found higher concentrations of N_2O in upland locations. Shorter and intermediate groundwater residence times can be associated with incomplete denitrification reactions, and result in more N_2O production (Jurado et al., 2017; McEachran et al., 2023; Nogueira et al., 2021; Reeder et al., 2018), but our upland locations are still within 150 m of the stream. Based on the close proximity of the denitrification wells to one another and the stream itself, we can speculate that groundwater residence times may not be the driving factor of N_2O production at our site, but it is rather the differences in environmental conditions driving the production of N_2O. In the plantation areas where N_2O production was high, there was higher DO and lower DOC than the valley and forest locations where N_2O production of low.

Environmental conditions ideal for preventing complete denitrification are likely driving high N_2O production. We found that RP was positively correlated with DOC and negatively correlated with DO, conductivity, GW_Z, and ORP. Acidic soil and groundwater are known to prevent complete denitrification, resulting in the production of more N_2O (Jurado et al., 2017; Nagele & Conrad, 1990; ŠImek & Cooper, 2002). The study catchment drains a blackwater stream with relatively low pH (4 – 5). There was not a significant relationship between pH and N_2O, but that is likely due to the narrow range in observed pH values throughout the study. Median pH was 4.5, with 83% of pH measurements falling between 4 – 5. Dissolved oxygen was much lower in the valley than any other landscape position, with median concentrations around 1 mg L^{-1}. Median concentrations in all other locations were between 2.2 and 3.4 mg L^{-1}. Conditions for complete denitrification typically require DO levels to be less than 2 mg L^{-1}

(Jahangir et al., 2013). Higher levels of DO upslope reflect a thicker vadose zone, and with that thicker vadose zone, a greater change in groundwater levels (ΔDTG) between sampling points introducing more air into groundwater. DO was positively correlated with depth to groundwater (DTG) and N_2O. Excess nitrate can limit complete denitrification, as microbes will use nitrate for respiration, instead of further reducing N_2O into N_2 (Jurado et al., 2017; Rivett et al., 2008; Zhou et al., 2018). Low pH in the presence of high levels of nitrate have been shown to inhibit the reduction of N_2O to N_2.

When observations of N_2 fell below that of water in equilibrium with the atmosphere, calculated excess N_2 values were negative. This occurred in 11.3% of potential N_2 samples, even when we set our pumping rate at 90 mL/min to discount the effects of ebullition. These samples were excluded from analysis due to the concerns of degassing and ebullition. Negative concentrations of excess N_2 can reflect degassing or ebullition during pumping. Degassing can occur from oversaturation of dissolved gases from gas producing processes (i.e., denitrification), or by the stripping of N_2 from other gas production procedures like methane. Ebullition during peristaltic pump operation is a concern when using pumping rates over 100 mL/min (Blicher-Mathiesen et al., 1998; Fox et al., 2014; Hester & Fox, 2020; Jahangir et al., 2013; Weymann et al., 2008).

4.4.3 Separating nitrate-reducing processes

Because of the combination of nitrate-reducing processes at play, it is difficult to separate which process is primarily contributing to N_2O production. The measurements of dissolved gases are estimates of net denitrification; we can only look at the driving or inhibiting factors of denitrification to define these different processes among landscape positions.

Transformation of nitrate to ammonium through dissimilatory nitrate reduction (DNRA) will produce N_2O, though typically only when nitrate levels are low (Rivett et al., 2008). Ammonium increased between the SMZ edge and the valley, where nitrate concentrations were lowest. The valley had much higher DOC and lower ORP values, which would benefit the DNRA process. However, ammonium concentrations were not significantly correlated with N_2O, and we did not find increasing N_2O concentrations with ammonium reduction, which would indicate nitrification is occurring in the valley rather than DNRA. There is evidence at our site that N cycling processes (nitrification and denitrification) are driven by seasonal changes to water chemistry, especially with regard to water temperature (Griffiths et al., 2017; Griffiths et al., 2016). Changes to temperature can regulate the availability of microsites for denitrification or nitrification, due partly to changes in oxygen conditions (Griffiths et al., 2016).

Nitrification in the vadose zone could be occurring at the boundary between the unsaturated soil and water table. This process would produce N_2O when ammonium is oxidized into nitrate. In environments with high concentrations of organic matter, high availability of ammonium, low pH, and high oxygen, the potential increases for this process to produce substantial amounts of N_2O (Marchant et al., 2016; Strauss et al., 2002; Wrage et al., 2001). The hydrology and environmental conditions of Watershed C fit those conditions where nitrification can play an outsized role in N_2O production. Further, coupled nitrification-denitrification can occur at the boundary between oxic and anoxic conditions, where there are persistent fluctuations in DO, and a ready supply of DOC and nitrogen.

4.4.4 Comparison to other studies of reaction progress

Higher reaction progress (RP) in the SMZ (valley and forest), corresponded with significant reductions in NO_3^-– N and TN concentrations within these zones. This is evidence of high rates of denitrification occurring within the SMZ, which is converting large loads of nitrate in hyporheic flowpaths of riparian groundwater into N_2O and N_2.

It is difficult to compare these estimates of RP with those of other studies due to differences in methods used to measure denitrification. This applies even to other studies which use the same N_2:Ar technique, as there are site and sample-specific factors to consider (e.g., how recharge temperature was measured, sampling equipment, calculations of atmospheric contributions). These comparisons are also made difficult by differences in how $N_{initial}$ is formulated, some studies are interested in nitrate reduction exclusively, keeping $N_{initial}$ and subsequent RP calculations as Böhlke et al. (2002) first presented which combines NO_3^- concentrations and denitrification end product concentrations to calculate $N_{initial}$. Others have incorporated TN, DON, NO_2, and other forms of nitrogen because of interests in gas production and separating the individual nitrogen reducing processes and intermediary denitrification components. Keeping in mind the differences between studies, there are similar studies which have directly measured $Excess_{N_2}$ and calculated RP as an estimate of in-situ denitrification. Jahangir et al. (2013) quantified denitrification and denitrification gas production in shallow groundwater at four agricultural sites, quantifying $N_{initial}$ based on N_2, N_2O, NO_2, NH_4^+, NO_3^-, and DON. Jahangir et al. (2013) found mean RP of 46% and 77% at sites with low permeability, and 4% and 8% at sites with high permeability, while noting in some of the low permeabilities sites a maximum reaction progress between 97% and 99%. Weymann et al. (2008) calculated RP at four NO_3^- contaminated watersheds in northern Germany using a conservative approach of Böhlke et al. (2002) by coupling it with addition measurements of intermediary denitrification (N_2O). Weymann et al. (2008) reports median RP values ranging from 33% to 68%, with ranges from 0 – 100%. McAleer et al. (2017) measured denitrification in deep and shallow groundwater of two agricultural catchments, one with slate bedrock and the other with a sandstone bedrock using the approach of Jahangir et al. (2013). McAleer et al. (2017) found denitrification reaction progress of 0 – 32% in the slate catchment, and 4 – 94% in the sandstone catchment. Zhou et al. (2018) investigated denitrification rates in three distinct agricultural settings in eastern China using the approach of Böhlke et al. (2002). They found that groundwater denitrification can consume 65 – 83% of leached nitrate. W. Zhang et al. (2022) present reaction progress in terms of N removal efficiency and found that shallow groundwater rates of between 14 – 35%, noting the high variability among sites, and the importance of supplies of carbon and nitrate on the estimate. W. Zhang et al. (2022) modifies the approach of Böhlke et al. (2002) and substitutes TN for NO_3^-. For this study, we found median RP values between 58 – 98.6%, with maximums between 80 – 100%, which is within the ranges reported from the aforementioned studies. Median values of RP in the riparian areas important for nitrate removal were between 97 – 98.6%.

4.5 Conclusions

The maintenance of a forested SMZ encompassing the stream valley and toeslopes supported conditions for the rapid transformation and denitrification of excess nitrate being transported in groundwater a fertilized pine plantation to the adjacent stream. We observed distinct gradients of nitrogen forms across hillslope positions from the pine plantation, downslope to the near-stream valley. Net denitrification was estimated to reduce 97 – 98.6% of nitrate in the shallow groundwater system within the near-stream valley, in contrast with upland locations which were reducing between 58 – 75% of nitrate. Complete denitrification is not occurring at upslope locations due in part to nitrate excess, as well as several environmental factors (e.g., high DO, low pH, large changes in groundwater level) that are likely allowing for N_2O, rather than N_2, production. We see evidence of this at upslope locations where the intermediate product of denitrification, N_2O, contributes between 85 – 92% to the total dissolved gas production, while in the forested valley N_2O only contributes between 56 – 64%.

The presence of a SMZ in this southeastern US Coastal Plain watershed provides an effective buffer in efforts to help mitigate the impacts of excess N fertilizer application, as the C-rich, low DO, warm conditions in the buffer are conducive to biogeochemical processes which aid in the mitigation of N losses to surface and groundwater. Runoff reduction from vegetation, vegetative and microbial uptake of N, dilution and dispersion of N to the vadose and groundwater flow paths, and denitrification are all processes which benefit from the presence of a riparian SMZ (Griffiths et al., 2019; Ice et al., 2010; Merill & Tonjes, 2014). We found that inclusion of an SMZ in the management practices of a SRWC plantation with low N fertilizer-use efficiency (Ferreira et al., 2021) effectively helped protect stream water from N pollution, despite evidence of nitrate concentrations in the surficial aquifer that were much higher than in the stream (Griffiths et al., 2019).

Atmospheric contamination, sample degassing, site-specific environmental conditions, and multiple biological processes and reactions producing gaseous N all add difficulty in measuring denitrification in-situ, as well as comparing denitrification rates between studies. These factors can make it difficult to understand and estimate the extent and magnitude of denitrification occurring from groundwater. Regardless, there is a need to understand and estimate the amount of N removal occurring in groundwater system with consideration to the amount of N-heavy fertilizer that is applied in agricultural settings. Forested riparian buffers were effective at mitigating excess nitrate leaching impacts on surface water, but incomplete reaction progress along the flow path may lead to large N_2O production. Increased N_2O production can be hazardous for the environment, as N_2O is a potent greenhouse gas with a warming effect more than 300 times that of carbon dioxide (CO_2) and a residence time in the atmosphere of over 100 years (Ravishankara et al., 2009; Z. Wang et al., 2017).

Figures

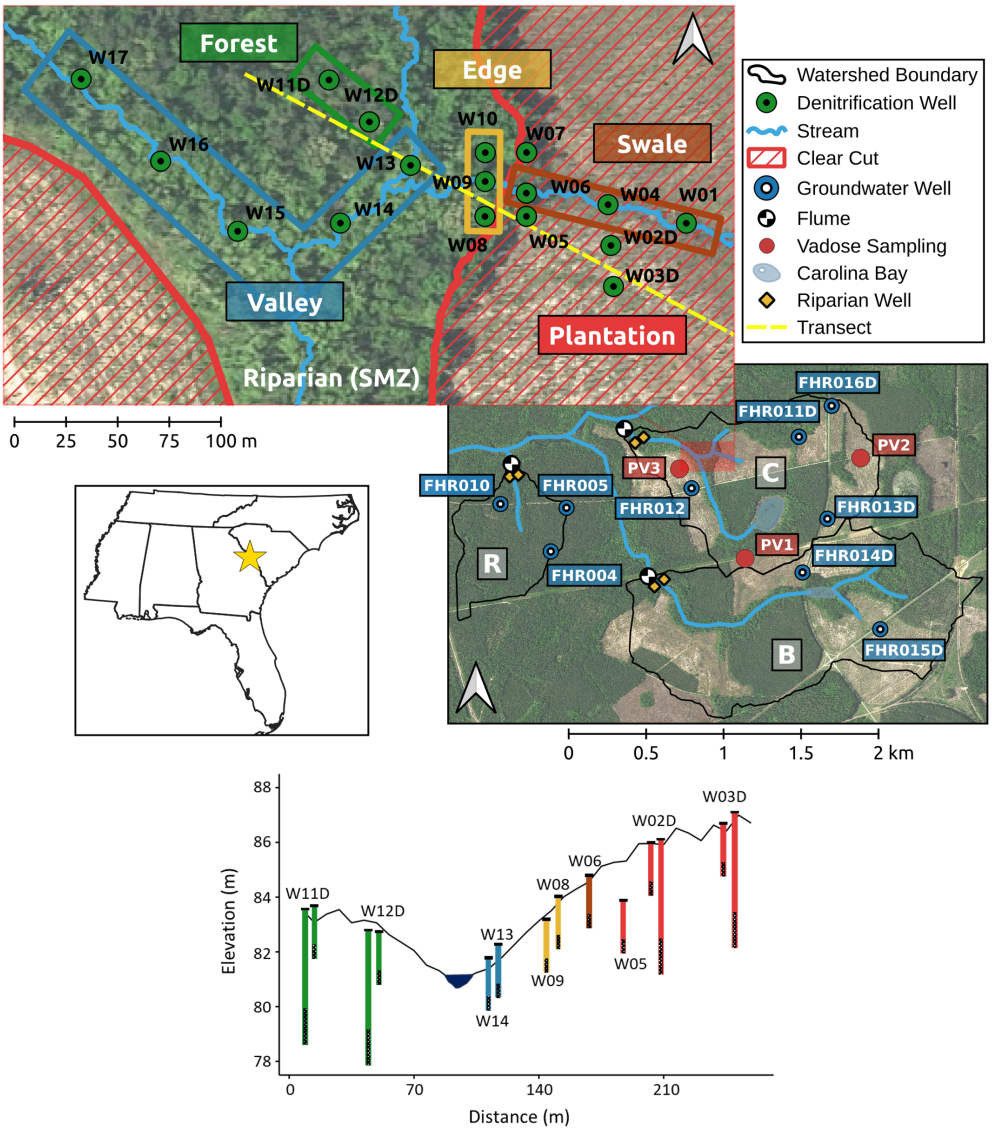

Figure 4.1: Location of Savannah River Site, South Carolina, USA (yellow star; middle left); Upper Fourmile Experimental Watersheds (middle right) showing locations of vadose sampling, groundwater wells, Carolina Bay wetlands, stream flumes, and denitrification well transects (red box); and the denitrification study area in Watershed C (upper left) showing the locations of denitrification sampling wells in the plantation and swale, and edge, valley, and unmanaged forest of the riparian zone. Denitrification study transect and locations of denitrification wells within 12 m of the transect (bottom). Aerial imagery shown is April 2015 NAIP orthophotography.

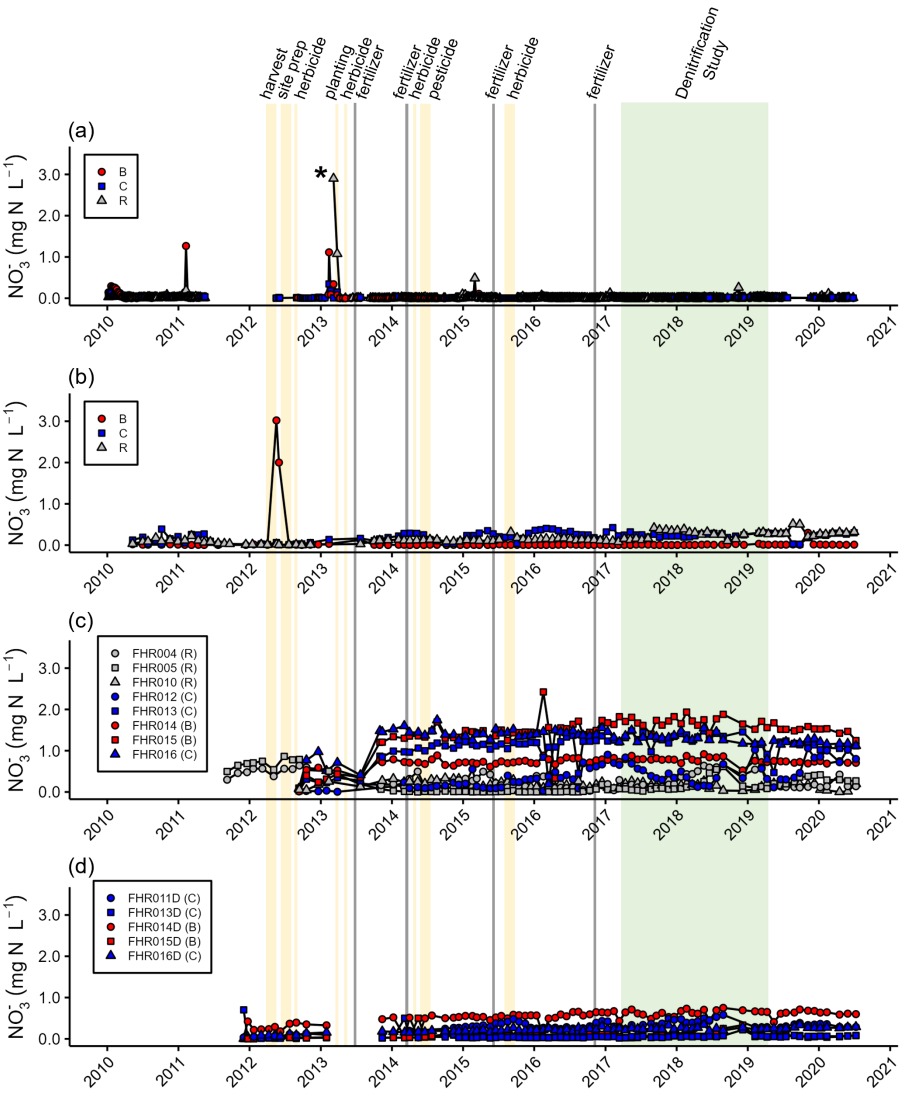

Figure 4.2: Nitrate (NO_3^-) concentrations over time in the study watershed (C) and in an adjacent treatment watershed (B) and reference (unmanaged) watershed (R). Nitrate concentrations are shown for: (a) streamwater; (b) riparian groundwater; (c) shallow groundwater; and (d) deep groundwater. The mean nitrate concentrations from the two riparian groundwater wells on each date are shown in (b). Yellow vertical bars show the timing of various silvicultural practices in Watersheds C and B. Grey vertical bars show the timing of fertilizer applications in Watersheds C and B. Green vertical vars show the measurement period for the denitrification study. Watersheds are identified by color, and individual wells within a watershed are identified by marker shape. The asterisk (*) in (a) reflects a single streamwater sample taken in the reference watershed (R) that measured off the figure scale at 8.4 mg N L^{-1}.

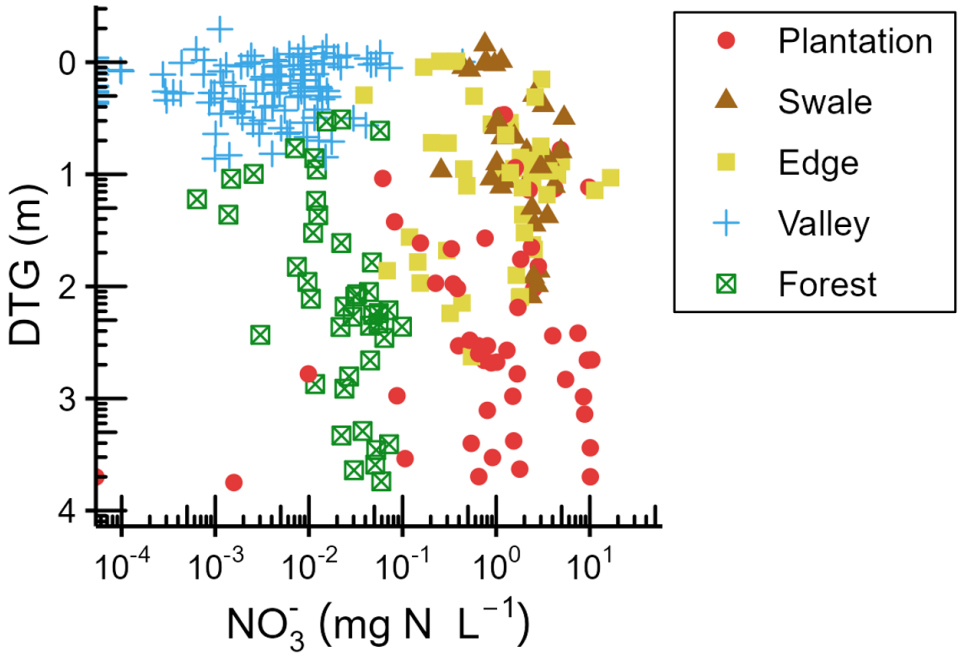

Figure 4.3: Plot of depth to groundwater (DTG) in meters (m) vs. the log of nitrate (NO_3^-) concentrations (mg N L^{-1}). Marker shape and color identify landscape position.

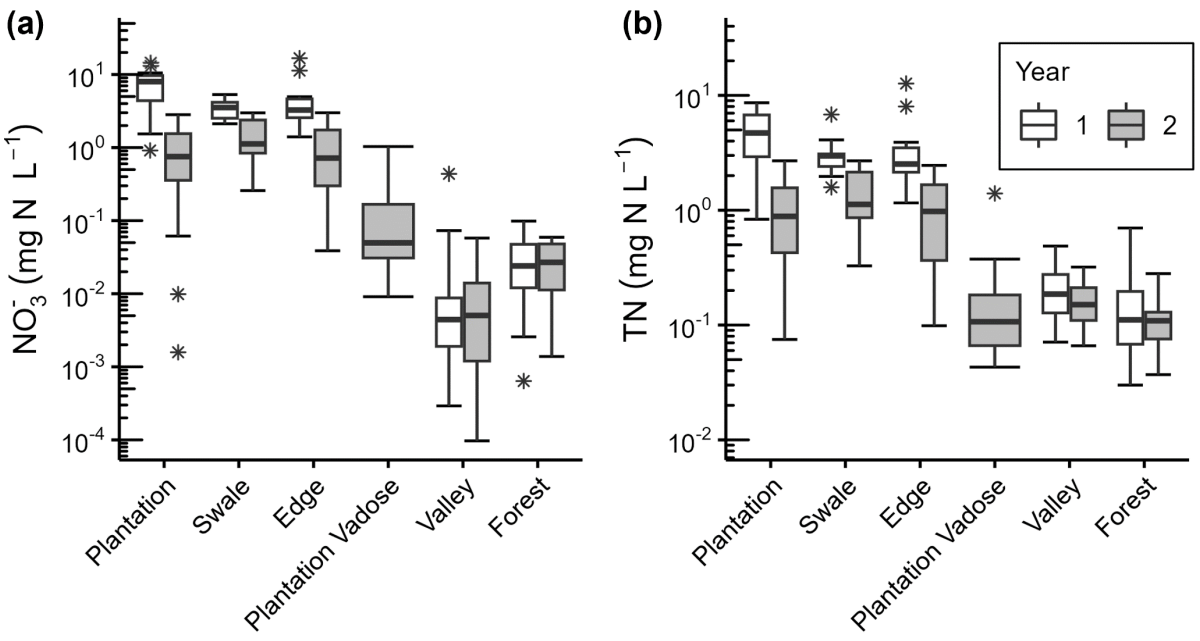

Figure 4.4: (a) NO_3^- – N concentrations by landscape position and sampling year. The y-axis is on a log scale. (b) Total nitrogen (TN) concentrations by landscape position and sampling year. The y-axis is on a log scale. Boxes represent the interquartile range (IQR) for each landscape position and year, with the edges representing the 25th and 75th percentiles. Whiskers represent 1.5 times the upper and lower limits of the IQR. Median values are represented by the bar across the IQR. Outliers are defined as values outside 1.5 times the limits of the IQR. Outliers are marked with an asterisk (*)

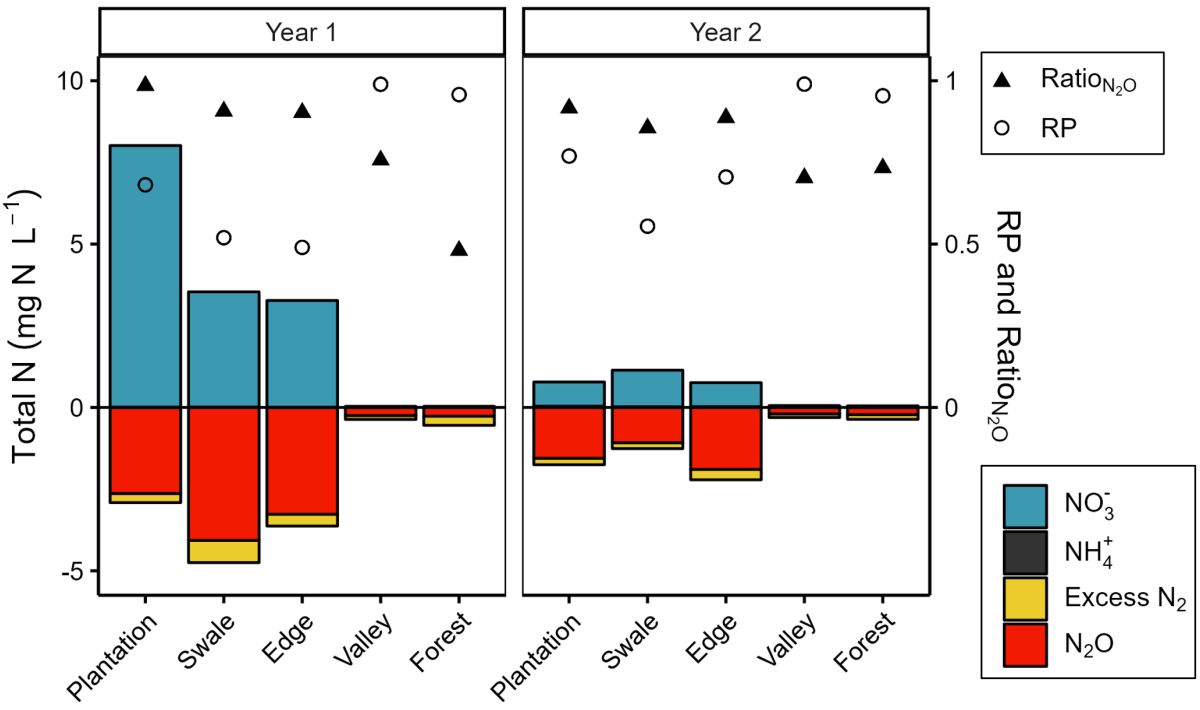

Figure 4.5: Median measurements of terminal Excess$_{N_2}$ and intermediary (N_2O) denitrification end products, as well as NO_3^-– N and NH_4^+– N represented as stacked bars. Reaction progress (RP; Equation 4.5) and the ratio of end products (Ratio$_{N_2O}$); Equation 4.6) are represented by circles and filled triangles respectively, on the secondary y-axis. Denitrification measurements are represented as negative values as they act as nitrogen reduction process.

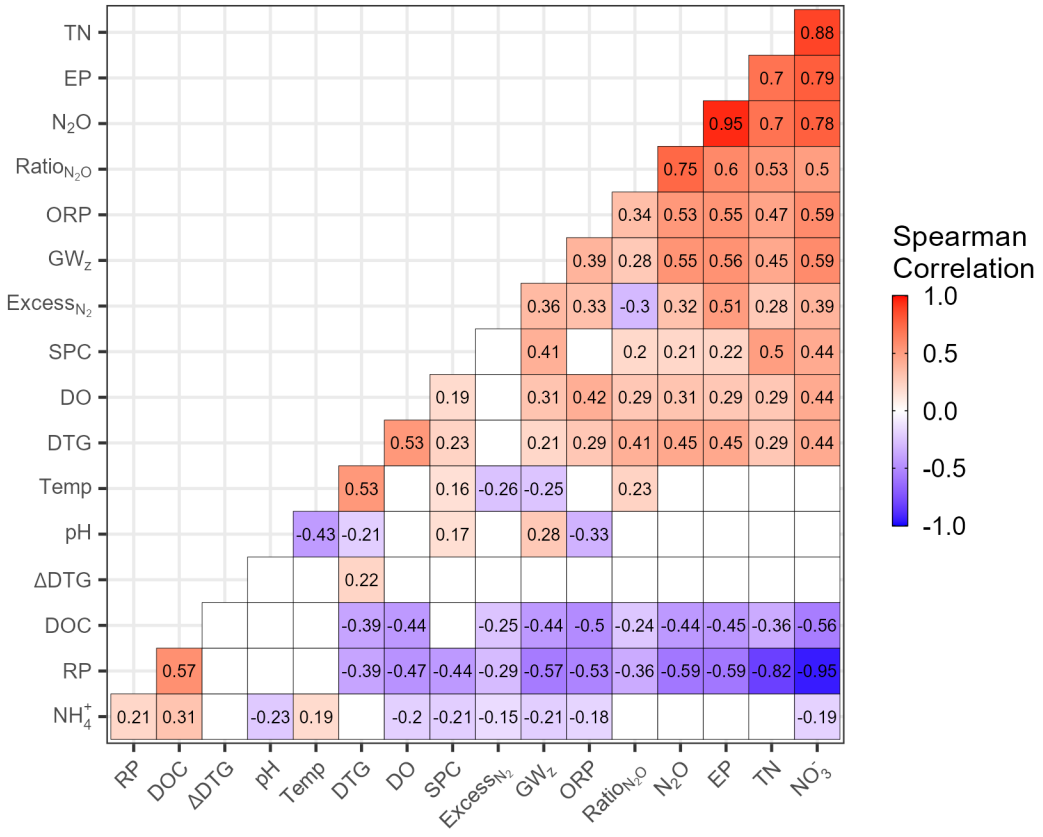

Figure 4.6: Spearman correlation matrix showing significant correlation coefficients ($p < 0.05$). Non-significant correlations are blank ($p \geq 0.05$).

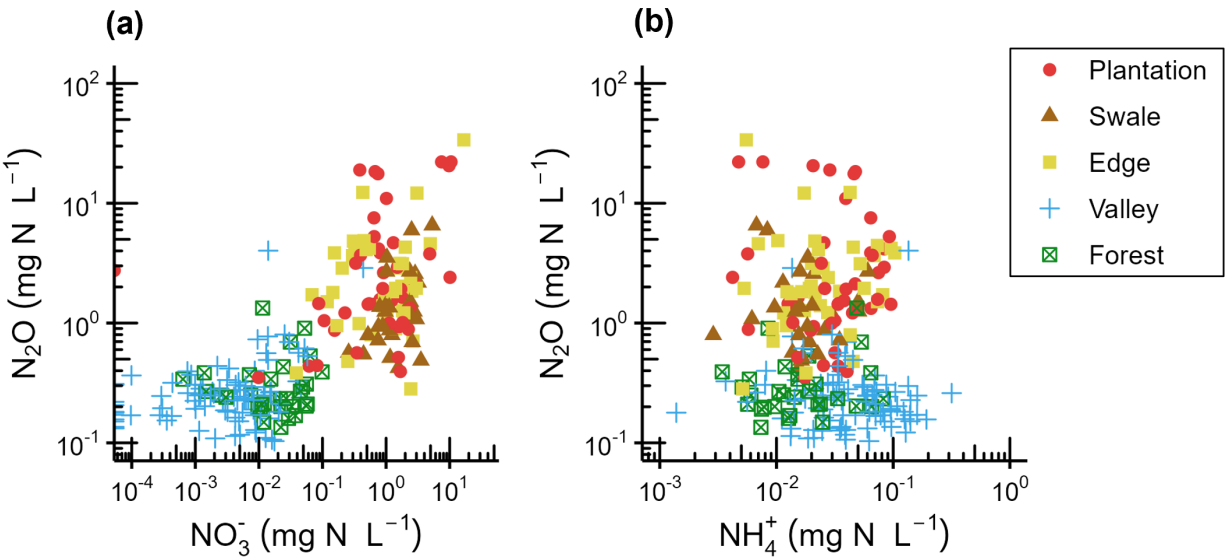

Figure 4.7: Plots of a) nitrous oxide (N_2O) vs. nitrate (NO_3^-) concentrations on a log-log scale; b) nitrous oxide (N_2O) vs. ammonium (NH_4^+) concentrations on a log-log scale. All nutrient and dissolved gas concentrations in mg N L^{-1}. Marker shape and color identify landscape position.

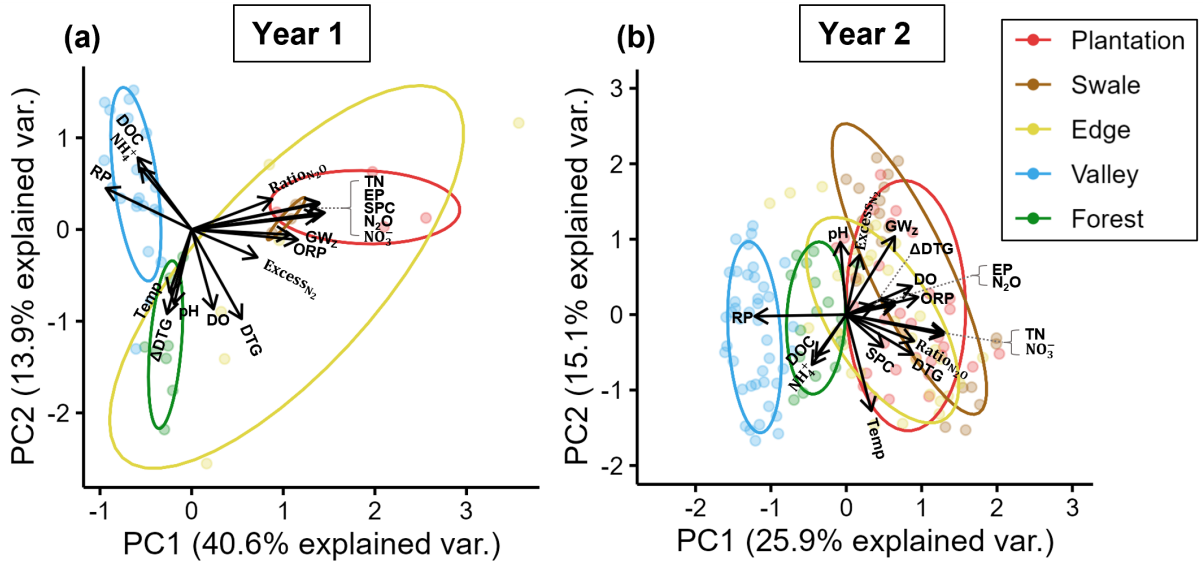

Figure 4.8: Principal component analysis of all measured and calculated parameters (water chemistry, nutrient concentrations, dissolved gas concentrations, and denitrification parameters) grouped and colored by landscape position for Year 1 of monitoring (a) and Year 2 (b).

Tables

Table 4.1: Fertilizer application rates to Watershed C and Watershed B.

Year	Rate of application (kg N ha^{-1})	Total applied (kg N)
2013	50.6	3,173
2014	110.9	6,953
2015	106.6	6,684
2016	196	12,289
Total	464.1	29,099

Table 4.2: Median values of measured parameters within the groundwater of the shallow denitrification wells by landscape position.

	DTG (m)	DO (mg L^{-1})	ORP (mV)	pH	Sp. Cond (μ S cm^{-1})	Temperature (°C)	DOC (mg L^{-1})	TN (mg N L^{-1})	NH_4^+ (mg N L^{-1})	NO_3^- (mg N L^{-1})
Plantation	2.19	3.43	296.1	4.55	33.4	16.2	1.34	0.964	0.034	0.807
Swale	0.58	2.27	301.1	4.75	39.4	13.6	0.98	1.124	0.018	1.123
Edge	0.99	2.2	317.5	4.4	32	16.3	1.02	1.188	0.021	1.261
Valley	0.16	0.92	198.2	4.58	29.8	15.5	2.87	0.134	0.034	0.005
Forest	1.89	2.89	256.8	4.5	29.6	17.5	1.24	0.096	0.015	0.014

Table 4.3: Median, minimum, and maximum measured values for denitrification reaction terminal ($Excess_{N_2}$) and intermediate (N_2O) end products, end product ratio ($Ratio_{N_2O}$), and reaction progress (RP). The number of samples 'n' varied by landscape position based on the number of sampling wells in Figure 4.1 and variation in the number of wells that were dry over time.

Landscape Position	n	$Excess_{N_2}$ (mg N L^{-1})			N_2O (mg N L^{-1})			$Ratio_{N_2O}$			RP		
		Median	Min	Max	Median	Min	Max	Median	Min	Max	Median	Min	Max
Plantation	37	0.23	0.02	0.74	1.92	0.39	22.13	0.92	0.60	0.99	0.75	0.27	0.97
Swale	23	0.26	0.09	0.88	1.25	0.55	6.54	0.85	0.54	0.97	0.58	0.24	0.80
Edge	39	0.32	0.09	0.81	1.95	0.28	33.80	0.90	0.31	0.98	0.69	0.26	0.97
Valley	67	0.14	0.01	0.64	0.23	0.10	4.02	0.64	0.16	0.97	0.99	0.89	1.00
Forest	24	0.24	0.02	0.50	0.25	0.14	1.33	0.56	0.33	0.93	0.97	0.80	0.99

Chapter 5

Conclusion

Representing watersheds and watershed characteristics in a longitudinal space can improve our understanding of watershed structure, connectivity, and behavior. Longitudinal examinations of stream network reveal high variation in the structure of low-order streams and in slope-area relationships. Furthermore, they indicate how geologic discontinuities affect network structure. Longitudinal topographic depictions can improve our understanding of groundwater-surface water interactions, as well as the flow permanence of streams, and increase the value of limited groundwater data. Finally, longitudinal depictions of land use can help researchers quantify and examine the importance of topographic position of developed land uses within watersheds.

A simple, parsimonious, GIS-based, steady-state water table model based on a deterministic 1D equation for groundwater flow can predict water table position, vadose zone thicknesses, and watershed travel times. Using GIS techniques, we apply this quasi-2D model at watershed scales within Upper Fourmile Creek. Sensitivity analysis indicated that model performance in the test watersheds was more sensitive to aquifer thickness below the stream valley than to aquifer-scale hydraulic conductivity. The model captured the range in water table elevations observed spatially and temporally within the test watershed. The model performed better than the CONUS-wide predictions of long-term average water table position generated from the USGS and presented in Zell and Sanford (2020). From the model output, we can see that depending on the location within the landscape there can be up to 30 m of vadose zone storage below the surface. Further, we utilized the model to estimate groundwater travel times and found groundwater travel times were highly right skewed with medians around 4.9 years but the longest travel times reaching 74.7 years.

A two-year study revealed that Toe-slope and riparian denitrification along a low gradient blackwater stream effectively prevented nitrate contaminated groundwater below adjacent pine plantations from reaching the stream. We evaluated denitrification within a series of wells distributed across a topographic gradient along a presumed groundwater flow pathway from the plantation down to the riparian valley. We found evidence that denitrification was reducing 97 – 99% of nitrate in the shallow groundwater system within the near-stream valley, in contrast with upland locations which were reducing between 58 – 75% of nitrate. Complete denitrification was not occurring at upslope locations likely due to site-specific

environmental factor known to control the reactions which reduce N_2O into inert N_2 gas. We see riparian buffers are effective at removing excess nitrate leaching, but incomplete denitrification at upslope sites is of concern because of the role N_2O plays as a potent greenhouse gas.

Bibliography

Aadland, R., Gellici, J., & Thayer, P. (1995). *Hydrogeologic framework of west-central south carolina* (No. 5). South Carolina Department of Natural Resources Water Resources Division.

Adams, J. M., Gasparini, N. M., Hobley, D. E., Tucker, G. E., Hutton, E. W., Nudurupati, S. S., & Istanbulluoglu, E. (2017). The landlab v1.0 OverlandFlow component: A python tool for computing shallow-water flow across watersheds. *Geoscientific Model Development*, *10*(4), 1645–1663. https://doi.org/10.5194/gmd-10-1645-2017

Adams, K. H., Reager, J. T., Rosen, P., Wiese, D. N., Farr, T. G., Rao, S., Haines, B. J., Argus, D. F., Liu, Z., Smith, R., Famiglietti, J. S., & Rodell, M. (2022). Remote sensing of groundwater: Current capabilities and future directions. *Water Resources Research*, *58*(10). https://doi.org/10.1029/2022WR032219

Alber, A., & Piégay, H. (2011). Spatial disaggregation and aggregation procedures for characterizing fluvial features at the network-scale: Application to the rhône basin (france). *Geomorphology*, *125*(3), 343–360. https://doi.org/10.1016/j.geomorph.2010.09.009

Altermatt, F. (2013). Diversity in riverine metacommunities: A network perspective. *Aquatic Ecology*, *47*(3), 365–377. https://doi.org/10.1007/s10452-013-9450-3

Ameli, A. A., Beven, K., Erlandsson, M., Creed, I. F., Mcdonnell, J. J., & Bishop, K. (2017). Primary weathering rates, water transit times, and concentration-discharge relations: A theoretical analysis for the critical zone. *Water Resources Research*, *53*, 942–960. https://doi.org/10.1002/2016WR019448

Anderson, M. P., Woessner, W. W., & Hunt, R. J. (2015). *Applied groundwater modeling: Simulation of flow and advective transport* (2nd ed). Academic Press.

Anderson, T. R., Goodale, C. L., Groffman, P. M., & Walter, M. T. (2014). Assessing denitrification from seasonally saturated soils in an agricultural landscape: A farm-scale mass-balance approach. *Agriculture, Ecosystems & Environment*, *189*, 60–69. https://doi.org/10.1016/j.agee.2014.03.026

Anderson, T. R., Groffman, P. M., Kaushal, S. S., & Walter, M. T. (2014). Shallow groundwater denitrification in riparian zones of a headwater agricultural landscape. *Journal of Environmental Quality*, *43*(2), 732–744. https://doi.org/10.2134/jeq2013.07.0303

Anovitz, L. M., & Cole, D. R. (2015). Characterization and analysis of porosity and pore structures. *Reviews in Mineralogy and Geochemistry*, *80*(1), 61–164. https://doi.org/10.2138/rmg.2015.80.04

Arora, B., Dwivedi, D., Faybishenko, B., Jana, R. B., & Wainwright, H. M. (2019). Understanding and predicting vadose zone processes. *Reviews in Mineralogy and Geochemistry*, *85*(1), 303–328. https://doi.org/10.2138/rmg.2019.85.10

Baalousha, H. (2009). Fundamentals of groundwater modelling. *Groundwater: Modelling, Management and Contamination*, 113–130.

Baker, M. E., Weller, D. E., & Jordan, T. E. (2006). Comparison of automated watershed delineations: Effects on land cover areas, percentages, and relationships to nutrient discharge. *Photogrammetric Engineering*, 10.

Barnhart, K. R., Hutton, E. W., Tucker, G. E., M. Gasparini, N., Istanbulluoglu, E., E. J. Hobley, D., J. Lyons, N., Mouchene, M., Siddhartha Nudurupati, S., M. Adams, J., & Bandaragoda, C. (2020). Short communication: Landlab v2.0: A software package for earth surface dynamics. *Earth Surface Dynamics*, *8*(2), 379–397. https://doi.org/10.5194/esurf-8-379-2020

Bear, J. (1972). *Hydraulics of groundwater*. McGraw-Hill Publishing Company.

Bear, J. (2018). *Modeling phenomena of flow and transport in porous media* (Vol. 31). Springer International Publishing. https://doi.org/10.1007/978-3-319-72826-1

Benda, L., Andras, K., Miller, D., & Bigelow, P. (2004). Confluence effects in rivers: Interactions of basin scale, network geometry, and disturbance regimes. *Water Resources Research*, *40*(5). https://doi.org/10.1029/2003WR002583

Benda, L., Veldhuisen, C., & Black, J. (2003). Debris flows as agents of morphological heterogeneity at low-order confluences, olympic mountains, washington. *Geological Society of America Bulletin*, *115*(9), 1110. https://doi.org/10.1130/B25265.1

Benettin, P., Rodriguez, N. B., Sprenger, M., Kim, M., Klaus, J., Harman, C. J., van der Velde, Y., Hrachowitz, M., Botter, G., McGuire, K. J., Kirchner, J. W., Rinaldo, A., & McDonnell, J. J. (2022). Transit time estimation in catchments: Recent developments and future directions. *Water Resources Research*, *58*(11). https://doi.org/10.1029/2022WR033096

Benettin, P., Soulsby, C., Birkel, C., Tetzlaff, D., Botter, G., & Rinaldo, A. (2017). Using SAS functions and high-resolution isotope data to unravel travel time distributions in headwater catchments. *Water Resources Research*, *53*(3), 1864–1878. https://doi.org/10.1002/2016WR020117

Berghuijs, W. R., & Kirchner, J. W. (2017). The relationship between contrasting ages of groundwater and streamflow. *Geophysical Research Letters*, *44*(17), 8925–8935. https://doi.org/10.1002/2017GL074962

Beven, K. (2006). Hydrology and earth system sciences searching for the holy grail of scientific hydrology: Q t =h (s ← , r ← ,t)a as closure. *Hydrology and Earth System Sciences*, *10*, 609–618. Retrieved June 13, 2019, from www.hydrol-earth-syst-sci.net/10/609/2006/

Binley, A., Hubbard, S. S., Huisman, J. A., Revil, A., Robinson, D. A., Singha, K., & Slater, L. D. (2015). The emergence of hydrogeophysics for improved understanding of subsurface processes over multiple scales. *Water Resources Research*, *51*(6), 3837–3866. https://doi.org/10.1002/2015WR017016

Blicher-Mathiesen, G., McCarty, G., & Nielsen, L. (1998). Denitrification and degassing in groundwater estimated from dissolved dinitrogen and argon. *Journal of Hydrology*, *208*(1), 16–24. https://doi.org/10.1016/S0022-1694(98)00142-5

Blodgett, D., & Johnson, J. (2022). *nhdplusTools: Tools for accessing and working with the NHDPlus*. https://doi.org/10.5066/P97AS8JD

Boddy, N. C., Booker, D. J., & McIntosh, A. R. (2019). Confluence configuration of river networks controls spatial patterns in fish communities. *Landscape Ecology*, *34*(1), 187–201. https://doi.org/10.1007/s10980-018-0763-4

Boerner, R. E. J. (2006). Unraveling the gordian knot: Interactions among vegetation, topography, and soil properties in the central and southern appalachians [Number: 2]. *The Journal of the Torrey Botanical Society*, *133*(2), 321–361. https://doi.org/10.3159/1095-5674(2006)133[321:UTGKIA]2.0.CO;2

Böhlke, J. K., Wanty, R., Tuttle, M., Delin, G., & Landon, M. (2002). Denitrification in the recharge area and discharge area of a transient agricultural nitrate plume in a glacial outwash sand aquifer, minnesota. *Water Resources Research*, *38*(7), 1–26. https://doi.org/10.1029/2001WR000663

Botter, G., Bertuzzo, E., & Rinaldo, A. (2011). Catchment residence and travel time distributions: The master equation. *Geophysical Research Letters*, *38*(11). https://doi.org/10.1029/2011GL047666

Boussinesq, J. (1904). Recherches théoriques sur l'écoulement des nappes d'eau infiltrées dans le sol et sur le débit des sources. *Journal de mathématiques pures et appliquées*, *10*, 5–78.

Boyer, E. W., Alexander, R. B., Parton, W. J., Li, C., Butterbach-Bahl, K., Donner, S. D., Skaggs, R. W., & Grosso, S. J. D. (2006). MODELING DENITRIFICATION IN TERRESTRIAL AND AQUATIC ECOSYSTEMS AT REGIONAL SCALES. *Ecological Applications*, *16*(6), 2123–2142. https://doi.org/10.1890/1051-0761(2006)016[2123:MDITAA]2.0.CO;2

Brauer, C. C., Teuling, A. J., Torfs, P. J., & Uijlenhoet, R. (2013). Investigating storage-discharge relations in a lowland catchment using hydrograph fitting, recession analysis, and soil moisture data. *Water Resources Research*, *49*(7), 4257–4264. https://doi.org/10.1002/wrcr.20320

Bresciani, E., Davy, P., & De Dreuzy, J.-R. (2014). Is the dupuit assumption suitable for predicting the groundwater seepage area in hillslopes? *Water Resources Research*, *50*(3), 2394–2406. https://doi.org/10.1002/2013WR014284

Bronstert, A. (1999). Capabilities and limitations of detailed hillslope hydrological modelling. *Hydrological Processes*, *13*(1), 21–48. https://doi.org/10.1002/(SICI)1099-1085(199901)13:1<21::AID-HYP702>3.0.CO;2-4

Brunke, M., & Gonser, T. (1997). The ecological significance of exchange processes between rivers and groundwater. *Freshwater Biology*, *37*(1), 1–33. https://doi.org/10.1046/j.1365-2427.1997.00143.x

Bruns, A. C. (2000). *Investigation of ground water level fluctuations at the savannah river site* (Master's thesis). University of Georgia. Athens.

Brutsaert, W., & Nieber, J. L. (1977). Regionalized drought flow hydrographs from a mature glaciated plateau. *Water Resources Research*, *13*(3), 637–643. https://doi.org/10.1029/WR013i003p00637

Buchanan, S., & Triantafilis, J. (2009). Mapping water table depth using geophysical and environmental variables. *Ground Water*, *47*(1), 80–96. https://doi.org/10.1111/j.1745-6584.2008.00490.x

Buttle, J. M. (2016). Dynamic storage: A potential metric of inter-basin differences in storage properties. *Hydrological Processes*, *30*(24), 4644–4653. https://doi.org/10.1002/hyp.10931

Cai, M., Li, S., Ye, F., Hong, Y., Lü, M., Op den Camp, H. J. M., & Wang, Y. (2022). Artificial ponds as hotspots of nitrogen removal in agricultural watershed. *Biogeochemistry*, *159*(3), 283–301. https://doi.org/10.1007/s10533-022-00928-6

Caldwell, P. V., Jackson, C. R., Miniat, C. F., Younger, S. E., Vining, J. A., McDonnell, J. J., & Aubrey, D. P. (2018). Woody bioenergy crop selection can have large effects on water yield: A southeastern united states case study. *Biomass and Bioenergy*, *117*, 180–189. https://doi.org/10.1016/j.biombioe.2018.07.021

Carbonneau, P., Fonstad, M. A., Marcus, W. A., & Dugdale, S. J. (2012). Making riverscapes real. *Geomorphology*, *137*(1), 74–86. https://doi.org/10.1016/j.geomorph.2010.09.030

Chang, B., Yan, Z., Ju, X., Song, X., Li, Y., Li, S., Fu, P., & Zhu-Barker, X. (2022). Quantifying biological processes producing nitrous oxide in soil using a mechanistic model. *Biogeochemistry*, *159*(1), 1–14. https://doi.org/10.1007/s10533-022-00912-0

Chang, K.-t., & Tsai, B.-w. (1991). The effect of DEM resolution on slope and aspect mapping. *Cartography and Geographic Information Systems*, *18*(1), 69–77. https://doi.org/10.1559/152304091783805626

Church, M. (1983). Pattern of instability in a wandering gravel bed channel. *Special Publications of the International Association of Sedimentologists*, *6*, 169–180.

Church, M. (1992). Channel morphology and typology. In *The rivers handbook* (pp. 126–143). Blackwell Scientific Publications.

Collins, S. E., Matter, S. F., Buffam, I., & Flotemersch, J. E. (2018). A patchy continuum? stream processes show varied responses to patch- and continuum-based analyses. *Ecosphere*, *9*(11), e02481. https://doi.org/10.1002/ecs2.2481

Condon, L. E., Kollet, S., Bierkens, M. F. P., Fogg, G. E., Maxwell, R. M., Hill, M. C., Fransen, H.-J. H., Verhoef, A., Van Loon, A. F., Sulis, M., & Abesser, C. (2021). Global groundwater modeling and monitoring: Opportunities and challenges. *Water Resources Research*, *57*(12). https://doi.org/10.1029/2020WR029500

Cooper, R. J., Hawkins, E., Locke, J., Thomas, T., & Tosney, J. (2020). Assessing the environmental and economic efficacy of two integrated constructed wetlands at mitigating eutrophication risk from sewage effluent. *Water and Environment Journal*, *34*(4), 669–678. https://doi.org/10.1111/wej.12605

Craft, C., Vymazal, J., & Kröpfelová, L. (2018). Carbon sequestration and nutrient accumulation in floodplain and depressional wetlands. *Ecological Engineering*, *114*, 137–145. https://doi.org/10.1016/j.ecoleng.2017.06.034

Craft, C. B., & Casey, W. P. (2000). Sediment and nutrient accumulation in floodplain and depressional freshwater wetlands of georgia, USA. *Wetlands*, *20*(2), 323–332. https://doi.org/10.1672/0277-5212(2000)020[0323:SANAIF]2.0.CO;2

Curran, J. C., & Hession, W. C. (2013). Vegetative impacts on hydraulics and sediment processes across the fluvial system. *Journal of Hydrology*, *505*, 364–376. https://doi.org/10.1016/j.jhydrol.2013.10.013

Danesh-Yazdi, M., Klaus, J., Condon, L. E., & Maxwell, R. M. (2018). Bridging the gap between numerical solutions of travel time distributions and analytical storage selection functions. *Hydrological Processes*, *32*(8), 1063–1076. https://doi.org/10.1002/hyp.11481

Dan-Jumbo, N. G., & Metzger, M. (2019). Relative effect of location alternatives on urban hydrology. the case of greater port-harcourt watershed, niger delta. *Hydrology*, *6*(3), 82. https://doi.org/10.3390/hydrology6030082

David, M. B., & Gentry, L. E. (2000). Anthropogenic inputs of nitrogen and phosphorus and riverine export for illinois, USA. *Journal of Environmental Quality*, *29*(2), 494–508. https://doi.org/10.2134/jeq2000.00472425002900020018x

Davie, T. (2019). *Fundamentals of hydrology* (3rd ed). Routledge, Taylor & Francis Group.

Dewitz, J., & USGS. (2021). National land cover database (NLCD) 2019 products (ver. 2.0, june 2021). *U.S. Geological Survey Data Release*. https://doi.org/10.5066/P9KZCM54

Doretto, A., Piano, E., & Larson, C. E. (2020). The river continuum concept: Lessons from the past and perspectives for the future. *Canadian Journal of Fisheries and Aquatic Sciences*, *77*(11), 1853–1864. https://doi.org/10.1139/cjfas-2020-0039

Du, E., Jackson, C. R., Klaus, J., McDonnell, J. J., Griffiths, N. A., Williamson, M. F., Greco, J. L., & Bitew, M. (2016). Interflow dynamics on a low relief forested hillslope: Lots of fill, little spill. *Journal of Hydrology*, *534*, 648–658. https://doi.org/10.1016/j.jhydrol.2016.01.039

Du, S., Shi, P., Van Rompaey, A., & Wen, J. (2015). Quantifying the impact of impervious surface location on flood peak discharge in urban areas. *Natural Hazards*, *76*(3), 1457–1471. https://doi.org/10.1007/s11069-014-1463-2

Dunne, T., Moore, T. R., & Taylor, C. H. (1975). Recognition and prediction of runoff-producing zones in humid regions. *Hydrological Sciences Bulletin*, *20*, 305–327.

Dupuit, J. (1848). *Etudes theoriques et pratiques sur le mouvement des eaux courantes*. Carilian-Goeury.

Edwards, P. J., Williard, K. W., & Schoonover, J. E. (2015). Fundamentals of watershed hydrology. *Journal of Contemporary Water Research & Education*, *154*(1), 3–20. https://doi.org/10.1111/j.1936-704X.2015.03185.x

Ehleringer, J., & Dawson, T. E. (1992). Water uptake by plants: Perspectives from stable isotope composition. *Plant, Cell, and Environment*, *15*, 1073–1082.

Elsen, P. R., & Tingley, M. W. (2015). Global mountain topography and the fate of montane species under climate change. *Nature Climate Change*, *5*(8), 772–776. https://doi.org/10.1038/nclimate2656

Elshall, A. S., Arik, A. D., El-Kadi, A. I., Pierce, S., Ye, M., Burnett, K. M., Wada, C. A., Bremer, L. L., & Chun, G. (2020). Groundwater sustainability: A review of the interactions between science and policy. *Environmental Research Letters*, *15*(9), 093004. https://doi.org/10.1088/1748-9326/ab8e8c

Erdbrügger, J., van Meerveld, I., Bishop, K., & Seibert, J. (2021). Effect of DEM-smoothing and -aggregation on topographically-based flow directions and catchment boundaries. *Journal of Hydrology*, *602*, 126717. https://doi.org/10.1016/j.jhydrol.2021.126717

Fan, Y., Clark, M., Lawrence, D. M., Swenson, S., Band, L. E., Brantley, S. L., Brooks, P. D., Dietrich, W. E., Flores, A., Grant, G., Kirchner, J. W., Mackay, D. S., McDonnell, J. J., Milly, P. C. D., Sullivan,

P. L., Tague, C., Ajami, H., Chaney, N., Hartmann, A., … Yamazaki, D. (2019). Hillslope hydrology in global change research and earth system modeling. *Water Resources Research*, *55*(2), 1737–1772. https://doi.org/10.1029/2018WR023903

Fang, K., Sivakumar, B., & Woldemeskel, F. M. (2017). Complex networks, community structure, and catchment classification in a large-scale river basin. *Journal of Hydrology*, *545*, 478–493. https://doi.org/10.1016/j.jhydrol.2016.11.056

Ferreira, G. W., Rau, B. M., & Aubrey, D. P. (2020). Herbicide, fertilization, and planting density effects on intensively managed loblolly pine early stand development. *Forest Ecology and Management*, *472*, 118206. https://doi.org/10.1016/j.foreco.2020.118206

Ferreira, G. W., Rau, B. M., & Aubrey, D. P. (2021). Temporal nitrogen dynamics in intensively managed loblolly pine early stand development. *Forest Ecology and Management*, *483*, 118890. https://doi.org/10.1016/j.foreco.2020.118890

Fetter, C. W. (2001). *Applied hydrogeology* (4th ed). Prentice Hall.

Fields, S. (2004). Global nitrogen: Cycling out of control. *Environmental Health Perspectives*, *112*(10), 557–563. https://doi.org/10.1289/ehp.112-a556

Flach, G. P., Harris, M. K., Hiergesell, R. A., Smits, A. D., & Hawkins, K. L. (1999). Regional groundwater flow model for c, k, l, and p reactor areas, savannah river site, aiken, south carolina (u), 488.

Flinchum, B. A., Holbrook, W. S., Grana, D., Parsekian, A. D., Carr, B. J., Hayes, J. L., & Jiao, J. (2018). Estimating the water holding capacity of the critical zone using near-surface geophysics. *Hydrological Processes*, *32*(22), 3308–3326. https://doi.org/10.1002/hyp.13260

Fonstad, M. A., & Andrew Marcus, W. (2010). High resolution, basin extent observations and implications for understanding river form and process. *Earth Surface Processes and Landforms*, *35*(6), 680–698. https://doi.org/10.1002/esp.1969

Fox, R. J., Fisher, T. R., Gustafson, A. B., Jordan, T. E., Kana, T. M., & Lang, M. W. (2014). Searching for the missing nitrogen: Biogenic nitrogen gases in groundwater and streams. *The Journal of Agricultural Science*, *152*, 96–106. https://doi.org/10.1017/S0021859614000070

Freeze, A., & Cherry, J. (1979). *Groundwater*. Prentice-Hall Publishing.

Freeze, R. A. (1971). Three-dimensional, transient, saturated-unsaturated flow in a groundwater basin‘. *Water Resources Research*.

Freeze, R. A., & Witherspoon, P. A. (1966). Theoretical analysis of regional groundwater flow: 1. analytical and numerical solutions to the mathematical model. *Water Resources Research*, *2*(4), 641–656. https://doi.org/10.1029/WR002i004p00641

Freeze, R. A., & Witherspoon, P. A. (1967). Theoretical analysis of regional groundwater flow: 2. effect of water-table configuration and subsurface permeability variation. *Water Resources Research*, *3*(2), 623–634. https://doi.org/10.1029/WR003i002p00623

Fürst, J., & Hörhan, T. (2009). Coding of watershed and river hierarchy to support GIS-based hydrological analyses at different scales. *Computers and Geosciences*, *35*(3), 688–696. https://doi.org/10.1016/j.cageo.2008.04.007

Gallen, S. F. (2018). Lithologic controls on landscape dynamics and aquatic species evolution in post-orogenic mountains. *Earth and Planetary Science Letters*, *493*, 150–160. https://doi.org/10.1016/j.epsl.2018.04.029

Gallen, S. F., Wegmann, K. W., & Bohnenstieh, D. R. (2013). Miocene rejuvenation of topographic relief in the southern appalachians. *GSA Today*, *23*(2), 4–10. https://doi.org/10.1130/GSATG163A.1

Gallen, S. F., Wegmann, K. W., Frankel, K. L., Hughes, S., Lewis, R. Q., Lyons, N., Paris, P., Ross, K., Bauer, J. B., & Witt, A. C. (2011). Hillslope response to knickpoint migration in the southern appalachians: Implications for the evolution of post-orogenic landscapes. *Earth Surface Processes and Landforms*, *36*(9), 1254–1267. https://doi.org/10.1002/esp.2150

Galloway, J. N., Dentener, F. J., Capone, D. G., Boyer, E. W., Howarth, R. W., Seitzinger, S. P., Asner, G. P., Cleveland, C. C., Green, P. A., Holland, E. A., Karl, D. M., Michaels, A. F., Porter, J. H., Townsend, A. R., & Vosmarty, C. J. (2004). Nitrogen cycles: Past, present, and future. *Biogeochemistry*, *70*(2), 153–226. https://doi.org/10.1007/s10533-004-0370-0

Gellici, J., Reed, R., Logan, W., Aadland, R., & Simones, G. (1995). *Hydrogeologic investigation and establishment of a permanent multi-observational well network in aiken, allendale, and barnwell counties, south carolina – eight-year interim report (1986 - 1994)*.

Gooseff, M. N., Wlostowski, A., McKnight, D. M., & Jaros, C. (2017). Hydrologic connectivity and implications for ecosystem processes - lessons from naked watersheds. *Geomorphology*, *277*, 63–71. https://doi.org/10.1016/j.geomorph.2016.04.024

Griffiths, N. A., Jackson, C. R., Bitew, M. M., Fortner, A. M., Fouts, K. L., McCracken, K., & Phillips, J. R. (2017). Water quality effects of short-rotation pine management for bioenergy feedstocks in the southeastern united states. *Forest Ecology and Management*, *400*, 181–198. https://doi.org/10.1016/j.foreco.2017.06.011

Griffiths, N. A., Jackson, C. R., Blake, J. I., Jeffers, J., Rau, B. M., Starr, G., & Vaché, K. (2019). *Environmental effects of short-rotation loblolly pine production for bioenergy and evaluation of current forestry best management practices* (ORNL/TM-2018/1055). Oak Ridge National Laboratory.

Griffiths, N. A., Jackson, C. R., McDonnell, J. J., Klaus, J., Du, E., & Bitew, M. M. (2016). Dual nitrate isotopes clarify the role of biological processing and hydrologic flow paths on nitrogen cycling in subtropical low-gradient watersheds. *Journal of Geophysical Research: Biogeosciences*, *121*, 1–16. https://doi.org/10.1002/2015JG003189

Griffiths, N. A., Rau, B. M., Vaché, K. B., Starr, G., Bitew, M. M., Aubrey, D. P., Martin, J. A., Benton, E., & Jackson, C. R. (2018). Environmental effects of short-rotation woody crops for bioenergy: What is and isn't known. *GCB Bioenergy*, *11*(4), 554–572. https://doi.org/10.1111/gcbb.12536

Groffman, P. M., Altabet, M. A., Böhlke, J. K., Butterbach-Bahl, K., David, M. B., Firestone, M. K., Giblin, A. E., Kana, T. M., Nielsen, L. P., & Voytek, M. A. (2006). Methods for measuring denitrification: Diverse approaches to a difficult problem. *Ecological Applications*, *16*(6), 2091–2122. https://doi.org/10.1890/1051-0761(2006)016[2091:MFMDDA]2.0.CO;2

Groh, T. A., Davis, M. P., Isenhart, T. M., Jaynes, D. B., & Parkin, T. B. (2019). In situ denitrification in saturated riparian buffers. *Journal of Environmental Quality*, *48*(2), 376–384. https://doi.org/10.2134/jeq2018.03.0125

Gruber, N., & Galloway, J. N. (2008). An earth-system perspective of the global nitrogen cycle [Publisher: Nature Publishing Group]. *Nature*, *451*(17), 293–296. https://doi.org/10.1038/nature06592

Guérin, A., Devauchelle, O., Robert, V., Kitou, T., Dessert, C., Quiquerez, A., Allemand, P., & Lajeunesse, E. (2019). Stream-discharge surges generated by groundwater flow. *Geophysical Research Letters*, *46*(13), 7447–7455. https://doi.org/10.1029/2019GL082291

Haitjema, H. M., & Mitchell-Bruker, S. (2005). Are water tables a subdued replica of the topography? *Ground Water*, *43*(6), 781–786. https://doi.org/10.1111/j.1745-6584.2005.00090.x

Hansen, W. F. (2001). Identifying stream types and management implications. *Forest Ecology and Management*, *143*(1), 39–46. https://doi.org/10.1016/S0378-1127(00)00503-X

Harman, C. J. (2015). Time-variable transit time distributions and transport: Theory and application to storage-dependent transport of chloride in a watershed. *Water Resources Research*, *51*(1), 1–30. https://doi.org/10.1002/2014WR015707

Harmon, R., Barnard, H. R., & Singha, K. (2020). Water table depth and bedrock permeability control magnitude and timing of transpiration-induced diel fluctuations in groundwater. *Water Resources Research*, *56*(5), 1–22. https://doi.org/10.1029/2019wr025967

Heasley, E. L., Clifford, N. J., & Millington, J. D. (2019). Integrating network topology metrics into studies of catchment-level effects on river characteristics. *Hydrology and Earth System Sciences*, *23*(5), 2305–2319. https://doi.org/10.5194/hess-23-2305-2019

Heaton, T., & Vogel, J. (1981). "excess air" in groundwater. *Journal of Hydrology*, *50*, 201–216. https://doi.org/10.1016/0022-1694(81)90070-6

Heckmann, T., Schwanghart, W., & Phillips, J. D. (2015). Graph theory-recent developments of its application in geomorphology. *Geomorphology*, *243*, 130–146. https://doi.org/10.1016/j.geomorph.2014.12.024

Hester, E. T., & Fox, G. A. (2020). Preferential flow in riparian groundwater: Gateways for watershed solute transport and implications for water quality management. *Water Resources Research*, *56*(12), 1–8. https://doi.org/10.1029/2020wr028186

Hiergesell, R. (1998). *The regional water table of the savannah river site and related coverages* (WSRC-TR-98-00045). Retrieved March 31, 2022, from http://www.osti.gov/servlets/purl/761146-vDIXc1/webviewable/

Hiergesell, R., & Jones, W. (2004). *An updated regional water table of the savannah river site and related coverages* (WSRC-TR-2003-00250). https://doi.org/10.2172/822081

Hill, A. R. (2019). Groundwater nitrate removal in riparian buffer zones: A review of research progress in the past 20 years. *Biogeochemistry*, *143*(3), 347–369. https://doi.org/10.1007/s10533-019-00566-5

Hobley, D. E., Adams, J. M., Siddhartha Nudurupati, S., Hutton, E. W., Gasparini, N. M., Istanbulluoglu, E., & Tucker, G. E. (2017). Creative computing with landlab: An open-source toolkit for building,

coupling, and exploring two-dimensional numerical models of earth-surface dynamics. *Earth Surface Dynamics*, *5*(1), 21–46. https://doi.org/10.5194/esurf-5-21-2017

Holbrook, W. S., Marcon, V., Bacon, A. R., Brantley, S. L., Carr, B. J., Flinchum, B. A., Richter, D. D., & Riebe, C. S. (2019). Links between physical and chemical weathering inferred from a 65-m-deep borehole through earth's critical zone. *Scientific Reports*, *9*(1), 4495. https://doi.org/10.1038/s41598-019-40819-9

Horton, R. E. (1932). Drainage-basin characteristics. *Transactions, American Geophysical Union*, *13*(1), 350–361. https://doi.org/10.1029/TR013i001p00350

Howarth, R. W. (2008). Coastal nitrogen pollution: A review of sources and trends globally and regionally. *Harmful Algae*, *8*(1), 14–20. https://doi.org/10.1016/j.hal.2008.08.015

Hrachowitz, M., & Clark, M. P. (2017). The complementary merits of competing modelling philosophies in hydrology. *Hydrol. Earth Syst. Sci*, *21*, 3953–3973. https://doi.org/https://doi.org/10.5194/hess-21-3953-2017

Humboldt, A. v., Bonpland, A., Jackson, S. T., & Romanowski, S. (2008). *Essay on the geography of plants*. University of Chicago Press.

Hursh, C. (1936). Storm water and absorption. *American Geophysical Union*, *17*, 301–302.

Hwang, T., Band, L. E., Vose, J. M., & Tague, C. (2012). Ecosystem processes at the watershed scale: Hydrologic vegetation gradient as an indicator for lateral hydrologic connectivity of headwater catchments. *Water Resources Research*, *48*(6). https://doi.org/10.1029/2011WR011301

Hynes, H. B. N. (1970). *The ecology of running waters*. University of Toronto Press.

Ice, G., Brown, G., Gravelle, J., Jackson, C. R., Light, J., Link, T., Martin, D., Mcgreer, D., Skaugset, A., Harvest, F., Ice, G., Brown, G., Gravelle, J., Jackson, C. R., Link, T., Martin, D., Mcgreer, D., & Skaugset, A. (2010). Discussion –"stream temperature relationships to forest harvest in western washington". *Journal of the American Water Resources Association*, *46*(4), 838–842. https://doi.org/10.1111/j.1752-1688.2010.00441.x

Jackson, C. R., Bahn, R. A., & Webster, J. R. (2017). Water quality signals from rural land use and exurbanization in a mountain landscape: What's clear and what's confounded? *JAWRA Journal of the American Water Resources Association*, *53*(5), 1212–1228. https://doi.org/10.1111/1752-1688.12567

Jackson, C. R., Bitew, M., & Du, E. (2014). When interflow also percolates: Downslope travel distances and hillsclope process zones. *28*(7), 3195–3200. https://doi.org/10.1002/hyp.10158

Jackson, C. R., Du, E., Klaus, J., Griffiths, N. A., Bitew, M. M., & McDonnell, J. J. (2016). Interactions among hydraulic conductivity distributions, subsurface topography, and transport thresholds revealed by a multitracer hillslope irrigation experiment. *Water Resources Research*, *52*, 6186–6206. https://doi.org/10.1002/2013WR015173

Jager, H. I., Bevelhimer, M. S., King, R. L., & Smith, K. A. (2011). Landscape influences on headwater streams on fort stewart, georgia, USA. *Environmental Management*, *48*(4), 795–807. https://doi.org/10.1007/s00267-011-9722-4

Jahangir, M. M. R., Johnston, P., Addy, K., Khalil, M. I., Groffman, P. M., & Richards, K. G. (2013). Quantification of in situ denitrification rates in groundwater below an arable and a grassland system. *Water, Air, & Soil Pollution*, *224*(9), 1693. https://doi.org/10.1007/s11270-013-1693-z

Jahangir, M., Johnston, P., Barrett, M., Khalil, M., Groffman, P., Boeckx, P., Fenton, O., Murphy, J., & Richards, K. (2013). Denitrification and indirect n20 emissions in groundwater: Hydrologic and biogeochemical influences. *Journal of Contaminant Hydrology*, *152*, 70–81. https://doi.org/10.1016/j.jconhyd.2013.06.007

Jahangir, M., Johnston, P., Khalil, M., Grant, J., Somers, C., & Richards, K. (2012). Evaluation of headspace equilibration methods for quantifying greenhouse gases in groundwater. *Journal of Environmental Management*, *111*, 208–212. https://doi.org/10.1016/j.jenvman.2012.06.033

James, A. L., & Roulet, N. T. (2007). Investigating hydrologic connectivity and its association with threshold change in runoff response in a temperate forested watershed. *Hydrological Processes*, *21*(25), 3391–3408. https://doi.org/10.1002/hyp.6554

Johnson, B., Smith, E., Ackerman, J. W., Dye, S., Polinsky, R., Somerville, E., Decker, C., Little, D., Pond, G. J., & D'Amico, E. (2019). Spatial convergence in major dissolved ion concentrations and implications of headwater mining for downstream water quality. *JAWRA Journal of the American Water Resources Association*, *55*(1), 247–258. https://doi.org/10.1111/1752-1688.12725

Jurado, A., Borges, A. V., & Brouyère, S. (2017). Dynamics and emissions of n20 in groundwater: A review. *Science of The Total Environment*, *584-585*, 207–218. https://doi.org/10.1016/j.scitotenv.2017.01.127

Kana, T. M., Darkangelo, C., Hunt, M. D., Oldham, J. B., Bennett, G. E., & Cornwell, J. C. (1994). Membrane lnlet mass spectrometer for rapid high-precision determination of n2, 02 , and ar in environmental water samples. *Analytical Chemistry*, *66*(23), 4166–4170. https://doi.org/10.1021/ac00095a009

Kilgo, J., & Blake, J. (2005). *Ecology and management of a forested landscape: Fifty years on the savannah river site.* USDA Forest Service, Savannah River, New Ellenton, SC.

Kim, M., & Harman, C. J. (2022). Transit times and StorAge selection functions in idealized hillslopes with steady infiltration. *Water Resources Research*, *58*(5). https://doi.org/10.1029/2019WR025917

Kim, M., Volkmann, T. H. M., Wang, Y., Meira Neto, A. A., Matos, K., Harman, C. J., & Troch, P. A. (2022). Direct observation of hillslope scale StorAge selection functions in experimental hydrologic systems: Geomorphologic structure and preferential discharge of old water. *Water Resources Research*, *58*(3). https://doi.org/10.1029/2020WR028959

Kirchner, J. W. (2009). Catchments as simple dynamical systems: Catchment characterization, rainfall-runoff modeling, and doing hydrology backward. *Water Resources Research*, *45*(2), 1–34. https://doi.org/10.1029/2008WR006912

Klaus, J., Chun, K. K., McGuire, K. J., & McDonnell, J. J. (2015). Temporal dynamics of catchment transit times from stable isotope data. *Water Resources Research*, *51*, 4208–4223. https://doi.org/10.1002/2014WR016247.Received

Klaus, J., McDonnell, J. J., Jackson, C. R., Du, E., & Griffiths, N. A. (2015). Where does streamwater come from in low-relief forested watersheds? a dual-isotope approach. *Hydrology and Earth System Sciences*, *19*(1), 125–135. https://doi.org/10.5194/hess-19-125-2015

Klaus, J., & Jackson, C. R. (2018). Interflow is not binary: A continuous shallow perched layer does not imply continuous connectivity. *Water Resources Research*, *54*(9), 5921–5932. https://doi.org/10.1029/2018WR022920

Kobayashi, S., & Yokoo, Y. (2013). Estimating watershed-scale storage changes from hourly discharge data in mountainous humid watersheds: Toward a new way of dominant process modeling. *Hydrological Research Letters*, *7*(4), 97–103. https://doi.org/10.3178/hrl.7.97

Koeniger, P., Marshall, J. D., Link, T., & Mulch, A. (2011). An inexpensive, fast, and reliable method for vacuum extraction of soil and plant water for stable isotope analyses by mass spectrometry: Vacuum extraction of soil and plant water for stable isotope analyses. *Rapid Communications in Mass Spectrometry*, *25*(20), 3041–3048. https://doi.org/10.1002/rcm.5198

Koh, E.-H., Lee, E., Kaown, D., Green, C. T., Koh, D.-C., Lee, K.-K., & Lee, S. H. (2018). Comparison of groundwater age models for assessing nitrate loading, transport pathways, and management options in a complex aquifer system. *Hydrological Processes*, *32*(7), 923–938. https://doi.org/10.1002/hyp.11465

Kolbe, T., Labasque, T., Marçais, J., & Bishop, K. (2020). Lagged rejuvenation of groundwater indicates internal flow structures and hydrological connectivity. *Hydrological Processes*, 2176–2189. https://doi.org/10.1002/hyp.13753

Kolbe, T., Marçais, J., Thomas, Z., Abbott, B. W., Rousseau-Gueutin, P., Aquilina, L., Labasque, T., & Pinay, G. (2016). Coupling 3d groundwater modeling with CFC-based age dating to classify local groundwater circulation in an unconfined crystalline aquifer. *Journal of Hydrology*, *543*, 31–46. https://doi.org/10.1016/J.JHYDROL.2016.05.020

Kong, J., Xin, P., Hua, G.-F., Luo, Z.-Y., Shen, C.-J., Chen, D., & Li, L. (2015). Effects of vadose zone on groundwater table fluctuations in unconfined aquifers. *Journal of Hydrology*, *528*, 397–407. https://doi.org/10.1016/j.jhydrol.2015.06.045

Krichels, A. H., Homyak, P. M., Aronson, E. L., Sickman, J. O., Botthoff, J., Shulman, H., Piper, S., Andrews, H. M., & Jenerette, G. D. (2022). Rapid nitrate reduction produces pulsed NO and n20 emissions following wetting of dryland soils. *Biogeochemistry*, *158*(2), 233–250. https://doi.org/10.1007/s10533-022-00896-x

Kumar, C. P. (2012). Groundwater modelling software – capabilities and limitations. *IOSR Journal of Environmental Science, Toxicology and Food Technology*, *1*(2), 46–57. https://doi.org/10.9790/2402-0124657

LaGro, J. (2005). Land-use classification. In D. Hillel (Ed.), *Encyclopedia of soils in the environment* (pp. 321–328). Elsevier. https://doi.org/10.1016/B0-12-348530-4/00530-0

Larsen, S., Bruno, M. C., Vaughan, I. P., & Zolezzi, G. (2019). Testing the river continuum concept with geostatistical stream-network models. *Ecological Complexity*, *39*, 100773. https://doi.org/10.1016/j.ecocom.2019.100773

Lenhart, S., Ortmeyer, F., & Banning, A. (2021). Denitrification in the vadose zone: Modelling with percolating water prognosis and denitrification potential. *Journal of Contaminant Hydrology*, *242*, 103843. https://doi.org/10.1016/j.jconhyd.2021.103843

Leray, S., Gauvain, A., & De Dreuzy, J.-R. (2019). Residence time distributions in non-uniform aquifer recharge and thickness conditions – an analytical approach based on the assumption of dupuit-forchheimer. *Journal of Hydrology*. https://doi.org/10.1016/j.jhydrol.2019.04.032

Lindsay, J. B., Francioni, A., & Cockburn, J. M. (2019). LiDAR DEM smoothing and the preservation of drainage features. *Remote Sensing*, *11*(16). https://doi.org/10.3390/rs11161926

Lindsay, J. B., Yang, W., & Hornby, D. D. (2019). Drainage network analysis and structuring of topologically noisy vector stream data. *ISPRS International Journal of Geo-Information*, *8*(9). https://doi.org/10.3390/ijgi8090422

Litwin, D., Tucker, G., Barnhart, K., & Harman, C. (2020). GroundwaterDupuitPercolator: A landlab component for groundwater flow. *Journal of Open Source Software*, *5*(46), 1935. https://doi.org/10.21105/joss.01935

Litwin, D., Tucker, G. E., Barnhart, K. R., & Harman, C. J. (2022). Groundwater affects the geomorphic and hydrologic properties of coevolved landscapes. *Journal of Geophysical Research*, *127*. https://doi.org/https://doi.org/10.1029/2021JF006239

Loáiciga, H. A. (2020). Seepage face in steady-state groundwater flow between two water bodies. *Journal of Hydrologic Engineering*, *25*(9), 06020005. https://doi.org/10.1061/(ASCE)HE.1943-5584.0001997

Lowe, E. F., & Keenan, L. W. (1997). Managing phosphorus-based, cultural eutrophication in wetlands: A conceptual approach. *Ecological Engineering*, *9*(1), 109–118. https://doi.org/10.1016/S0925-8574(97)00035-9

Lowrance, R. (1992). Groundwater nitrate and denitrification in a coastal plain riparian forest. *Journal of Environmental Quality*, *21*(3), 401–405. https://doi.org/10.2134/jeq1992.00472425002100030017x

Lowrance, R., Altier, L. S., Newbold, J. D., Schnabel, R. R., Groffman, P. M., Denver, J. M., Correll, D. L., Gilliam, J. W., Robinson, J. L., Brinsfield, R. B., Staver, K. W., Lucas, W., & Todd, A. H. (1997). Water quality functions of riparian forest buffers in chesapeake bay watersheds. *Environmental Management*, *21*(5), 687–712. https://doi.org/10.1007/s002679900060

Lowrance, R., Vellidis, G., & Hubbard, R. K. (1995). Denitrification in a restored riparian forest wetland. *Journal of Environmental Quality*, *24*(5), 808–815. https://doi.org/10.2134/jeq1995.00472425002400050003x

Lürling, M., & Mucci, M. (2020). Mitigating eutrophication nuisance: In-lake measures are becoming inevitable in eutrophic waters in the netherlands. *Hydrobiologia*, *847*(21), 4447–4467. https://doi.org/10.1007/s10750-020-04297-9

Lutz, S. R., Trauth, N., Musolff, A., Van Breukelen, B. M., Knöller, K., & Fleckenstein, J. H. (2020). How important is denitrification in riparian zones? combining end-member mixing and isotope modeling to quantify nitrate removal from riparian groundwater. *Water Resources Research*, *56*(1). https://doi.org/10.1029/2019WR025528

Marchant, H. K., Holtappels, M., Lavik, G., Ahmerkamp, S., Winter, C., & Kuypers, M. M. M. (2016). Coupled nitrification-denitrification leads to extensive n loss in subtidal permeable sediments: Coupled nitrification-denitrification in sands. *Limnology and Oceanography*, *61*(3), 1033–1048. https://doi.org/10.1002/lno.10271

Mathes, S., Rasmussen, T., & Reed, J. (2001). GIS mapping of groundwater contamination at the savannah river site.

McAleer, E., Coxon, C., Richards, K., Jahangir, M., Grant, J., & Mellander, P. (2017). Groundwater nitrate reduction versus dissolved gas production: A tale of two catchments. *Science of The Total Environment*, *586*, 372–389. https://doi.org/10.1016/j.scitotenv.2016.11.083

McClain, M. E., Boyer, E. W., Dent, C. L., Gergel, S. E., Grimm, N. B., Groffman, P. M., Hart, S. C., Harvey, J. W., Johnston, C. A., Mayorga, E., McDowell, W. H., & Pinay, G. (2003). Biogeochemical hot spots and hot moments at the interface of terrestrial and aquatic ecosystems. *Ecosystems*, *6*(4), 301–312. https://doi.org/10.1007/s10021-003-0161-9

McDonnell, J. J., McGuire, K., Aggarwal, P., Beven, K. J., Biondi, D., Destouni, G., Dunn, S., James, A., Kirchner, J., Kraft, P., Lyon, S., Maloszewski, P., Newman, B., Pfister, L., Rinaldo, A., Rodhe, A., Sayama, T., Seibert, J., Solomon, K., … Wrede, S. (2010). How old is streamwater? open questions in catchment transit time conceptualization, modelling and analysis. *Hydrological Processes*, *24*(12), 1745–1754. https://doi.org/10.1002/hyp.7796

McEachran, A. R., Dickey, L. C., Rehmann, C. R., Isenhart, T. M., Groh, T. A., Perez, M. A., & Rutherford, C. J. (2023). Groundwater flow in saturated riparian buffers and implications for nitrate removal. *Journal of Environmental Quality*, *52*(1), 64–73. https://doi.org/10.1002/jeq2.20428

McGuire, K. J., & McDonnell, J. J. (2006). A review and evaluation of catchment transit time modeling. *Journal of Hydrology*, *330*(3), 543–563. https://doi.org/10.1016/j.jhydrol.2006.04.020

McGuire, K. J., Torgersen, C. E., Likens, G. E., Buso, D. C., Lowe, W. H., & Bailey, S. W. (2014). Network analysis reveals multiscale controls on streamwater chemistry. *Proceedings of the National Academy of Sciences*, *111*(19), 7030–7035. https://doi.org/10.1073/pnas.1404820111

McMillan, H. (2020). Linking hydrologic signatures to hydrologic processes: A review. *Hydrological Processes*, *34*(6), 1393–1409. https://doi.org/10.1002/hyp.13632

McMillan, H. (2022). A taxonomy of hydrological processes and watershed function. *Hydrological Processes*, *36*(3). https://doi.org/10.1002/hyp.14537

Meade, R. H., Rayol, J. M., Da Conceicão, S. C., & Natividade, J. R. G. (1991). Backwater effects in the amazon river basin of brazil. *Environmental Geology and Water Sciences*, *18*(2), 105–114. https://doi.org/10.1007/BF01704664

Meding, S., Morris, L. A., Hoover, C. M., Nutter, W. L., & Cabrera, M. L. (2001). Denitrification at a long-term forested land treatment system in the piedmont of georgia. *Journal of Environmental Quality*, *30*(4), 1411–1420. https://doi.org/10.2134/jeq2001.30414111x

Mejía, A. I., & Moglen, G. E. (2010). Impact of the spatial distribution of imperviousness on the hydrologic response of an urbanizing basin. *Hydrological Processes*, *24*(23), 3359–3373. https://doi.org/10.1002/hyp.7755

Meles, M. B., Younger, S. E., Jackson, C. R., Du, E., & Drover, D. (2020). Wetness index based on landscape position and topography (WILT): Modifying TWI to reflect landscape position. *Journal of Environmental Management*, *255*, 109863. https://doi.org/10.1016/j.jenvman.2019.109863

Meles Bitew, M., Jackson, C. R., Goodrich, D. C., Younger, S. E., Griffiths, N. A., Vaché, K. B., & Rau, B. (2020). Dynamic domain kinematic modelling for predicting interflow over leaky impeding layers. *Hydrological Processes*, *34*(13), 2895–2910. https://doi.org/10.1002/hyp.13778

Merill, L., & Tonjes, D. J. (2014). A review of the hyporheic zone, stream restoration, and means to enhance denitrification. *Critical Reviews in Environmental Science and Technology*, *44*(21), 2337–2379. https://doi.org/10.1080/10643389.2013.829769

Millar, C., Pratt, D., Schneider, D. J., & McDonnell, J. J. (2018). A comparison of extraction systems for plant water stable isotope analysis. *Rapid Communications in Mass Spectrometry*, *32*(13), 1031–1044. https://doi.org/10.1002/rcm.8136

Montgomery, D. R. (1999). Process domains and the river continuum. *Journal of the American Water Resources Association*, *35*(2), 397–410. https://doi.org/10.1111/j.1752-1688.1999.tb03598.x

Munoth, P., & Goyal, R. (2019). Effects of DEM source, spatial resolution and drainage area threshold values on hydrological modeling. *Water Resources Management*, *33*(9), 3303–3319. https://doi.org/10.1007/s11269-019-02303-x

Musolff, A., Schmidt, C., Rode, M., Lischeid, G., Weise, S. M., & Fleckenstein, J. H. (2016). Groundwater head controls nitrate export from an agricultural lowland catchment. *Advances in Water Resources*, *96*, 95–107. https://doi.org/10.1016/j.advwatres.2016.07.003

Nagele, W., & Conrad, R. (1990). Influence of soil pH on the nitrate-reducing microbial populations and their potential to reduce nitrate to NO and n_2o. *FEMS Microbiology Letters*, *74*(1), 49–57. https://doi.org/10.1111/j.1574-6968.1990.tb04051.x

Nogueira, G. E. H., Schmidt, C., Brunner, P., Graeber, D., & Fleckenstein, J. H. (2021). Transit-time and temperature control the spatial patterns of aerobic respiration and denitrification in the riparian zone. *Water Resources Research*, *57*(12), 1–25. https://doi.org/10.1029/2021WR030117

Paerl, H. W., Havens, K. E., Xu, H., Zhu, G., McCarthy, M. J., Newell, S. E., Scott, J. T., Hall, N. S., Otten, T. G., & Qin, B. (2020). Mitigating eutrophication and toxic cyanobacterial blooms in large lakes: The evolution of a dual nutrient (n and p) reduction paradigm. *Hydrobiologia*, *847*(21), 4359–4375. https://doi.org/10.1007/s10750-019-04087-y

Paniconi, C., & Putti, M. (2015). Physically based modeling in catchment hydrology at 50: Survey and outlook. *Water Resources Research*, *51*(9), 7090–7129. https://doi.org/10.1002/2015WR017780

Parsekian, A. D., Singha, K., Minsley, B. J., Holbrook, W. S., & Slater, L. (2015). Multiscale geophysical imaging of the critical zone: Geophysical imaging of the critical zone. *Reviews of Geophysics*, *53*(1), 1–26. https://doi.org/10.1002/2014RG000465

Payne, W. (1976). Denitrification. *Trends in Biochemical Sciences*, *1*(4), 220–222. https://doi.org/10.1016/S0968-0004(76)80094-1

Pepper, I., Gerba, C., & Gentry, T. (2015). Preface. In *Environmental microbiology* (p. xvii). Elsevier. https://doi.org/10.1016/B978-0-12-394626-3.00035-1

Petroff, A. P., Devauchelle, O., Seybold, H., & Rothman, D. H. (2013). Bifurcation dynamics of natural drainage networks. *Philosophical Transactions of the Royal Society A: Mathematical, Physical and Engineering Sciences*, *371*(2004), 20120365. https://doi.org/10.1098/rsta.2012.0365

Phillips, J. D., Schwanghart, W., & Heckmann, T. (2015). Graph theory in the geosciences. *Earth-Science Reviews*, *143*, 147–160. https://doi.org/10.1016/j.earscirev.2015.02.002

Picourlat, F., Mouche, E., & Mügler, C. (2022). Upscaling hydrological processes for land surface models with a two-hydrologic-variable model: Application to the little washita watershed. *Water Resources Research*, *58*(9). https://doi.org/10.1029/2021WR030997

Poeppl, R. E., Fryirs, K. A., Tunnicliffe, J., & Brierley, G. J. (2020). Managing sediment (dis)connectivity in fluvial systems. *Science of The Total Environment*, *736*, 139627. https://doi.org/10.1016/j.scitotenv.2020.139627

Popp, A. L., Manning, C. C., Brennwald, M. S., & Kipfer, R. (2020). A new in situ method for tracing denitrification in riparian groundwater. *Environmental Science & Technology*, *54*(3), 1562–1572. https://doi.org/10.1021/acs.est.9b05393

Pringle, C. M., Naiman, R. J., Bretschko, G., Karr, J. R., Oswood, M. W., Webster, J. R., Welcomme, R. L., & Winterbourn, M. J. (1988). Patch dynamics in lotic systems: The stream as a mosaic. *Journal of the North American Benthological Society*, *7*(4), 503–524. https://doi.org/10.2307/1467303

Prowell, D. C. (1996). *GEOLOGIC MAP OF THE SAVANNAH RIVER SITE, AIKEN, ALLENDALE, AND BARNWELL COUNTIES, SOUTH CAROLINA*.

Rabalais, N. N., Turner, R. E., Sen Gupta, B. K., Boesch, D. F., Chapman, P., & Murrell, M. C. (2007). Hypoxia in the northern gulf of mexico: Does the science support the plan to reduce, mitigate, and control hypoxia? *Estuaries and Coasts*, *30*(5), 753–772. https://doi.org/10.1007/BF02841332

Rabalais, N. N., & Turner, R. E. (2019). Gulf of mexico hypoxia: Past, present, and future. *Limnology and Oceanography Bulletin*, *28*(4), 117–124. https://doi.org/10.1002/lob.10351

Rabalais, N. N., Turner, R. E., & Wiseman, W. J. (2002). Gulf of mexico hypoxia, a.k.a. "the dead zone". *Annual Review of Ecology and Systematics*, *33*(1), 235–263. https://doi.org/10.1146/annurev.ecolsys.33.010802.150513

Rahmati, O., Naghibi, S. A., Shahabi, H., Bui, D. T., Pradhan, B., Azareh, A., Rafiei-Sardooi, E., Samani, A. N., & Melesse, A. M. (2018). Groundwater spring potential modelling: Comprising the capability and robustness of three different modeling approaches. *Journal of Hydrology*, *565*, 248–261. https://doi.org/10.1016/j.jhydrol.2018.08.027

Rasmussen, T. C., Haborak, K. G., & Young, M. H. (2003). Estimating aquifer hydraulic properties using sinusoidal pumping at the savannah river site, south carolina, USA. *Hydrogeology Journal*, *11*, 466–482. https://doi.org/10.1007/s10040-003-0255-7

Rasmussen, T. C., & Mote, T. L. (2007). Monitoring surface and subsurface water storage using confined aquifer water levels at the savannah river site, USA. *Vadose Zone Journal*, *6*(2), 327. https://doi.org/10.2136/vzj2006.0049

Ravishankara, A. R., Daniel, J. S., & Portmann, R. W. (2009). Nitrous oxide (n_2o): The dominant ozone-depleting substance emitted in the 21st century. *Science*, *326*(5949), 123–125. https://doi.org/10.1126/science.1176985

Razavi, T., & Coulibaly, P. (2017). An evaluation of regionalization and watershed classification schemes for continuous daily streamflow prediction in ungauged watersheds. *Canadian Water Resources Journal*, *42*(1), 2–20. https://doi.org/10.1080/07011784.2016.1184590

Reeder, W. J., Quick, A. M., Farrell, T. B., Benner, S. G., Feris, K. P., Marzadri, A., & Tonina, D. (2018). Hyporheic source and sink of nitrous oxide. *Water Resources Research*, *54*(7), 5001–5016. https://doi.org/10.1029/2018WR022564

Ren, S., Gragg, S., Zhang, Y., Carr, B. J., & Yao, G. (2018). Borehole characterization of hydraulic properties and groundwater flow in a crystalline fractured aquifer of a headwater mountain watershed, laramie range, wyoming. *Journal of Hydrology*, *561*, 780–795. https://doi.org/10.1016/j.jhydrol.2018.04.048

Ren, S., Parsekian, A. D., Zhang, Y., & Carr, B. J. (2019). Hydraulic conductivity calibration of logging NMR in a granite aquifer, laramie range, wyoming. *Groundwater*, *57*(2), 303–319. https://doi.org/10.1111/gwat.12798

Rice, S., Greenwood, M., & Joyce, C. (2001). Tributaries, sediment sources, and the longitudinal organization mof macroinvertebrate fauna along river systems. *Canadian Journal of Fisheries and Aquatic Sciences*, *58*, 828–840. https://doi.org/https://doi.org/10.1139/f01-022

Richey, A. S., Thomas, B. F., Lo, M.-H., Famiglietti, J. S., Swenson, S., & Rodell, M. (2015). Uncertainty in global groundwater storage estimates in a total groundwater stress framework. *Water Resources Research*, *51*(7), 5198–5216. https://doi.org/10.1002/2015WR017351

Rinaldo, A., Banavar, J. R., & Maritan, A. (2006). Trees, networks, and hydrology. *Water Resources Research*, *42*, 1–19. https://doi.org/10.1029/2005WR004108

Rinaldo, A., Rigon, R., Banavar, J. R., Maritan, A., & Rodriguez-Iturbe, I. (2014). Evolution and selection of river networks: Statics, dynamics, and complexity. *Proceedings of the National Academy of Sciences*, *111*(7), 2417–2424. https://doi.org/10.1073/pnas.1322700111

Rivenbark, B. L., & Jackson, C. R. (2004). AVERAGE DISCHARGE, PERENNIAL FLOW INITIATION, AND CHANNEL INITIATION - SMALL SOUTHERN APPALACHIAN BASINS. *Journal of the American Water Resources Association*, *40*(3), 639–646. https://doi.org/10.1111/j.1752-1688.2004.tb04449.x

Rivett, M. O., Buss, S. R., Morgan, P., Smith, J. W. N., & Bemment, C. D. (2008). Nitrate attenuation in groundwater: A review of biogeochemical controlling processes. *Water Research*, *42*, 4215–4232. https://doi.org/10.1016/j.watres.2008.07.020

Robertson, G. P., & Vitousek, P. M. (2009). Nitrogen in agriculture: Balancing the cost of an essential resource. *Annual Review of Environment and Resources*, *34*(1), 97–125. https://doi.org/10.1146/annurev.environ.032108.105046

Robinson, T. P., & Metternicht, G. (2006). Testing the performance of spatial interpolation techniques for mapping soil properties. *Computers and Electronics in Agriculture*, *50*(2), 97–108. https://doi.org/10.1016/j.compag.2005.07.003

Rodriguez, N. B., McGuire, K. J., & Klaus, J. (2018). Time-varying storage–water age relationships in a catchment with a mediterranean climate. *Water Resources Research*, *54*(6), 3988–4008. https://doi.org/10.1029/2017WR021964

Rogers, V. A. (1990). *Soil survey of savannah river plant area, parts of aiken, barnwell, and allendale counties, south carolina*. https://www.osti.gov/biblio/5383134

Roy, A. G., & Roy, R. (1988). Changes in channel size at river confluences with coarse bed material. *Earth Surface Processes and Landforms*, *13*(1), 77–84. https://doi.org/10.1002/esp.3290130110

Ruzol, R., Staudhammer, C. L., Younger, S., Aubrey, D. P., Loescher, H. W., Jackson, C. R., & Starr, G. (2022). Water use in a young *Pinus taeda* bioenergy plantation: Effect of intensive management on stand evapotranspiration. *Ecosphere*, *13*(6), 1–19. https://doi.org/10.1002/ecs2.4100

Saksena, S., & Merwade, V. (2015). Incorporating the effect of DEM resolution and accuracy for improved flood inundation mapping. *Journal of Hydrology*, *530*, 180–194. https://doi.org/10.1016/j.jhydrol.2015.09.069

Sayama, T., McDonnell, J. J., Dhakal, A., & Sullivan, K. (2011). How much water can a watershed store? *Hydrological Processes*, *25*(25), 3899–3908. https://doi.org/10.1002/hyp.8288

Scher, H., Margolin, G., Metzler, R., Klafter, J., & Berkowitz, B. (2002). The dynamical foundation of fractal stream chemistry: The origin of extremely long retention times. *Geophysical Research Letters*, *29*(5), 1–4. https://doi.org/10.1029/2001gl014123

Schlesinger, W. H., & Bernhardt, E. S. (2013). *Biogeochemistry: An analysis of global change* (3rd ed.). Elsevier.

Schlosser, I. J. (1991). Stream fish ecology: A landscape perspective. *BioScience*, *41*(10), 704–712. https://doi.org/10.2307/1311765

Schoonover, J. E., Lockaby, B. G., & Helms, B. S. (2006). Impacts of land cover on stream hydrology in the west georgia piedmont, USA. *Journal of Environmental Quality*, *35*(6), 2123–2131. https://doi.org/10.2134/jeq2006.0113

Schoorl, J. M., Sonneveld, M. P. W., & Veldkamp, A. (2000). Three-dimensional landscape process modelling: The effect of DEM resolution. *Earth Surface Processes and Landforms*, *25*(9), 1025–1034. https://doi.org/10.1002/1096-9837(200008)25:9<1025::AID-ESP116>3.0.CO;2-Z

Schumm, S. (1977). *The fluvial system*. John Wiley; Sons.

Schwanghart, W., & Scherler, D. (2014). Short communication: TopoToolbox 2 – MATLAB-based software for topographic analysis and modeling in earth surface sciences. *Earth Surface Dynamics*, *2*(1), 1–7. https://doi.org/10.5194/esurf-2-1-2014

Schwanghart, W., & Kuhn, N. J. (2010). TopoToolbox: A set of matlab functions for topographic analysis. *Environmental Modelling and Software*, *25*(6), 770–781. https://doi.org/10.1016/j.envsoft.2009.12.002

Schwanghart, W., & Scherler, D. (2020). Divide mobility controls knickpoint migration on the roan plateau (colorado, USA). *Geology*, *48*(7), 698–702. https://doi.org/10.1130/G47054.1

Schwartz, F. W., & Zhang, H. (2003). *Fundamentals of ground water*. Wiley.

Schwientek, M., Maloszewski, P., & Einsiedl, F. (2009). Effect of the unsaturated zone thickness on the distribution of water mean transit times in a porous aquifer. *Journal of Hydrology*, *373*(3), 516–526. https://doi.org/10.1016/j.jhydrol.2009.05.015

Seitzinger, S., Harrison, J. A., Böhlke, J. K., Bouwman, A. F., Lowrance, R., Peterson, B., Tobias, C., & Drecht, G. V. (2006). DENITRIFICATION ACROSS LANDSCAPES AND WATERSCAPES: A SYNTHESIS. *Ecological Applications*, *16*(6), 2064–2090. https://doi.org/10.1890/1051-0761(2006)016[2064:DALAWA]2.0.CO;2

Senbayram, M., Chen, R., Budai, A., Bakken, L., & Dittert, K. (2012). N20 emission and the n20/(n20+n2) product ratio of denitrification as controlled by available carbon substrates and nitrate concentrations. *Agriculture, Ecosystems & Environment*, *147*, 4–12. https://doi.org/10.1016/j.agee.2011.06.022

Senbayram, M., Wei, Z., Wu, D., Shan, J., Yan, X., & Well, R. (2022). Inhibitory effect of high nitrate on n20 reduction is offset by long moist spells in heavily n loaded arable soils. *Biology and Fertility of Soils*, *58*(1), 77–90. https://doi.org/10.1007/s00374-021-01612-x

Sigler, W. A., Ewing, S. A., Wankel, S. D., Jones, C. A., Leuthold, S., Brookshire, E. N. J., & Payn, R. A. (2022). Isotopic signals in an agricultural watershed suggest denitrification is locally intensive in riparian areas but extensive in upland soils. *Biogeochemistry*, *158*(2), 251–268. https://doi.org/10.1007/s10533-022-00898-9

Silvanima, J., Woeber, A., Sunderman-Barnes, S., Copeland, R., Sedlacek, C., & Seal, T. (2018). A synoptic survey of select wastewater-tracer compounds and the pesticide imidacloprid in florida's ambient freshwaters. *Environmental Monitoring and Assessment*, *190*(7), 435. https://doi.org/10.1007/s10661-018-6782-4

ŠImek, M., & Cooper, J. E. (2002). The influence of soil pH on denitrification: Progress towards the understanding of this interaction over the last 50 years: Soil pH and denitrification. *European Journal of Soil Science*, *53*(3), 345–354. https://doi.org/10.1046/j.1365-2389.2002.00461.x

Somarriba, E., Valdivieso, R., Vásquez, W., & Galloway, G. (2001). Survival, growth, timber productivity and site index of cordia alliodora in forestry and agroforestry systems. *Agroforestry Systems*, *51*, 111–118.

Spence, C., & Phillips, R. W. (2015). Refining understanding of hydrological connectivity in a boreal catchment: CONNECTIVITY IN a BOREAL CATCHMENT. *Hydrological Processes*, *29*(16), 3491–3503. https://doi.org/10.1002/hyp.10270

Staudinger, M., Stoelzle, M., Cochand, F., Seibert, J., Weiler, M., & Hunkeler, D. (2019). Your work is my boundary condition!: Challenges and approaches for a closer collaboration between hydrologists and hydrogeologists. *Journal of Hydrology*, *571*, 235–243. https://doi.org/10.1016/j.jhydrol.2019.01.058

Staudinger, M., Stoelzle, M., Seeger, S., Seibert, J., Weiler, M., & Stahl, K. (2017). Catchment water storage variation with elevation. *Hydrological Processes*, *31*(11), 2000–2015. https://doi.org/10.1002/hyp.11158

Strauss, E. A., Mitchell, N. L., & Lamberti, G. A. (2002). Factors regulating nitrification in aquatic sediments: Effects of organic carbon, nitrogen availability, and pH. *Canadian Journal of Fisheries and Aquatic Sciences*, *59*(3), 554–563. https://doi.org/10.1139/f02-032

Thompson Tew, D., Morris, L., Lee Allen, H., & Wells, C. (1986). Estimates of nutrient removal, displacement and loss resulting from harvest and site preparation of a pinus taeda plantation in the piedmont of north carolina. *Forest Ecology and Management*, *15*(4), 257–267. https://doi.org/10.1016/0378-1127(86)90163-5

Thorp, J. H., Thoms, M. C., & Delong, M. D. (2006). The riverine ecosystem synthesis: Biocomplexity in river networks across space and time. *River Research and Applications*, *22*(2), 123–147. https://doi.org/10.1002/rra.901

Tóth, J. (1963). A theoretical analysis of groundwater flow in small drainage basins. *Journal of Geophysical Research*, *68*(16), 4795–4812. https://doi.org/10.1029/jz068i016p04795

Townsend, C. R. (1989). The patch dynamics concept of stream community ecology [Number: 1]. *Journal of the North American Benthological Society*, *8*(1), 36–50. https://doi.org/10.2307/1467400

Troch, P. A., Berne, A., Bogaart, P., Harman, C., Hilberts, A. G., Lyon, S. W., Paniconi, C., Pauwels, V. R., Rupp, D. E., Selker, J. S., Teuling, A. J., Uijlenhoet, R., & Verhoest, N. E. (2013). The importance of hydraulic groundwater theory in catchment hydrology: The legacy of wilfried brutsaert and jean-yves parlange. *Water Resources Research*, *49*(9), 5099–5116. https://doi.org/10.1002/wrcr.20407

USGS. (2018). *NHDPlus high resolution* (Version USGS National Hydrography Dataset Plus High Resolution). https://www.usgs.gov/core-science-systems/ngp/national-hydrography/access-national-hydrography-products

Vache, K., Meles, M. B., Griffiths, N. A., & Jackson, C. R. (2021). Ensemble modeling of watershed-scale hydrologic effects of short-rotation woody crop production. *Biofuels, Bioproducts and Biorefining*, *15*(5), 1345–1359. https://doi.org/10.1002/bbb.2247

van Meerveld, H. J., Seibert, J., & Peters, N. E. (2015). Hillslope-riparian-stream connectivity and flow directions at the panola mountain research watershed: Hillslope-riparian-stream connectivity and flow directions at panola. *Hydrological Processes*, *29*(16), 3556–3574. https://doi.org/10.1002/hyp.10508

van Meerveld, H. J. I., Kirchner, J. W., Vis, M. J. P., Assendelft, R. S., & Seibert, J. (2019). Expansion and contraction of the flowing stream network changes hillslope flowpath lengths and the shape of the travel time distribution. *Hydrology and Earth System Sciences Discussions*, 1–18. https://doi.org/10.5194/hess-2019-218

Vannote, R., Minshall, G., Cummins, K., Sedell, J., & Crushing, C. (1980). The river continuum concept. *Canadian Journal of Fisheries and Aquatic Sciences*, *37*(1), 130–137.

Vidon, P., Allan, C., Burns, D., Duval, T. P., Gurwick, N., Inamdar, S., Lowrance, R., Okay, J., Scott, D., & Sebestyen, S. (2010). Hot spots and hot moments in riparian zones: Potential for improved water quality management. *Journal of the American Water Resources Association*, *46*(2), 278–298. https://doi.org/10.1111/j.1752-1688.2010.00420.x

Vitousek, P. M., Aber, J. D., Howarth, R. W., Likens, G. E., Matson, P. A., Schindler, D. W., Schlesinger, W. H., & Tilman, D. G. (1997). HUMAN ALTERATION OF THE GLOBAL NITROGEN CYCLE: SOURCES AND CONSEQUENCES. *Ecological Applications*, *7*(3).

Vitousek, P. M., Treseder, K. K., Howarth, R. W., & Menge, D. N. L. (2022). A "toy model" analysis of causes of nitrogen limitation in terrestrial ecosystems. *Biogeochemistry*, *160*(3), 381–394. https://doi.org/10.1007/s10533-022-00959-z

Wagener, T., Sivapalan, M., Troch, P., & Woods, R. (2007). Catchment classification and hydrologic similarity. *Geography Compass*, *1*(4), 901–931. https://doi.org/10.1111/j.1749-8198.2007.00039.x

Wagner, M. J., Bladon, K. D., Silins, U., Williams, C. H. S., Martens, A. M., Boon, S., MacDonald, R. J., Stone, M., Emelko, M. B., & Anderson, A. (2014). Catchment-scale stream temperature response to land disturbance by wildfire governed by surface-subsurface energy exchange and atmospheric controls. *Journal of Hydrology*, *517*, 328–338. https://doi.org/10.1016/j.jhydrol.2014.05.006

Walsh, D. O., Grunewald, E. D., Turner, P., Hinnell, A., & Ferre, T. P. (2014). Surface NMR instrumentation and methods for detecting and characterizing water in the vadose zone. *Near Surface Geophysics*, *12*(2), 271–284. https://doi.org/10.3997/1873-0604.2013066

Wang, G. G., & Klinka, K. (1996). Use of synoptic variables in predicting white spruce site index. *Forest Ecology and Management*, *80*(1), 95–105. https://doi.org/10.1016/0378-1127(95)03630-x

Wang, K., Yan, D., Qin, T., Weng, B., Wang, H., Bi, W., Li, X., & Dorjsuren, B. (2020). A new topological and hierarchical river coding method based on the hydrology structure. *Journal of Hydrology*, *580*, 124243. https://doi.org/10.1016/j.jhydrol.2019.124243

Wang, Z., Fei, X., He, S., Huang, J., & Zhou, W. (2017). Comparison of heterotrophic and autotrophic denitrification processes for treating nitrate-contaminated surface water. *Science of The Total Environment*, *579*, 1706–1714. https://doi.org/10.1016/j.scitotenv.2016.11.194

Warburton, J., Holden, J., & Mills, A. J. (2004). Hydrological controls of surficial mass movements in peat. *Earth-Science Reviews*, *67*(1), 139–156. https://doi.org/10.1016/j.earscirev.2004.03.003

Webster, J. R., Benfield, E., Cecala, K., Chamblee, J., Dehring, C., Gragson, T., Cymerman, J., Jackson, C. R., Knoepp, J. D., Maerz, J., Pringle, C. M., & Valett, H. M. (2012). Water quality and exurbanization in southern appalachian streams. In P. Boon & P. Raven (Eds.), *River conservation and management* (pp. 91–106). Wiley-Blackwell.

Wells, D. (2009). *SRS groundwater* (SRNS–STI–2010–00175).

Welsh, M. K., Vidon, P. G., & McMillan, S. K. (2021). Riparian seasonal water quality and greenhouse gas dynamics following stream restoration. *Biogeochemistry*, *156*(3), 453–474. https://doi.org/10.1007/s10533-021-00866-9

Weymann, D., Well, R., Flessa, H., von der Heide, C., Deurer, M., Meyer, K., Konrad, C., & Walther, W. (2008). Groundwater n2o emission factors of nitrate-contaminated aquifers as derived from

denitrification progress and n20 accumulation. *Biogeosciences*, *5*(5), 1215–1226. https://doi.org/10.5194/bg-5-1215-2008

Wickham, J., Wade, T., & Norton, D. (2014). Spatial patterns of watershed impervious cover relative to stream location. *Ecological Indicators*, *40*, 109–116. https://doi.org/10.1016/j.ecolind.2014.01.013

Wilusz, D. C., Harman, C. J., Ball, W. P., Maxwell, R. M., & Buda, A. R. (2020). Using particle tracking to understand flow paths, age distributions, and the paradoxical origins of the inverse storage effect in an experimental catchment. *Water Resources Research*, *56*(4). https://doi.org/10.1029/2019WR025140

Withers, P., Neal, C., Jarvie, H., & Doody, D. (2014). Agriculture and eutrophication: Where do we go from here? *Sustainability*, *6*(9), 5853–5875. https://doi.org/10.3390/su6095853

Wohl, E., Bledsoe, B. P., Jacobson, R. B., Poff, N. L., Rathburn, S. L., Walters, D. M., & Wilcox, A. C. (2015). The natural sediment regime in rivers: Broadening the foundation for ecosystem management. *BioScience*, *65*(4), 358–371. https://doi.org/10.1093/biosci/biv002

Wrage, N., Velthof, G. L., van Beusichem, M. L., & Oenema, O. (2001). Role of nitrifier denitrification in the production of nitrous oxide. *Soil Biology*, *33*, 1723–1732.

Wurtsbaugh, W. A., Paerl, H. W., & Dodds, W. K. (2019). Nutrients, eutrophication and harmful algal blooms along the freshwater to marine continuum. *WIREs Water*, *6*(5), 1–27. https://doi.org/10.1002/wat2.1373

Yang, G., Bowling, L. C., Cherkauer, K. A., & Pijanowski, B. C. (2011). The impact of urban development on hydrologic regime from catchment to basin scales. *Landscape and Urban Planning*, *103*(2), 237–247. https://doi.org/10.1016/j.landurbplan.2011.08.003

Yeo, I.-Y., & Guldmann, J.-M. (2006). Land-use optimization for controlling peak flow discharge and nonpoint source water pollution. *Environment and Planning B: Planning and Design*, *33*(6), 903–921. https://doi.org/10.1068/b31185

Younger, S. E., Jackson, C. R., Dix, M. J., Caldwell, P. V., & Aubrey, D. P. (2023). Evapotranspiration partitioning of eucalyptus benthamii and pinus taeda during early stand development. *BioEnergy Research*. https://doi.org/10.1007/s12155-023-10591-w

Younger, S. E., Jackson, C. R., & Rasmussen, T. C. (2020). Relationships among forest type, watershed characteristics, and watershed ET in rural basins of the southeastern US. *Journal of Hydrology*, *591*, 125316. https://doi.org/10.1016/j.jhydrol.2020.125316

Zaliapin, I., Foufoula-Georgiou, E., Ghil, M., Foufoula-Georgiou, E., & Ghil, M. (2010). Transport on river networks: A dynamic tree approach. *Journal of Geophysical Research: Earth Surface*, *115*. https://doi.org/10.1029/2009jf001281

Zell, W. O., & Sanford, W. E. (2020). Calibrated simulation of the long-term average surficial groundwater system and derived spatial distributions of its characteristics for the contiguous united states. *Water Resources Research*, *56*(8), 1–16. https://doi.org/10.1029/2019WR026724

Zettler-Mann, A., & Fonstad, M. (2020). Riverscape mapping and hyperscale analysis of the sediment links concept. *Geomorphology*, *350*, 106920. https://doi.org/10.1016/j.geomorph.2019.106920

Zhang, W., Li, H., & Pueppke, S. G. (2022). Direct measurements of dissolved n2 and n20 highlight the strong nitrogen (n) removal potential of riverine wetlands in a headwater stream. *Science of The Total Environment*, *848*, 157538. https://doi.org/10.1016/j.scitotenv.2022.157538

Zhang, Y., Hassan, M. A., King, L., Fu, X., Istanbulluoglu, E., & Wang, G. (2020). Morphometrics of china's loess plateau: The spatial legacy of tectonics, climate, and loess deposition history. *Geomorphology*, *354*, 107043. https://doi.org/10.1016/j.geomorph.2020.107043

Zhou, W., Ma, Y., Well, R., Wang, H., & Yan, X. (2018). Denitrification in shallow groundwater below different arable land systems in a high nitrogen-loading region. *Journal of Geophysical Research: Biogeosciences*, *123*(3), 991–1004. https://doi.org/10.1002/2017JG004199

Zimmerman, D. L., & Ver Hoef, J. M. (2017). The torgegram for fluvial variography: Characterizing spatial dependence on stream networks. *Journal of Computational and Graphical Statistics*, *26*(2), 253–264. https://doi.org/10.1080/10618600.2016.1247006

Zimmermann, B., Zimmermann, A., Turner, B. L., Francke, T., & Elsenbeer, H. (2014). Connectivity of overland flow by drainage network expansion in a rain forest catchment. *Water Resources Research*, *50*(2), 1457–1473. https://doi.org/10.1002/2012WR012660

Živković, J. (2019). Human settlements and climate change [Series Title: Encyclopedia of the UN Sustainable Development Goals]. In W. Leal Filho, T. Wall, U. Azeiteiro, A. M. Azul, L. Brandli, & P. G. Özuyar (Eds.), *Good health and well-being* (pp. 1–11). Springer International Publishing. https://doi.org/10.1007/978-3-319-71063-1_88-1